# Context-dependent roles of BCL2L13 in autophagy, mitochondrial respiration, ceramide remodeling, and temozolomide resistance in glioblastoma

By

**Courtney Clark**

A Thesis submitted to the Faculty of Graduate and Postdoctoral Studies

of The University of Manitoba

in partial fulfilment of the requirements of the degree of

**Master of Science**

Biomedical Engineering

University of Manitoba

Winnipeg, Canada

**Abstract**

**Background:** Glioblastoma (**GBM**) is the most common and aggressive malignant primary brain tumor in adults, marked by rapid cellular proliferation, infiltrative growth, and high resistance to standard therapies. Despite surgical resection followed by radiotherapy and chemotherapy with temozolomide (**TMZ**), patient prognosis remains dismal, with median survival rarely exceeding 15 months. A major contributor to this therapeutic failure is the development of chemoresistance, particularly to TMZ, which significantly impairs treatment efficacy. Emerging evidence implicates dysregulated autophagy, mitochondrial dysfunction, and sphingolipid remodeling—including altered ceramide metabolism—as cellular adaptations associated with TMZ resistance. Among key molecular regulators, BCL-2-like protein 13 (**BCL2L13**), a mitochondria-localized member of the B-cell lymphoma-2 (**BCL2**) family, has been linked to apoptosis, mitochondrial stress responses, autophagy-related processes, and ceramide-associated signalling; however, its role in TMZ-resistant (**TMZ-R**) GBM remains underexplored. This study examined associations between BCL2L13 expression, autophagy flux, mitochondrial respiration, ceramide profiles, and TMZ response in GBM cells.

**Hypothesis:** We hypothesize that BCL2L13 expression contributes to cellular processes associated with TMZ resistance in GBM, including autophagy, mitochondrial function, and ceramide remodeling.

**Methods:** A clinically relevant TMZ-R U251 GBM cell line was established using an 18-week pulsed selection protocol and compared to TMZ-non-resistant (**TMZ-NR**) U251 cells. Cell viability and drug sensitivity were assessed by PrestoBlue and 3-(4,5-dimethyl-2-thiazolyl)-2,5-diphenyl-2H-tetrazolium bromide (**MTT**) cell viability assays. Flow cytometry was used to

analyze apoptosis and cell cycle distribution. Autophagy flux was evaluated via immunoblotting for LC3B-II and p62, with additional confirmation by immunocytochemistry (**ICC**) and transmission electron microscopy (**TEM**). Autophagosome–lysosome fusion was assessed using Bafilomycin A1 (**BafA1**). Stable knockdown of BCL2L13 was achieved through lentiviral transduction with puromycin selection. Mitochondrial respiration parameters—including ATP-linked respiration, spare capacity, and proton leak—were measured using the Seahorse XF Analyzer. Finally, targeted lipidomic profiling of ceramide species and their derivatives was performed using Liquid chromatography-tandem mass spectrometry (**LC-MS/MS**) in TMZ-R, TMZ-NR, and BCL2L13 knockdown variants.

**Results:** TMZ-R cells displayed marked resistance to high-dose TMZ (up to 5000μM), with significantly less apoptosis and G2-M cell cycle arrest than TMZ-NR cells. Autophagy marker dynamics were consistent with marked impairment of late-stage autophagic processing in TMZ-R cells, as indicated by accumulation of LC3B-II and p62, reduced responsiveness to BafA1, increased LC3B-positive puncta, and increased double-membrane autophagic vacuoles. BCL2L13 expression was significantly upregulated in TMZ-R cells ($P < 0.01$), and its knockdown altered autophagy-marker dynamics in a context-dependent manner without restoring autophagy flux or TMZ-induced apoptosis. Seahorse analysis revealed that BCL2L13 knockdown significantly increased proton leak and decreased spare respiratory capacity in TMZ-NR cells, while ATP-linked respiration and maximal respiration showed more modest, nonsignificant reductions. In TMZ-R cells, BCL2L13 knockdown produced minimal additional impairment. Targeted lipidomic analysis revealed that ceramide metabolism is profoundly altered in TMZ-R cells and further modulated by BCL2L13 knockdown. In wild-type TMZ-R cells, ceramide species such as Cer 18:0, Cer 20:0, and Cer 22:0 were significantly enriched relative to TMZ-NR cells. Knockdown

of BCL2L13 in TMZ-R cells led to selective enrichment of complex glycosylated ceramides including dihexosylceramides (DHC 18:0, 20:0, 22:0) and trihexosylceramides (THC 18:0, 20:0, 22:0), while reducing levels of THC 16:0, 24:0, and 24:1. Dihydroceramides (e.g., dhCer 16:0 and dhCer 22:0) also demonstrated distinct shifts between resistant and non-resistant states, with dhCer 16:0 significantly decreased in BCL2L13 knockdown TMZ-R cells. Monohexosylceramides (e.g., MHC 24:0 and 24:1) were enriched in TMZ-R wild-type cells but suppressed upon BCL2L13 knockdown. Principal component analysis demonstrated clear separation of TMZ-R and TMZ-NR cells based on their ceramide profiles. Overall, TMZ-NR cells displayed C16:0 and mid-chain ceramide changes consistent with CerS6-associated remodeling, whereas TMZ-R cells showed altered very-long-chain C22-C24 and glycosylated ceramide profiles consistent with CerS2-associated remodeling. Together, these findings support a context-dependent association between BCL2L13 and ceramide metabolism rather than direct regulation of CerS2 and CerS6.

**Conclusion:** This study demonstrates that BCL2L13 is associated with context-dependent changes in autophagy-marker dynamics, mitochondrial bioenergetics, and ceramide lipid remodeling in GBM. Although BCL2L13 is strongly upregulated in TMZ-R cells, it's knockdown does not restore TMZ-induced apoptosis, indicating that it is not a direct determinant of established TMZ-resistance. Instead, the findings support a role for BCL2L13 as a modifier of a stress-adaptive network involving autophagy, mitochondrial respiration, and ceramide metabolism. These pathways represent candidate mechanisms requiring further functional and mechanistic investigation.

**Acknowledgments**

I would first like to express my sincere gratitude to my super, Dr. Saeid Ghavami, for his guidance, mentorship, and support throughout my master's degree. Thank you for giving me the opportunity to undertake this work, for encouraging me to think critically and independently, and for supporting my growth as a researcher throughout this process. I am grateful for the knowledge and experience I have gained under your supervision and for your support in bringing this work to completion.

I would also like to sincerely thank my committee members, Dr. Miller and Dr. Moussavi, for their time, thoughtful feedback, expertise and guidance throughout my degree and during my thesis defence. Your questions and perspectives strengthened both this work and my development as a scientist. I am deeply grateful to the members of Dr. Ghavami's laboratory, past and present, for their support, collaboration, and friendship. Research is never accomplished alone, and I am thankful to everyone who shared their knowledge, helped me troubleshoot experiments, answered many questions, and contributed to an environment in which I could learn and grow. I would also like to acknowledge the faculty, staff, collaborators and colleagues who contributed their expertise, resources, and support to this work. I am especially grateful for those who assisted with the experimental techniques and analyses that made this project possible.

To my loved ones , thank you for your patience, encouragement, humour, and support through this defrgee. You celebrated the successes with me, carried me through the difficult stretches, and reminded me that there was a world outside of the laboratory. I could not have reached this point without the community of people who stood beside me.

Finally, I want to acknowledge the personal significance of completing this work as a Two-Spirit Red River Métis student. I carry the strength, knowledge, and resilience of the people and

communities who came before me. I am especially grateful to Ongomizwiin – Indigenous Institute of Health and Healing and to the Indigenous and Two-Spirit Elders, mentors, and organizations that have supported me throughout my education and helped create spaces where I could bring my whole self to this work.

This thesis is dedicated

to my loved ones, to those who believed in and me and loved me through every version of this journey. You all kept me going through every high and low that brought me here. And to Piggy, my constant little companion who stuck with me through the long days and late nights, and far too many hours spent at my computer. I could not have done this without all of you.

## Table of Contents

**List of Tables**

**List of Figures**

**List of Abbreviations**

| | |
|---|---|
| 3-MA | 3-methyladenine |
| ABC | ATP-binding cassette |
| ALDH1 | Aldehyde dehydrogenase 1 |
| ALL | Acute lymphoblastic leukemia |
| AMPK | 5'-AMP-activated protein kinase |
| ANT | Adenine nucleotide translocator |
| ATG | Autophagy-related genes |
| BafA1 | Bafilomycin A1 |
| BBB | Blood-brain barrier |
| BCL-2 | B-cell lymphoma-2 |
| BCL2L13 | BCL-2-like protein 13 |
| BER | Base excision repair |
| BH | BCL-2 homology |
| BNIP3 | BCL2 interacting protein 3 |
| BNIP3L/Nix | BCL2 interacting protein 3 like |
| BSA | Bovine serum albumin |
| CerS | Ceramide synthases |
| CerS2/6 | Ceramide synthases 2 and 6 |
| CHO | Chinese hamster ovary cells |
| CMA | Chaperone-mediated autophagy |
| CNS | Central nervous system |
| Co-IP | Co-immunoprecipitation |
| CSC | Cancer stem cells |
| DAG | Diacylglycerol |
| dckl1 | Doublecortin-like kinase 1 |
| DHC | Dihexosylceramides |
| dhCer | Dihydroceramides |
| DMSO | Dimethyl sulfoxide |
| DNM1L | Dynamin-1-like protein |
| DPBS | Dulbecco's phosphate-buffered saline |
| ESI+ | Positive electrospray ionization mode |
| FAs | Fatty acids |
| FDS | False discovery rate |
| GBM | Glioblastoma Multiforme |
| GIC | GBM-initiating cells |
| GSCs | Glioma stem cells |
| HGG | High-grade glioma |
| HOPS | Homotypic fusion and protein sorting |
| HNSCC | Head and neck squamous cell carcinoma |
| Hsc70 | Heat shock protein 70 |
| ICC | Immunocytochemistry |
| IDH | Isocitrate dehydrogenase |
| KD | Knockdown |
| KEGG | Kyoto Encyclopedia of Genes and Genomes Analysis |

| | |
|---|---|
| LAMP2 | Lysosome-associated membrane protein 2 |
| LAMP2A | Lysosomal-associated membrane protein 2A |
| LC-MS/MS | Liquid chromatography-tandem mass spectrometry |
| LC3β | Microtubule-associated protein 1A/1B-light chain 3B |
| LGG | Low-grade glioma |
| LIR | LC3-interacting region |
| MGMT | $O^6$-methylguanine-DNA methyltransferase |
| MHC | Monohexosylceramides |
| miRNA | MicroRNA |
| MMR | Mismatch repair |
| MOMP | Mitochondrial outer membrane permeabilization |
| MPG | N3-methylpurine-DNA-glycosylase |
| mRNA | Messenger RNA |
| MTT | 3-(4,5-dimethyl-2-thiazolyl)-2,5-diphenyl-2H-tetrazolium bromide |
| mTOR | Mechanistic target of rapamycin |
| OCR | Oxygen consumption rate |
| OGD | Oxygen-glucose deprivation |
| OXPHOS | Oxidative phosphorylation |
| PARP | Poly(ADP-ribose) polymerase |
| PAS | Phagophore assembly site |
| PBS | Phosphate buffered saline |
| PI3K | Phosphoinositide 3-kinase |
| PINK1 | Phosphatase and tensin homolog-induced kinase 1 |
| PL | Phospholipids |
| PLS-DA | Partial least squares discriminant analysis |
| pRB | Retinoblastoma protein |
| Q-TOF LC/MS. | Quadruple time-of-flight liquid chromatography-mass spectrometry |
| RT | Room temperature |
| S1P | Sphingosine-1-phosphate |
| scRNA | Scramble RNA |
| shRNA | Short hairpin RNA |
| SNAREs | Soluble NSF attachment protein receptors |
| TAG | Triacylglycerols |
| THC | Trihexosylceramides |
| TEM | Transmission electron microscopy |
| TM | Transmembrane |
| TMZ | Temozolomide |
| TMZ-NR | Temozolomide non-resistant |
| TMZ-R | TMZ-resistant |
| TNF | Tumour necrosis factor |
| TRAIL | Tumour-necrosis-factor-related apoptosis-induing ligand |
| ULK1 | Unc-51-like kinase |
| VDAC | Voltage-dependent anion channel |
| VIP | Variable Importance in Projection |
| VLC | Very-long chain |
| WT | Wildtype |

# CHAPTER 1: Literature Review

## *1.1 Glioblastoma*

Glioblastoma (**GBM**) is the most common primary malignant brain tumour in adults and is commonly known for its rapidly progressive and deadly nature (1). It comprises 75% of all high-grade gliomas and has an annual incidence of 4.5 per 100,000 people in Canada (2). Under the current World Health Organization classification, GBM is an IDH-wildtype, grade 4 adult brain tumour characterized by diffuse infiltration, aggressive cellular proliferation, genomic instability, angiogenesis, and resistance to therapy (**Figure 1.1**). The current classification incorporates both histological and molecular characteristics in the diagnosis of GBM, reflecting the increasing importance of tumour genetics in defining the disease.

Astrocytomas are a subset of gliomas derived from astrocytes, non-neuronal brain cells that provide structure and metabolic support for surrounding neurons (3, 4). Isocitrate dehydrogenase (**IDH**) is an important biomarker in the classification of adult diffuse gliomas. IDH enzymes play an important role in cellular metabolism, including the conversion of isocitrate to α-ketoglutarate. Mutations in IDH1 or IDH2 confer neomorphic enzymatic activity that results in production of the oncometabolite D-2-hydroxyglutarate, which can alter epigenetic regulation and cellular metabolism (5). Historically, glioblastomas were categorized as primary or secondary, with secondary GBMs frequently harbouring IDH mutations (3, 6). Under the current World Health Organization classification, however, the diagnosis of GBM is reserved for IDH-wildtype tumours, while IDH-mutant tumours previously classified as secondary GBM are now classified separately as astrocytoma, IDH-mutant (7).

Several methods exist for determining the morbidity and mortality associated with cancer. The five-year relative survival rate is defined as the percentage of people alive five years post-

diagnosis. It depends on several factors, including age, sex, and place of residence (8). Median survival refers to the period during which half of a group of people with cancer are still alive, while the other half will live less than this amount of time. When compared to other cancers of the central nervous system (**CNS**), GBM falls short in both areas, with the lowest five-year survival rate (6.8%) of all CNS cancers and a median overall survival of approximately 14 months (9, 10).

A significant factor contributing to poor GBM prognosis is extensive inter-tumoural (between tumours) and intra-tumoural (within a tumour) heterogeneity (11). Heterogeneity manifests as differences in cellular morphology, gene expression, metabolism, motility, proliferation, and metastatic potential (12). These differences are potentiated by variations in the tumour microenvironment, which imposes selective pressures on tumour cells, thereby increasing the proportion of subpopulations in various regions of the tumour (13). Another hallmark of GBM that poses a direct challenge to developing effective therapeutic strategies and drug delivery is disruption of the blood-brain barrier (**BBB**). The BBB is a neurovascular unit that evolved to maintain brain homeostasis and restrict the passage of solutes in the circulating blood from crossing into the extracellular fluid of the CNS (14). It acts as a physical barrier to foreign molecules entering cerebral circulation. Tumours of the CNS have been shown to infiltrate the BBB, resulting in the development of a distinct neurovascular unit called the blood-brain tumour barrier, a derivative of the BBB characterized by increased perfusion and enhanced permeability to solutes. However, the increased permeability of the blood-brain tumour barrier is nonuniform and does not include the advancing tumour boundary; this is a rate-limiting factor in optimizing drug delivery and concentrations of chemotherapy agents within the tumour (15). The standard of care for patients with GBM includes maximal surgical resection, radiotherapy, and concurrent or adjuvant chemotherapy with temozolomide (**TMZ**), a DNA alkylating drug (11). This multimodal

approach improves median survival to approximately 14.6 months, compared to 12 months with radiotherapy alone (1). The following section provides background on the development and mechanism of action of TMZ, highlighting key challenges researchers and clinicians face in its use for the treatment of GBM.

Glioblastoma is predominantly a sporadic malignancy; however, inherited genetic factors can contribute to disease susceptibility. A small proportion of cases occur in association with hereditary cancer predisposition syndromes, including Li-Fraumeni syndrome, neurofibromatosis type 1, Lynch syndrome, and Turcot syndrome (16, 17). These syndromes involve germline alterations affecting tumour suppressor and DNA repair pathways, including TP53, NF1, and DNA mismatch repair genes such as MLH1, MSH2, MSH6, and PMS2 (17). Beyond these rate hereditary syndromes, inherited susceptibility to glioblastoma may also be influenced by common genetic variation (18). Genome-wide association studies examining glioma, a broader group of primary brain tumours that includes glioblastoma, have identified susceptibility loci involving genes such as TERT, CCDC26, CDKN2A/CDKN2B, and RTEL1, with some associations varying according to tumour subtype (18, 19). Thus, while hereditary predisposition accounts for only a small proportion of glioblastoma cases, inherited genetic factors represent a recognized component of disease susceptibility.

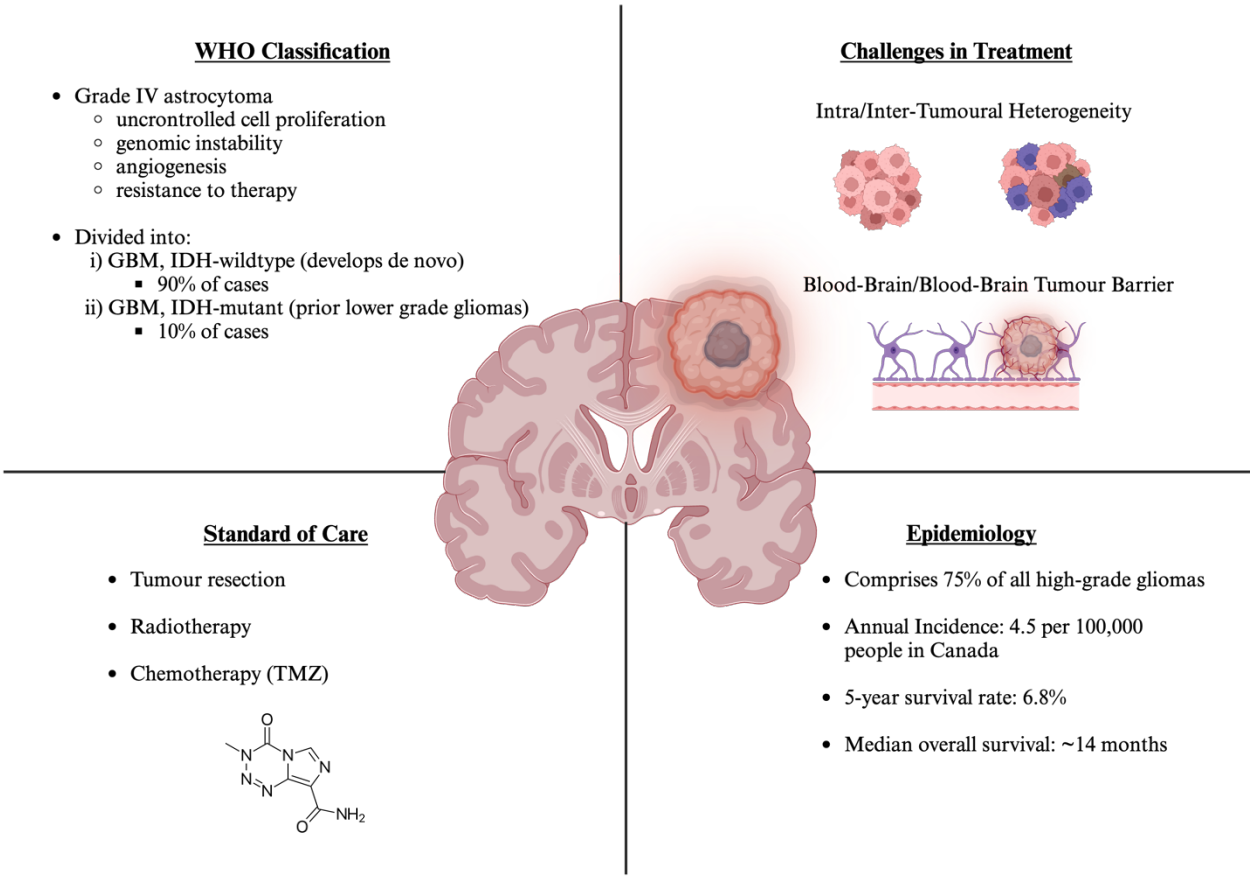


**Figure 1.1.** Classification and epidemiological overview of glioblastoma multiforme.

### *1.1.1 TMZ discovery, mechanism of action, and therapy in GBM*

Temozolomide is the most commonly prescribed chemotherapeutic drug used to treat GBM. The cytotoxic effect depends on its ability to alkylate DNA, resulting in DNA damage and tumour cell death. TMZ induces cell cycle arrest at G2/M, preventing cells with damaged DNA from undergoing mitosis and eventually leading to programmed cell death (apoptosis) (20). Prior to its discovery by medical chemist Malcolm Stevens in the 1980s, triazenes – molecules with a linear chain of three nitrogen atoms – were already recognized for their anti-tumour activity (21). Stevens built on this knowledge and applied a newly described method for synthesizing tetrazine ring systems to produce the first imidazotetrazine derivative of dacarbazine, a triazene then used to treat malignant melanoma. TMZ and its precursor molecules were characterized by a triazene

group in a cyclic form and an imidazole ring backbone (21, 22). TMZ's novelty lies in its small molecular weight and lipophilic characteristics, which make it orally bioavailable and capable of penetrating the BBB (22, 23).

Further investigation has established TMZ as a pro-drug that, once ingested, remains highly stable at the acidic pH of the stomach. However, after being absorbed in the digestive tract and encountering the slightly basic pH of the blood, TMZ undergoes spontaneous hydrolysis to form the active methylating agent MTIC (3-methyl-(trizen-1-yl) imidazole-4-carboximide). MTIC is then rapidly metabolized to produce the reactive methyldiazonium ion, which methylates purine bases of DNA (N7meG, N3meA, and O6meG) (24). Specifically, alkylation of the O6 position on guanine results in the insertion of a thymine instead of a cytosine base during DNA replication, which can lead to cell death (25, 26). Enzymes involved in different DNA repair pathways recognize these mispaired bases and induce double-strand breaks, ultimately leading to programmed cell death (**Figure 1.2**) (27).

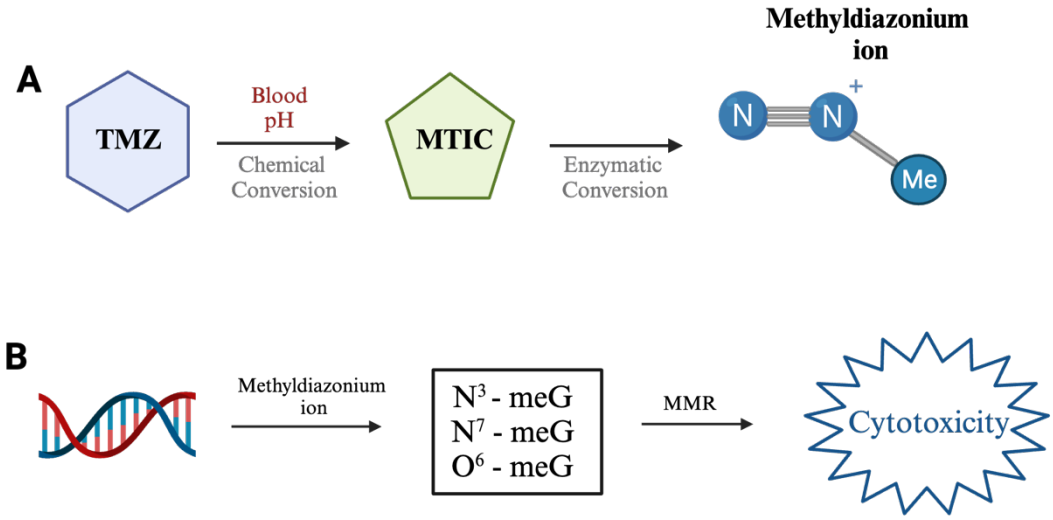


**Figure 1.2. Metabolic activation of temozolomide and DNA damage-induced cytotoxicity (A)** Different stages of TMZ metabolism: TMZ is orally ingested and is stable at the acidic pH (stomach). At physiologic (blood) pH, it is converted to the short-lived MTIC, which is metabolized to produce the diazonium ion. **(B)** Mechanism of action of TMZ: Diazonium ion modifies purine bases of DNA at N3, N7, and O6 sites. MMR results in double-strand breaks and leads to programmed cell death.

TMZ does not require metabolic activation and is spontaneously converted to its active compound at blood pH, deeming it a strong clinical candidate that was ultimately approved for market use in 1999 (28, 29). Unlike other chemotherapeutic compounds such as nitrosoureas, TMZ does not induce interstrand cross-linking of DNA, reducing its toxicity to hematopoietic progenitor cells in the bone marrow. Damage to these cells may lead to aplastic anemia (deficiency in blood cell production) or myelodysplastic syndrome (abnormal blood cell development) (30-32). A pivotal 2005 clinical trial published by Stupp et al. compared outcomes in GBM patients receiving

radiotherapy alone to those receiving radiotherapy in combination with TMZ. Their findings showed that the median survival rate increased from 12.1 months with radiotherapy alone to 14.6 months with the combined approach. Additionally, they reported a two-year survival rate of 26.5% for the combination group, compared to 10.4% with radiotherapy alone (33). These results demonstrated a statistically significant and clinically meaningful survival benefit, leading to the incorporation of TMZ into the standard of care for GBM (34). However, despite its initial efficacy, resistance to TMZ emerges in nearly all patients, often resulting in tumour recurrence that is more aggressive and unresponsive to further TMZ treatment – presenting a major obstacle to long-term therapeutic success (35).

### *1.1.2 Temozolomide chemoresistance in glioblastoma*

Many cellular mechanisms contribute to TMZ resistance in glioblastoma. TMZ acts on cells by inducing DNA damage that leads to programmed cell death. However, in TMZ-resistant glioblastoma cells, DNA repair pathways are often altered, suggesting that these cells recover from TMZ-induced damage through alternative repair mechanisms (35). This section describes different cellular mechanisms involved in TMZ chemoresistance, such as $O^6$-methylguanine-DNA methyltransferase (**MGMT**) overexpression, mismatch repair (**MMR**), base excision repair (**BER**), glioma stem cells (**GSCs**), the role of microRNAs (**miRNA**), potentiated drug efflux, and survival autophagy.

#### *1.1.2.1 Role of MGMT in TMZ chemoresistance in GBM*

MGMT is a DNA repair enzyme that removes methyl groups from $O^6$-methylguanine (O6-MeG) derivatives, a lesion induced by alkylating agents such as TMZ. This direct reversal of DNA

damage prevents errors during replication and transcription, thereby promoting cell survival and contributing to chemoresistance (36-39).

Expression of MGMT is transcriptionally regulated by methylation of the CpG (cytosine phosphate guanine) island in its promoter region. Transcriptionally regulated means the cell controls protein levels by controlling how much mRNA is produced from a gene. Promoter methylation leads to epigenetic silencing of MGMT expression, compromising DNA repair and enhancing the cytotoxic effects of TMZ (36, 40). In an orthotopic GBM xenograft model, MGMT protein levels were inversely correlated with TMZ response, while promoter methylation was positively correlated, indicating that lower MGMT expression enhances TMZ sensitivity (41). Clinical data also support this association: patients with MGMT promoter methylation demonstrate improved prognosis and overall survival compared to those with unmethylated MGMT promoters (42, 43).

However, the relationship between MGMT methylation, protein expression, and patient outcomes is not always consistent, as highlighted by discordant findings in several studies (44-46). Although promoter methylation is a key mechanism of MGMT silencing, additional layers of regulation influence MGMT expression and activity. For example, MGMT can be post-translationally regulated by poly(ADP-ribose) polymerase (**PARP**). Following TMZ treatment, PARP interacts with MGMT and facilitates its binding to chromatin, which is essential for the removal of $O^6$-MetG lesions from methylated DNA. Interestingly, PARP inhibition disrupts this PARP-MGMT interaction, thereby suppressing MGMT activity and restoring TMZ sensitivity in MGMT-expressing GBM models (47).

Moreover, a clinical study investigated the prevalence of genomic alterations in GBM and their association with MGMT promoter methylation. Mutations in TP53, CDKN2A, PTEN, and

PIK3CA were found to be four times more frequent in tumours with methylated MGMT compared to those with unmethylated MGMT. These cases were also associated with improved patient survival, suggesting that the co-occurrence of MGMT methylation and specific genetic mutations may have a synergistic impact on treatment response or disease progression (48). Despite MGMT's role in conferring TMZ resistance, approximately 50% of patients with primary GBM are MGMT-deficient and still resistant to TMZ, indicating that other mechanisms must also drive resistance to TMZ in these tumours (49).

#### *1.1.2.2 Role of DNA mismatch repair in TMZ chemoresistance in GBM*

DNA mismatch repair is a highly conserved pathway that plays a critical role in maintaining genomic stability by repairing base-base mismatches that are generated during DNA replication (50). MMR functions by identifying and correcting mismatched bases in the newly synthesized daughter strand, thereby preventing replication-associated damage to the cell. Briefly, MMR machinery consists of the dimers MutSα, MutLα, and MutH. MutSα recognizes and binds to the region of the mismatched base in the newly synthesized DNA strand. Next, MutH binds along the parent strand and is only activated upon contact with the MutLα dimer, which binds the MutS-DNA complex and acts as a mediator between MutSα and MutH, thereby activating the latter. The DNA is looped out to search for the nearest native methylation site on the parent strand closest to the mismatched base. Upon activation by the MutS-DNA complex, MutH introduces a nick in the daughter strand. MutLα then recruits DNA helicase, which separates the two strands. The entire MMR complex then progresses along the DNA, displacing the strand that needs to be excised. Exonuclease, which removes nucleotides from the ends of DNA, follows behind the complex and digests the single-stranded DNA tail. Throughout this process, nucleotides

surrounding the mismatch site are entirely removed. The single-strand gap created by the exonuclease is filled by DNA polymerase III, which uses the intact strand of DNA as a template. Lastly, DNA ligase joins the newly synthesized strand to the rest of the daughter strand (51).

However, extensive MMR can also have detrimental effects on the cell, such as programmed cell death. Recall that cytotoxicity from TMZ partially depends on a properly functioning DNA MMR system. Exposure to TMZ activates DNA repair mechanisms, such as MMR, due to TMZ-induced O6-meG mismatched bases. MMR recognizes these lesions and generates recurrent double-strand breaks, leading to apoptosis. It has been shown that cells that develop resistance to alkylating agents, like TMZ, are deficient in MMR. For instance, the human lymphoblastoid cell line MT1, which carries a defect in hMSH6, was derived by culturing TK6 cells in the presence of alkylating agent MNNG to establish MNNG-resistant MT1 cells. These MNNG-resistant cells are defective in strand-specific MMR (52). Reduction or loss of function in key MMR components has been reported following TMZ treatment, frequently appears in GBM recurrences, and is associated with poor response to TMZ and overall survival (53-55). Because MMR genes are susceptible to TMZ-induced mutations, disruption of MMR gene function is another mechanism that may contribute to TMZ resistance in GBM. One study demonstrated that small decreases in amounts of MutSα resulted in significant progression of GBM tumour cell growth in an in vivo mouse model and suggested that low MutSα levels in GBM tumours could be used as a prognostic tool for patient survival after TMZ treatment (54).

#### *1.1.2.3 Role of base excision repair in TMZ chemoresistance in GBM*

BER functions to reverse DNA damage caused by oxidation, deamination, single-strand breaks, and alkylation (56). DNA glycosylase, an enzyme that recognizes and removes small base

lesions, initiates BER. Removal of a base in DNA results in the production of an apurinic/apyrimidinic site in DNA that is subsequently repaired by DNA-replication machinery, which restores the original and correct DNA sequence (35, 57). N3-methyladenine and N7-methylguanine derivatives, which result from TMZ treatment, are substrates of N3-methylpurine-DNA-glycosylase (**MPG**), which removes the alkyl group from these adducts. Interestingly, a TMZ-resistant phenotype in patient-derived glioma cells has been linked to higher expression of MPG (58). It has also been shown that higher nuclear levels of MPG correlate with poorer overall survival compared to patients lacking MPG expression (59). These studies highlight BER as a possible target for tackling TMZ-resistant GBM.

#### *1.1.2.4 Role of glioma stem cells in TMZ chemoresistance in GBM*

A large body of evidence links chemoresistance with stem cell characteristics in GBM. These tumour-propagating cancer stem cells (**CSCs**) are more specifically referred to as GSCs. GSCs are considered key drivers of tumour progression and recurrence due to their capacity for self-renewal, multilineage differentiation, and their ability to replenish the highly transient tumour cell population. Through differentiation, GSCs form the bulk of the tumour and contribute significantly to its histological heterogeneity (60, 61).

Functionally, GSCs isolated from malignant glioma exhibit tumour-initiating properties (62) and enhanced DNA repair capacity – features that likely underlie both chemoresistance and disease relapse in patients (63). To better understand their role in acquired resistance, researchers have identified cellular markers unique to this subpopulation. In vitro, GSCs are commonly identified by their ability to self-renew in suspension cultures (tumour sphere formation) under serum-free conditions supplemented with basic fibroblast growth factor and epidermal growth

factor (64). When cultured in this stem cell medium, GSCs have been shown to recapitulate the genotype and phenotype of the original tumour, supporting their role in maintaining histological heterogeneity observed in glioma (65).

GSCs expressing the stem-cell marker CD133 (Prominin 1) have been shown to initiate glioblastoma tumour growth *in vivo* when transplanted into mice and are often referred to as GBM-initiating cells (**GICs**) (66). Several markers for GSCs have been identified, including CD133, SSEA1, nestin, integrin alpha 6, CD15, and A2B5 (67). However, controversy persists regarding the reliability of these markers – particularly whether they are consistent indicators of GIC capabilities. For example, a 2008 study revealed that GBM cells lacking Prominin 1 expression were also capable of initiating tumour formation in mice (68). GSCs may also be identified functionally by their notably high activity of aldehyde dehydrogenase 1 (**ALDH1**) (69). ALDH1 activity supports self-renewal, differentiation, and cellular protection and is associated with poor cancer prognosis (70). However, ALDH1 activity and the presence of stem cell markers are not consistent among various GBM tumours.

Such inconsistency likely reflects multiple sources of variability. Differences in experimental protocols across laboratories contribute, but a more profound cause lies in the heterogeneity that exists among GSCs within the same tumour (71). This intratumoural heterogeneity arises from genomic instability, a defining feature of cancer, which leads to diverse subpopulations of cells. Supporting this, Meacham and Morrison showed that even tumour-initiating cells isolated from the same tumour can give rise to genetically distinct populations when transplanted into mice (72).

The cancer stem cell model, also called the hierarchical stem cell concept, offers a compelling framework for understanding such tumour heterogeneity (**Figure 1.3**). According to

this model, cancers are hierarchically organized, with a small population of tumourigenic CSCs at the apex giving rise to and non-tumourigenic progeny. In glioblastoma, these CSCs are referred to as GSCs. A defining feature of these cells is their capacity for self-renewal, enabling them to maintain the CSC pool over time while also producing more differentiated progeny that constitute the bulk of the tumour. This self-renewing ability is central to their role in sustaining long-term tumour growth.

The interconversion between these subpopulations is influenced by factors in the tumour microenvironment. For example, GBM stemness has been shown to increase in response to alkylating agents like TMZ (73), as well as exposure to growth factors (e.g. bFGF) (74), transcription factors (e.g. Oct4, Sox2, Nanog) (75), and cytokine-driven STAT3 signaling activated from astrocytes (76). Tumourigenic CSCs, including GSCs in GBM, are thought to drive tumour growth and disease progression through their therapy-resistant phenotype and potential for metastasis. Whereas their non-tumourigenic progeny make up the bulk of the tumour mass (72, 77, 78).

Bidirectional interconversion between differentiated non-progenitor cells and undifferentiated GSCs further contributes to intratumoural heterogeneity and maintains the pool of tumour propagating cells (79). This model explains one potential source of intratumoural heterogeneity and its role in therapy resistance while emphasizing the likelihood of tumour development from genetically distinct GSCs. Meyer et al. demonstrated that the expression of MGMT, MGMT promoter methylation, and cellular response to TMZ varied among distinct clones isolated from the same tumour (80). This finding suggests that TMZ resistance exists at the clonal level within a tumour and illustrates the importance of GSC heterogeneity in driving clonal-level resistance and treatment failure in GBM.

#### *1.1.2.5 Role of miRNAs in TMZ chemoresistance in GBM*

MicroRNAs (miRNAs) are small, single-stranded non-coding RNA molecules approximately 21-23 nucleotides in length. miRNAs are generated by an enzyme called Dicer, which processes ~70 nucleotide-long precursor RNA molecules into mature miRNAs. Rather than encoding proteins, they bind to complementary sequences on target messenger RNAs (**mRNAs**), thereby repressing protein translation or promoting mRNA degradation (81, 82). In cancer, miRNAs serve dual roles: they function intracellularly to regulate gene expression and also act as extracellular signalling molecules. Tumour cells often package miRNA molecules into exosomes, microvesicles, and high-density lipoproteins to shield them from enzymatic degradation, facilitating their intracellular communication (83-85). Several miRNA molecules are involved in the maintenance and progression of cancer cells through mechanisms including CSC regulation; promotion of cell proliferation, invasion, and angiogenesis; induction of autophagy; upregulation of DNA repair pathways; and evasion of apoptosis (86-88). Unsurprisingly, many of these mechanisms are implicated in resistance to TMZ.

For example, the downregulation of miRNA-101 has been shown to contribute to TMZ resistance, whereas its overexpression increases sensitivity to TMZ in U251 GBM cells by repressing MGMT expression through promoter methylation (89). Similarly, the upregulation of miRNA-21 inhibits TMZ-induced apoptosis by reducing caspase activity. In contrast, inhibition of miRNA-21 enhances TMZ sensitivity in resistant GBM cells to TMZ (90, 91).

High-throughput miRNA profiling has identified numerous miRNAs associated with GBM pathogenesis (92), including those involved in regulating and maintaining CSC characteristics (93). In a study by Srinivasan et al., a ten-miRNA signature was found to correlate with patient survival: three miRNAs (miR-20a, miR-106a, and miR-17-5p) displayed tumour-suppressive

functions, while the remaining seven (hsa-miR-31, hsa-miR-222, hsa-miR-148a, hsa-miR-221, hsa-miR-146b, hsa-miR-200b and hsa-miR-193a) were associated with tumour-promoting roles. Based on this signature, patients were stratified into high and low-risk groups, with high-risk patients exhibiting significantly poorer overall survival (94). By contributing to tumour heterogeneity and enabling risk stratification, miRNAs offer both mechanistic insight and potential as therapeutic targets – supporting the broader view that resistance in GBM is shaped by complex, multi-level regulation.

#### *1.1.2.6 Role of drug efflux in TMZ chemoresistance in GBM*

Drug efflux transporters reduce intracellular drug accumulation by actively transporting cytotoxic agents out of the cell. The ATP-binding cassette (**ABC**) transporter family is one of the comprising over 40 transporters in humans, plays a key role in this process. Beyond drug transport, ABC proteins also regulate osmotic balance, lipid trafficking, and cell division (95). These integral membrane proteins use ATP to power the translocation of various substrates across the plasma membrane (96-98). In GBM, ABCB1 (also known as MDR1) is frequently overexpressed and has been implicated in TMZ resistance (99, 100). Notably, a single-nucleotide polymorphism in the MDR1 gene (C1236T) has been associated with survival outcomes in patients treated with TMZ (101).

These findings suggest that ABC transporters contribute to chemoresistance and may serve as both therapeutic and prognostic biomarkers in GBM. Taken together with other resistance mechanisms – such as DNA repair pathways, glioma stem cells, and miRNAs – drug efflux transporters form part of a multifaceted resistance network against TMZ therapy in GBM (**Figure 1.3**). Understanding these interconnected pathways is critical to developing strategies that

overcome or bypass resistance. This complexity is further exemplified by the role of autophagy, a stress response mechanism that has emerged as both a contributor to and potential target for overcoming TMZ.

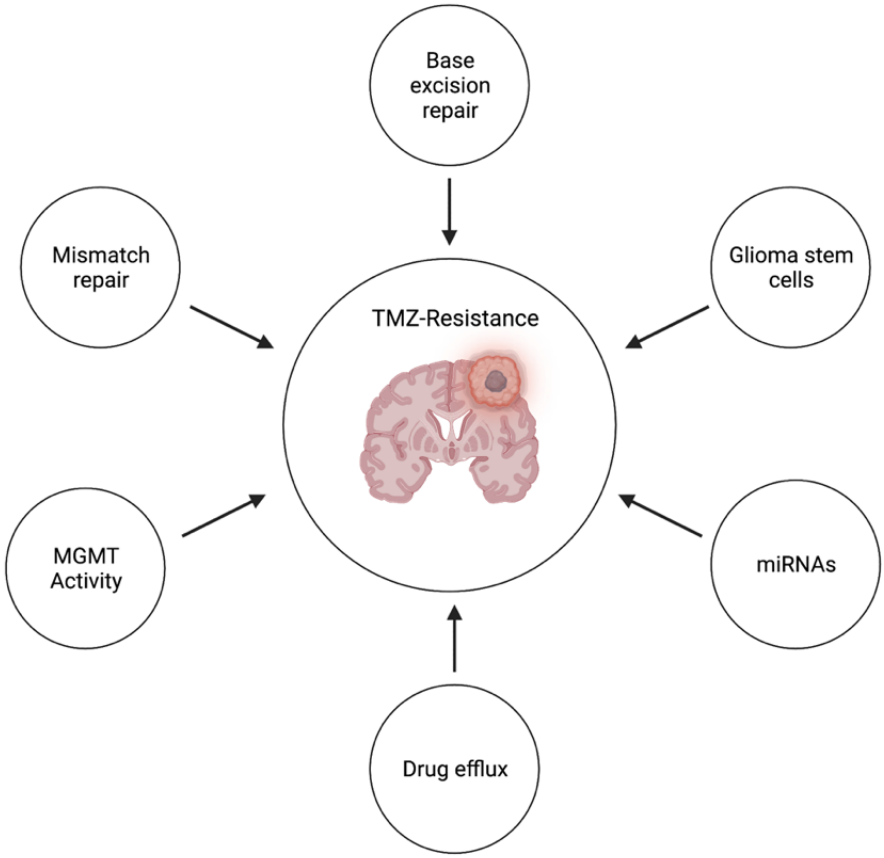


**Figure 1.3. Cellular mechanisms underlying TMZ resistance in GBM.** Overview of cellular mechanisms contributing to TMZ-resistance in GBM, including base excision repair, glioma stem cells, miRNAs, drug efflux, MGMT activity, and mismatch repair.

### *1.1.3 Autophagy and TMZ chemoresistance*

Autophagy is a highly conserved catabolic process that enables cells to degrade and recycle damaged organelles and macromolecules, often as a survival strategy under stress. In GBM, TMZ

induces DNA damage that can activate autophagy. Paradoxically, this activation may protect tumour cells by clearing cytotoxic components and supplying essential metabolic substrates, ultimately promoting survival. This pro-survival role of autophagy has been implicated in resistance to TMZ. As a result, autophagy inhibitors are being investigated as adjuvant therapies to improve TMZ efficacy. Elucidating the mechanisms by which autophagy contributes to chemoresistance is crucial for developing more effective therapeutic approaches for GBM (102).

#### *1.1.3.1 Autophagy mechanism*

Autophagy operates through several evolutionarily conserved pathways that mediate the lysosomal degradation and recycling of intracellular components, including misfolded proteins, damaged organelles, and invading pathogens (103). While autophagy occurs constitutively at basal levels to maintain cellular homeostasis, it is markedly upregulated in response to cellular stressors such as hypoxia, nutrient deprivation, or exposure to cytotoxic agents. In mammalian cells, three distinct types of autophagy have been characterized: macroautophagy, microautophagy, and chaperone-mediated autophagy (**CMA**). All converge on the lysosome for degradation and recycling of cargo. Macroautophagy and microautophagy are conserved in eukaryotic cells, whereas CMA is restricted to mammalian cells.

Macroautophagy is characterized by the formation of double-membrane vesicles called autophagosomes, which sequester cytoplasmic material and deliver it to the acidic lysosome for degradation. In contrast, microautophagy involves the direct engulfment of cytoplasmic components by lysosomal membrane invagination, bypassing the need for autophagosomes. CMA is distinguished by the presence of a specific pentapeptide motif (Lys-Phe-Glu-Arg-Gln) in substrate proteins, which targets them for lysosomal degradation via recognition by heat shock

cognate protein 70 (**Hsc70**) and interaction with lysosomal-associated membrane protein 2A (**LAMP2A**) (103).

Of these, macroautophagy (hereafter referred to simply as autophagy) is the most extensively studied and will be the focus of this section. Autophagy is regulated by a set of proteins encoded by approximately 30 autophagy-related genes (**ATGs**), including components that form the ULK1 complex, the phosphoinositide 3-kinase (**PI3K**) complex, and various ubiquitin-like conjugation systems (**Figure 1.4**)(103). Central to autophagy regulation is the mechanistic target of rapamycin (**mTOR**), which suppresses the process by inhibiting the kinase activity of unc-51-like kinase (**ULK1**), thereby blocking autophagy induction (103). Under cellular stress, autophagy is initiated via activation of 5'-AMP-activated protein kinase (**AMPK**), which phosphorylates ULK1. This phosphorylation triggers a conformational change in ULK1, enabling its interaction with FIP200, ATG13, and ATG101 to form the ULK1 complex. Activated ULK1 then phosphorylates its own complex components, enhancing their activity and directing the complex to the phagophore assembly site (**PAS**) (104-106).

AMPK also phosphorylates Beclin-1, leading to the formation of the class III PI3K-VPS34 complex, which contains Beclin-1, VPS34, VPS15, and ATG14L (107, 108). These functional units – the ULK1 complex, PI3K complex, ATG12-conjugation system, and microtubule-associated protein 1A/1B-light chain 3B (hereafter referred to as **LC3β**)-conjugation system – are recruited to the PAS to drive nucleation, the early stage of phagophore formation (109-111).

In the ATG12-mediated pathway, ATG12 is activated by ATG7 and conjugated to ATG5. ATG16L stabilizes the ATG12-ATG5 conjugate to form the ATG12-ATG5-ATg16L complex, which is essential for the LC3 conjugation system. In parallel, pro-LC3 (cytosolic form) is cleaved at its C-terminal by ATG4B to generate LC3β-I (112, 113). LC3βI is then lipidated with

phosphatidylethanolamine by ATG7 and ATG3, producing LC3βII, which embeds into the growing autophagosomal membrane (114, 115).

Finally, lysosome-associated membrane protein 2 (**LAMP2**), soluble NSF attachment protein receptors (**SNAREs**), and the homotypic fusion and protein sorting (**HOPS**) complex mediate fusion of the autophagosome with the lysosome. Within the resulting autolysosome, enzymes such as proteases, acid phosphatases, lipases, and nucleases degrade the autophagosome cargo (116).

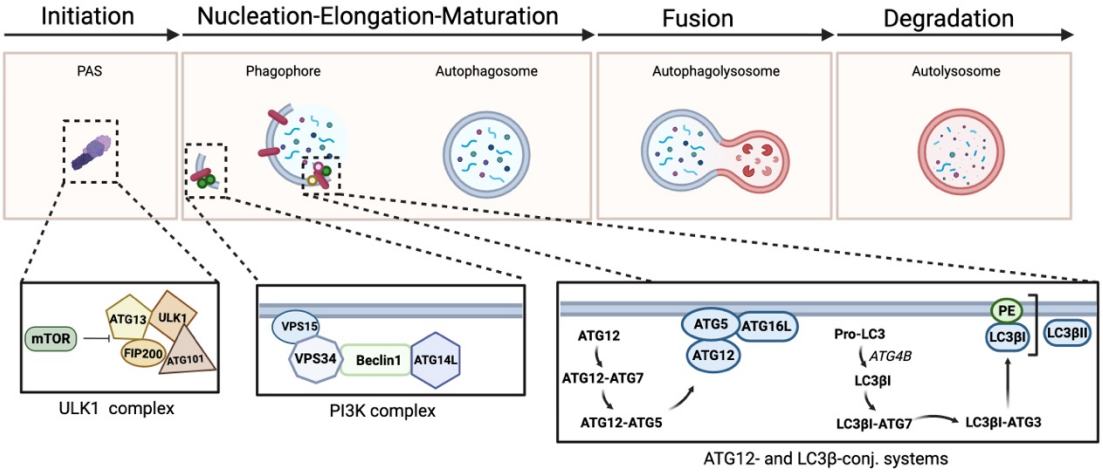


**Figure 1.4. Autophagy signalling pathway and autophagosome formation.** Autophagy is primarily regulated by mTOR, which inhibits ULK and blocks autophagy induction. Under cellular stress, autophagy is initiated by AMPK overexpression, which phosphorylates ULK1 to promote the formation of the ULK1 complex and the PAS. AMPK also phosphorylates Beclin-1, facilitating the formation of the PI3K complex. The ULK1 complex, PI3K complex, and the ATG12- and LC3-conjugation systems are recruited to the PAS, where they participate in autophagosome formation. Finally, degradation of the sequestered cellular contents occurs after fusion of the autophagosome with the lysosome.

### *1.1.3.2 Tumour-suppressing and tumour-promoting autophagy in cancer*

Autophagy has a controversial role in cancer because it can promote or antagonize tumour progression. Tumour-suppressing autophagy protects against tumour development by maintaining cellular homeostasis primarily through the removal of damaged cell organelles and proteins, and by mitigating oxidative stress (117, 118). Tumour-promoting autophagy can contribute to cancer progression by supplying cells with energy and metabolic substrates necessary for rapid growth and proliferation. Autophagy also acts as a critical adaptive response to cellular stressors such as hypoxia, nutrient deprivation, and cytotoxic challenges (119, 120). Defects in autophagic machinery or alterations in ATGs have been implicated in various human diseases, including neurodegenerative disorders, lysosomal storage diseases, and multiple types of cancer (121, 122).

Different studies highlight the function of Beclin 1 as a tumour suppressor, with the deletion of the BECN1 gene observed in human breast, prostate, and ovarian cancers (118, 123, 124). Takamura et al. investigated the role of ATG5 and ATG7 in the progression of liver cancers. They used knockout mice models to show that the deletion of ATG5 and ATG7 promotes liver tumourigenesis through accumulation of damaged mitochondria and oxidative stress (125).

Autophagy is believed to have an essential role in colorectal cancer progression. The co-localization of p62 with CSC marker doublecortin-like kinase 1 (**dckl1**) contributes to tumour growth and progression by impeding dckl1's elimination during colon cancer development (126). Autophagy inhibitors, such as 3-methyladenine (**3-MA**), have been shown to increase the sensitivity of hepatocellular carcinoma to chemotherapy, demonstrating autophagy's role in therapy resistance (127). Contrastingly, an anti-tumour compound known as dihydroartemisinic, stimulates tumour-suppressing autophagy in cervical and endometrial cancers (128).

Autophagy's dual role as both a tumour-promoting and tumour-suppressing factor in cancers makes it a complex and debated topic, with its ultimate function being highly context-dependent. This complexity exemplifies autophagy's "double-edged sword" nature in tumours (129, 130). Autophagy's role in tumour development and chemotherapy response remains a significant focus of cancer research. Many studies confirm that, in established tumours deprived of nutrients or oxygen, autophagy promotes tumour growth and can undermine the efficacy of chemotherapeutic agents such as TMZ (131-133). Thus, inhibiting autophagy is intuitively considered a potential strategy to improve treatment efficacy. As previously mentioned, a significant challenge in the standard of care for GBM is that, in most cases, patients develop mechanisms of resistance against TMZ, which contributes to low OS and poor prognosis. Increasing studies demonstrate that TMZ treatment may induce autophagy. However, the mechanisms involved are not fully understood. Elucidating how autophagy is involved in GBM tumour progression is critical to developing therapeutic strategies to improve patient outcomes.

#### *1.1.3.3 Survival autophagy and its role in TMZ-resistant GBM*

DNA alkylating drugs, like TMZ, are integral to treating patients with GBM. However, activation of intracellular pathways can lead to the development of resistance via circumventing cell death mechanisms (134, 135). Several studies demonstrate TMZ's ability to induce autophagy – which has been suggested as a mechanism of chemoresistance to alkylating drugs in GBM (135-137). Autophagy has been shown to have a pro-survival role in tumours, where it is further induced in response to imposed stress, such as limited nutrient availability, hypoxic environments, and DNA damage. Understanding how autophagy is involved in GBM tumour development and its response to TMZ has been a significant focus of basic science research. Liu et al. demonstrated

that autophagy was induced following treatment of GBM cells with cisplatin, a platinum-based chemotherapy medication used to treat several cancers. When the retinoblastoma protein (**pRB**), a key regulator of cell cycle and survival, was knocked down, GBM cells became more dependent on autophagy for survival. Inhibiting autophagy under these conditions sensitized the cells to apoptosis, indicating that autophagy helps protect pRB-deficient GBM cells from chemotherapy-induced cell death (138).

A study using GBM xenografts investigated the effects of blocking autophagy with chloroquine, a drug that prevents autophagosomes from fusing with lysosomes – a crucial step in the autophagy process. Treatment with bevacizumab caused hypoxia in tumour cells, which triggered autophagy, helping the cells survive and resist chemotherapy. However, when chloroquine was combined with bevacizumab, this protective autophagy was blocked, resulting in reduced tumour growth reduced tumour growth (139). These findings suggest that inhibiting autophagy can make GBM tumours more sensitive to treatment and help overcome drug resistance. Wojton et al. hypothesized that autophagy may prevent tumour formation in early stages but later supports tumour growth and resistance to chemotherapy in GBM (140). Supporting this, Kanzawa et al. found that blocking autophagy early with class III PI3K inhibitors like 3-MA reduced the effectiveness of TMZ, whereas blocking autophagy at a later stage with bafilomycin A1 (**BafA1**) increased TMZ's ability to kill tumour cells (141).

These findings highlight autophagy as a promising target to improve the efficacy of drugs such as bevacizumab and TMZ, which induce autophagy as a protective response. A clearer understanding of autophagy's role in GBM progression and TMZ resistance will guide the development of therapies that manipulate autophagy to improve patient outcomes.

Mitochondria play a significant role in regulating cellular stress responses, including apoptosis. Damaged mitochondria are typically removed by mitophagy, the selective degradation of mitochondria by autophagy, which counteracts cell death. B-cell lymphoma-2 (**BCL-2**) family proteins are closely involved in these processes as they interact with pro- and anti-apoptotic proteins at the mitochondria to determine their fate. The following section will detail how BCL-2 family proteins are understood to be involved in these cell stress responses.

### *1.1.4 BCL-2 protein family*

BCL-2 family proteins are critical regulators of intrinsic (mitochondria-mediated) apoptosis and are characterized by the presence of one or more conserved regions known as BCL-2 homology (**BH**) domains (142, 143). Most BCL-2 family members also contain a hydrophobic transmembrane (**TM**) domain that anchors them to membranous organelles such as mitochondria (144, 145). The BH domains mediate interactions among family members and determine their pro- or anti-apoptotic function.

The BCL-2 family is broadly divided into three groups: multi-domain anti-apoptotic proteins, multi-domain pro-apoptotic (pore-forming) proteins, and BH3-only pro-apoptotic proteins (146). The anti-apoptotic subfamily includes proteins containing four BH domains (BH1-4), with the BH4 domain being essential for their anti-apoptotic function (147). The pore-forming pro-apoptotic proteins, such as BAX and BAK, possess BH1-3 domains, while the BH3-only pro-apoptotic proteins contain only the BH3 domain (148, 149). BH3-only pro-apoptotic proteins activate BAX or BAK either directly or by inhibiting anti-apoptotic members, leading to mitochondrial outer membrane permeabilization (**MOMP**) cytochrome c release, which triggers

apoptosis (150). Anti-apoptotic members prevent apoptosis by sequestering and inhibiting pro-apoptotic proteins, effectively balancing cell survival and death.

Pro-apoptotic 'activator' proteins are upregulated in response to cellular stress or damage. Anti-apoptotic proteins can bind and neutralize these activators, preventing apoptosis. However, if anti-apoptotic proteins are insufficient to sequester activators, pore-forming proteins promote apoptosis (151, 152). BH3-only 'sensitizer' proteins, also induced by stress, do not directly activate BAX and BAK but can release sequestered activators by binding to anti-apoptotic proteins, tipping the balance towards apoptosis (146). Thus, tight regulation of the expression and interaction of BCL-2 family members is critical in determining cell fate.

Many isoforms of the BCL-2 protein family exist (**Table 1.1**). The following sections will focus primarily on BCL-2-like protein 13 (**BCL2L13**), a recently identified member that exhibits both pro- and anti-apoptotic functions (149).

**Table 1.1.** Classification of BCL-2 family proteins by apoptotic activity and domain composition.

| Subfamily | Activity | BH Domain | TM Domain | Members |
|---|---|---|---|---|
| Anti-apoptotic | Anti-apoptotic | BH1-4 | Yes | BCL-2<br>BCL-$X_L$<br>BCL-W<br>BCL-B<br>MCL-1 |
| Pore-forming | Pro-apoptotic | BH1-3 | Yes | BAX<br>BAK<br>BOK |
| BH3-only | Pro-apoptotic | BH3 | No | BNIP3L/Nix[†]<br>BIM<br>BIK<br>HRK<br>NIP3 |
| | | BH3 | No | Noxa<br>BAD<br>BID |

| | | | | |
|---|---|---|---|---|
| | | | | PUMA<br>BMF<br>MAP-1 |
| Other | Mixed | BH1-4<br>(+BHNo) | Yes | BCL2L13 |

† BNIP3L/Nix is an exception as it has a TM domain, but most BH-3 only proteins lack TM domains.

#### *1.1.4.1 BCL2L13 structure, function, and tissue distribution*

BCL2L13, also referred to as BCL-rambo, is a novel member of the BCL-2 protein family. It contains all four conserved BH domains, a unique c-terminal 250-amino acid region called the BHNo domain, and a TM domain (153). Initial studies found that overexpression of BCL2L13 induced apoptosis in mammalian cells independently of its conserved BH domains. Instead, apoptosis was mediated by its BHNo and TM domains (153). Another study showed that the TM domain is essential for BCL2L13's pro-apoptotic activity, as its deletion abolished the protein's ability to induce cell death (154). The TM domain also enables BCL2L13 to localize to the outer membrane of mitochondria (153, 155).

More recently, BCL2L13 was shown to have anti-apoptotic activity in SF767 human GBM cells. Here, the BHNo domain interacted with ceramide synthases 2 and 6, preventing their dimerization and thereby inhibiting pro-apoptotic BAX activity (156). These findings suggest that BCL2L13 has dual, context-dependent functions, acting as either a pro- or anti-apoptotic protein.

Subcellular proteome mapping revealed that BCL2L13 is most often located in the outer mitochondrial membrane (157). Using an integrated omics approach, Uhlén et al. found that BCL2L13 protein expression is highest in the cerebral cortex, oral mucosa, and skeletal muscle (158). BCL2L13 has been implicated in physiological processes such as growth and development (via its its pro-apoptotic function) and energy metabolism (through mitochondrial regulation) (159,

160). The next section will describe experimental model systems used to investigate the role of BCL2L13.

#### *1.1.4.2 Genetic models available*

Early studies using human embryonic kidney 293T cells showed that overexpression of BCL2L13 localized the protein to mitochondria and induced apoptosis (153). Subsequent work ectopically expressed human BCL2L13 in *Drosophila melanogaster*, where it also localized to mitochondria in Schneider 2 cells. Full-length BCL2L13 induced apoptosis, whereas a variant lacking the C-terminal transmembrane domain did not (161).

BCL2L13 is the functional mammalian homolog of ATG32, a mitochondrial receptor essential for mitophagy in yeast (162). To determine which ATGs are required for BCL2L13-mediated mitophagy, Murakawa et al. expressed BCL2L13 in *Saccharomyces cerevisiae* strains individually lacking different ATGs. Mitophagy activity was assessed by monitoring degradation of the fluorescent reporter mCherry. The results showed that BCL2L13 requires ATG1, 13, 17, 29, and 31 – but not ATG11 – to induce mitophagy, indicating that the machinery driving ATG32-dependent mitophagy in yeast is only partially conserved in mammals. Notably, BCL2L13 was able to compensate for the absence of ATG32 under nitrogen starvation by recruiting the mammalian ULK1 complex, which restored mitochondrial degradation in ATG32-deficient yeast. In contrast, cells lacking both ATG32 and BCL2L13 showed no evidence of mitophagy. These findings reveal that BCL2L13 retains a conserved mitophagy-inducing capacity across species, while employing partially distinct molecular components, making it a valuable model for studying mitochondrial quality control mechanisms (163).

More recently, Drosophila models have been used to investigate the regulation of BCL2L13 in apoptosis, mitochondrial fragmentation, and mitophagy. This work identified phosphoglycerate mutase family member 5 (PGAM5) as an interacting partner that promotes BCL2L13-dependent apoptosis but inhibits its role in mitophagy (164). Collectively, studies in human cell lines, *Drosophila*, and yeast have established BCL2L13 as a conserved mitochondrial protein capable of inducing apoptosis and mediating mitophagy, while revealing both shared and distinct molecular requirements across species. These genetic studies set the stage for examining BCL2L13's specific contributions to autophagy and mitophagy.

#### *1.1.4.3 BCL2L13: Role in autophagy and mitophagy*

Autophagy is a fundamental cellular process that sequesters and degrades cytosolic components, breaking down macromolecules into their constituent part to maintain energetic demands and metabolic homeostasis. It's ability to catabolize damaged, aging, or excess organelles is central to cellular maintenance and prevents accumulation of cellular damage (165, 166). Mitochondria, beyond being the primary energy producers of eukaryotic cells, also play key roles in tissue homeostasis and aging, influencing cellular senescence, stem cell function, apoptosis, and gene expression (167-171). Maintaining healthy mitochondria – and, by extension, metabolic homeostasis – depends largely on mitophagy, the selective autophagic degradation of damaged or dysfunctional mitochondria (172, 173).

Two well-characterized mitophagy pathways exist: parkin-mediated and non-parkin-mediated. In healthy mitochondria, phosphatase and tensin homolog (PTEN)-induced kinase 1 (**PINK1**) is cleaved and degraded. In dysfunctional mitochondria, which are often depolarized or contain misfolded protein aggregates, PINK1 accumulates on the outer mitochondrial membrane.

There, it phosphorylates ubiquitin on mitochondrial proteins – the signal that marks mitochondria for degradation – and phosphorylates Parkin, activating its ligase activity to amplify ubiquination and the phosphor-ubiquitin signal (174, 175).

The non-parkin-mediated pathway relies on mitochondrial receptors such as BCL2 interacting protein 3 (**BNIP3**), BCL2 interacting protein 3 like (**BNIP3L/Nix**), and BCL2L13. These receptors contain conserved regions that interact with LC3β, recruiting mitochondria to the phagophore (173, 176). Specifically, BCL2L13 binds directly to the LC3/GABARAP family of proteins via an LC3-interacting region (**LIR**), demonstrating its function as a mitophagy receptor (177, 178) (**Figure 1.6**).

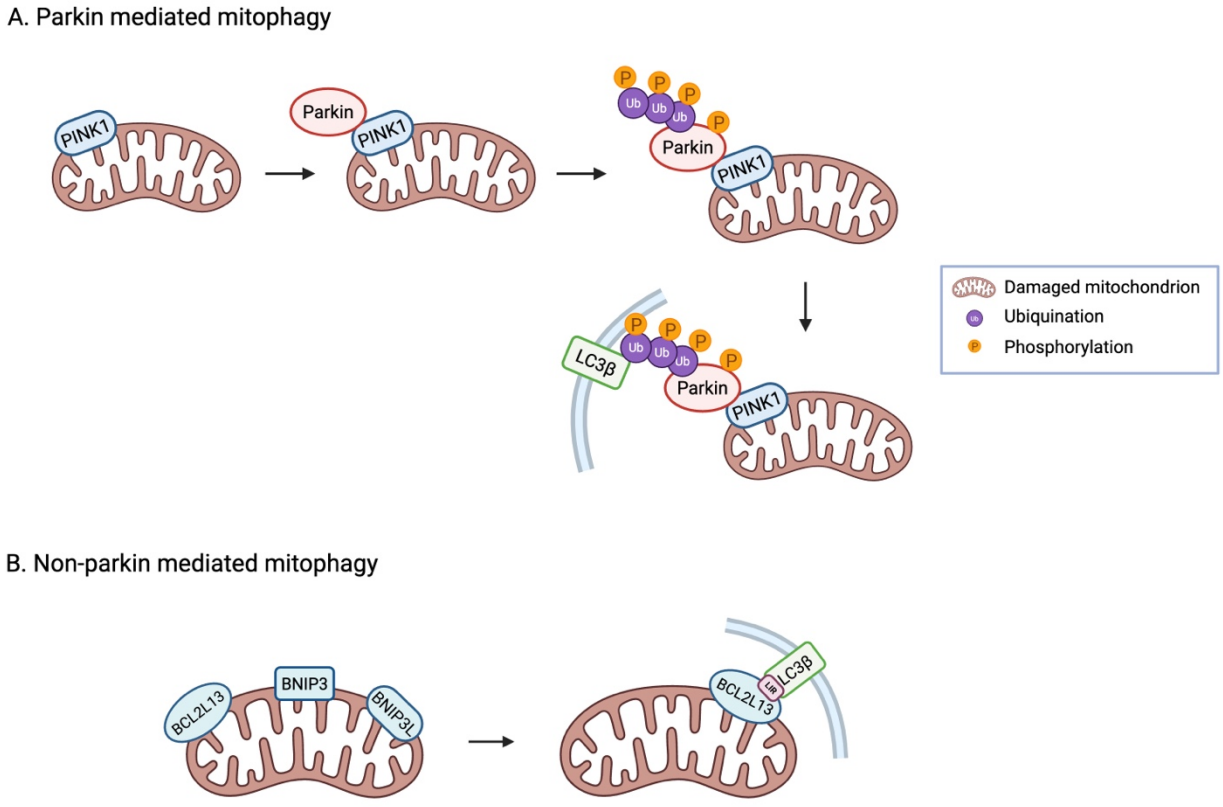


**Figure 1.5**. **Mechanisms of parkin-dependent and parkin-independent mitophagy (A)** Parkin-mediated mitophagy: PINK1 accumulates on damaged mitochondria and phosphorylates both

ubiquitin (Ub) and parkin, activating parkin's ligase activity and flagging the mitochondria for recruitment to the autophagosome. **(B)** Non-parkin mediated mitophagy: outer mitochondrial membrane receptors, including BCL2L13, interact with LC3β via their LIR, targeting mitochondria to the autophagosome.

#### *1.1.4.4 BCL2L13: Role in cancer and other known pathologies*

BCL2L13 regulates mitophagy, cell growth, development, and energy metabolism. Dysregulation of these processes can contribute to various pathologies, including neurodegenerative diseases, cardiovascular diseases, infections, and cancer. Neurons, due to their high energy demand, are particularly sensitive to mitochondrial damage. Consequently, impaired mitophagy has been linked to Parkinson's and Alzheimer's diseases (179, 180). Mutations in Parkin and PINK1 cause the autosomal recessive form of Parkinson's disease (181, 182). In Alzheimer's disease, neurons exhibit mitochondrial dysfunction disrupted mitophagy, leading to accumulation of damaged mitochondria (183-185).

BCL2L13 also plays a role in cardiovascular disease. For example, miR-484 expression is down-regulated in neurons subjected to oxygen-glucose deprivation (**OGD**), and its upregulation alleviates cerebral ischemia/reperfusion injury by inhibiting apoptosis via post-transcriptional silencing of BCL2L13 (186). Additionally, phosphorylation of PINK1 by AMPKα2 is critical for proper mitophagy and preventing heart failure progression, while the dominant AMPKα isoform in the heart is AMPKα1 (187).

BCL2L13 is implicated in bacterial infections as well. Specifically, *Legionella pneumophila* expresses a virulence factor, anhydromevalonyl-CoA transferase, that counteracts

BNIP3 and BCL2L13 activity in lung macrophages, preventing apoptosis and enabling bacterial replication (188).

In cancer, BCL2L13 continues to be extensively studied. It is elevated in childhood acute lymphoblastic leukemia (**ALL**) and involved in L-asparaginase resistance, serving as an adverse prognostic factor (189). Its expression is higher in proximal versus distal gastric cancer, suggesting a role as a disease progression marker. Conversely, downregulation of BCL2L13 correlates with poor prognosis in clear and papillary renal cell carcinoma (190). These contrasting findings underscore the complexity of BCL2L13's role in cell signaling across different contexts. From a mitophagy perspective, one might hypothesize that inhibiting mitophagy could benefit cancer therapy, whereas activating it might support cell survival by maintaining mitochondrial homeostasis. However, cancer cells' adaptive nature and resilience suggest that the relationship is not this straightforward.

#### *1.1.4.5 BCL2L13: Role in glioblastoma*

BCL2L13 is expressed at higher levels in GBM, where it displays complex functional roles. Beyond promoting apoptosis and mediating the selective mitochondria degradation, BCL2L13 also exhibits anti-apoptotic functions. Upregulation of BCL2L13 blocks caspase activation, whereas its knockdown increases caspase activation. Jensen et al. showed that this anti-apoptotic effect is mediated through lipid synthesis. Specifically, BCL2L13 uses its BHNo domain to bind pro-apoptotic ceramide synthases 2 and 6 (**CerS2/6**), preventing their homo- and heterodimerization and inhibiting apoptosis upstream of Bax activation and MOMP. Furthermore, CerS2/6 activity inversely correlates with BCL2L13 in GBM tumours (156). Because effective

chemotherapeutic agents such as TMZ rely on inducing apoptosis, understanding lipid profiles in GBM is critical to addressing chemoresistance.

## *1.2 Lipidomics*

### *1.2.1 Lipids*

Lipids are a major class of biomolecules in cells, characterized by a wide structural diversity that underlies their numerous functions. Primarily, lipids are critical for forming and maintaining the structure and fluidity of biological membranes, which in turn influence membrane dynamics such as fission, fusion, and budding – processes essential for cell division and autophagy (191, 192). The fluid nature of membranes also facilitates the aggregation and dispersion of membrane proteins, modulating their activity and interactions (193).

Beyond structural roles, lipids serve as high-energy storage molecules due to their relatively reduced state. They are also involved in signalling: hydrolysis of polar headgroups can generate second messengers, metabolism of hydrocarbon tails can produce lipid messengers, and lipids can regulate protein function and localization. Additionally, lipids act as precursors for the synthesis of signalling molecules known as lipid mediators (194-200).

Fatty acids (**FAs**) are one of the primary lipids in eukaryotic cells (201). FAs are aliphatic molecules with both hydrophobic and hydrophilic regions. They vary in carbon chain length, degree and position of unsaturation, and polar head groups. FAs are the building blocks of more complex lipids, including phospholipids and sphingolipids (202).

Phospholipids consist of a glycerol backbone attached to two fatty acid chains and a polar phosphate head group, enabling them to form the lipid bilayers essential for membrane integrity and dynamics. Sphingolipids, in contrast, contain a sphingosine backbone linked to both a polar

head group and an acyl group, often a fatty acid. The simplest sphingolipid, ceramide, has only a hydrogen as its polar head group (202). These structural differences contribute to the diverse roles of phospholipids and sphingolipids in membrane organization, signaling, and cellular processes. Among sphingolipids, ceramides are particularly important as bioactive molecules that connect lipid structure to key cellular functions including apoptosis, stress responses, and metabolic regulation. The following section will focus on ceramides, their synthesis, metabolism, and regulation in mammalian cells.

### *1.2.2 Ceramides*

Ceramide is an essential intermediate in sphingolipid metabolism in mammalian cells (203). Ceramides are bioactive sphingolipids that regulate numerous cellular processes, including cell cycle arrest, apoptosis, senescence, and stress responses (204, 205). Ceramides of different acyl chain lengths are primarily synthesized by ceramide synthases (**CerS**). Six distinct CerS enzymes are encoded by separate genes, each with specificity for particular acyl-CoA chain lengths, producing ceramide species with distinct, but overlapping, acyl chains (206, 207).

Structurally, ceramide comprises a sphingosine backbone linked to a fatty acid via an amide bond (208, 209). Ceramides serve as precursors for more complex sphingolipids, including glucosylceramide, ceramide-1-phosphate, sphingomyelin, and galactosylceramide, and can also be generated through the catabolism of these complex sphingolipids. Figure 7 illustrates major pathways of ceramide production in the cell.

Endogenous ceramides are synthesized *de novo* in the endoplasmic reticulum, beginning with the condensation of L-serine and palmitoyl-CoA, followed by several enzymatic reactions that lead to the production of ceramide (210). Ceramide can also be generated through the salvage pathway, where it is hydrolyzed to sphingosine and then acylated back to ceramide (211).

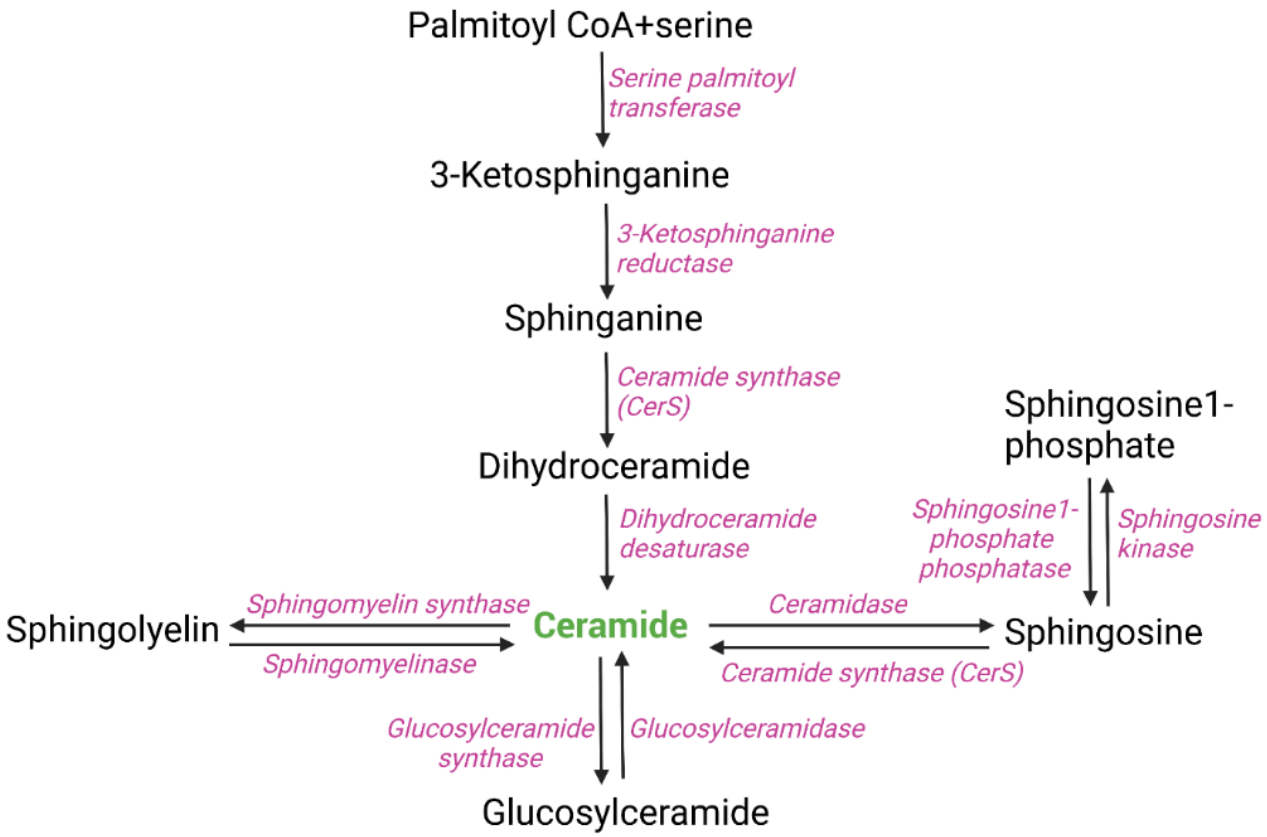


**Figure 1.6**. **Major pathways of ceramide metabolism.** Ceramide occupies a central position in sphingolipid metabolism and is generated through de novo synthesis from palmitoyl-CoA and serine. Ceramide can be interconverted with sphingomyelin, glucosylceramide, sphingosine, and sphingosign-1-phosphate through the actions of key metabolic enzymes, which are shown in pink.

### *1.2.2.1 Ceramide synthase activity regulation*

The mechanisms that regulate CerS activity are not yet fully understood. Recent studies suggest that the dimerization of different CerS enzymes may play a role in regulating ceramide synthesis. In this context, the activity of individual CerS enzymes in homo- or heterodimers may depend on, and be modulated by, the other monomers, indicating that dimerization could serve as a regulatory mechanism (212). CerS monomers and dimers exist in equilibrium in the endoplasmic

reticulum, and the processes of dimerization or dissociation may contribute to rapid and efficient regulation of activity (212).

Post-translational modifications of CerS are also implicated in regulation, although the mechanisms remain incompletely elucidated. Evidence suggests that CerS phosphorylation can influence activity; for example, increased *de novo* ceramide synthesis has been linked to activation of protein kinase C and subsequent upregulation of CerS5 activity (213, 214). Additionally, high-performance mass spectrometry has shown that CerS can be phosphorylated and glycosylated, supporting the idea that rapid changes in CerS activity may occur through post-translational modification (215-218).

#### *1.2.2.2 Ceramides' role in regulating apoptosis*

Apoptosis is a form of programmed cell death characterized by distinct morphological features and biochemical mechanisms (219, 220). Two main types of apoptosis exist: intrinsic and extrinsic. The loss of integrity of the mitochondrial outer membrane is a crucial determinant of intrinsic pathway execution. Different proteins contribute to apoptosis initiation and subsequent MOMP by forming pores (221). For example, pro-apoptotic members of the BCL-2 protein family, BAX and BAK, are key regulators (222, 223).

Ceramides also form channels in the mitochondrial outer membrane (224-226). Although most studies link ceramides' role in apoptosis to channel formation and MOMP, they also regulate apoptosis through interactions with both anti- and pro-apoptotic BCL-2 family proteins (227, 228). Ceramide channel formation depends on the specific structure of ceramides, including the degree and location of unsaturation. Recent studies demonstrate that different ceramides form channels of varying sizes and numbers in isolated mitochondria (228). Overexpression of ceramide

synthases in HEK cells increases production of specific ceramides (229). Furthermore, the addition of very-long chain ceramides can interfere with C16-ceramide-induced channel formation (228).

Ceramides also regulate apoptosis through anti-apoptotic BCL-2 family proteins, BCL-2 and BCL-xL. BCL-2 phosphorylation is required for its anti-apoptotic function (230). Ceramides may influence BCL-2 phosphorylation and function by activating protein phosphatase 2A, which removes the phosphate group from BCL-2. The fatty acid chain lengths of ceramides are important for regulating ceramide channels in the presence of BCL-xL (231). BCL-xL prevents ceramide channels formation, and hence ceramide-induced apoptosis (232). This prevention is less effective when ceramide has truncated fatty acyl chains, suggesting a critical role for acyl chain length in binding to BCL-xL. One study found that BCL-xL inhibits channel formation by C17-, C18-, and C20-ceramides (233).

Finally, ceramides also act through pro-apoptotic BCL-2 proteins BAX and BAK. BAX plays a central role in maintaining mitochondrial outer membrane integrity, directly participating in pore formation and the release of cytochrome c, a key apoptotic mediator (234-238). Evidence suggests that BAX and ceramide synergistically promote MOMP (239). Loss of BAX inhibits the C2-ceramide-induced apoptosis in colorectal cancer cells, highlighting the dependence of ceramide-induced apoptosis on BAX [98,99]. Recently, cell-permeable ceramides have been shown to induce conformational changes in the N-terminus of BAX, further promoting apoptosis (240).

#### *1.2.2.3 Ceramides role in regulating apoptosis in cancer*

Owing to their regulatory role in apoptosis, CerS and ceramides have been implicated in the pathogenesis of various cancers. For example, CerS1 overexpression sensitizes human

embryonic kidney cells to multiple chemotherapeutic agents such as carboplatin, cisplatin, vincristine, and doxorubicin. In contrast, CerS5 increases sensitivity only to doxorubicin and vincristine, whereas CerS4 appears to have no impact on drug responsiveness (241). Similarly, CerS1 plays a key role in doxorubicin-induced, caspase-dependent apoptosis in head and neck squamous cell carcinoma (**HNSCC**) (242). In this context, silencing CerS1 expression with siRNA reduced apoptosis by approximately 50%, accompanied by diminished activation of caspase-3 and caspase-9. Liquid chromatography-mass spectroscopy analysis further revealed that only C18-ceramide, the principle product of CerS1, accumulated following doxorubicin treatment. These findings identify C18-ceramide as a central mediator of doxorubicin-induced apoptosis in HNSCC (242). The CD95 (Fas) death receptor and its ligand CD95L act together to induce apoptosis (243). CerS6 has been shown to modulate the activation of CD95 and the subsequent induction of apoptosis (244). The tumour-necrosis-factor related apoptosis-induing ligand (**TRAIL**), another member of the tumour-necrosis-factor (**TNF**) superfamily, induces apoptosis through its death receptors DR4 and DR5, initiating caspase-8 and caspase-10 activation (245, 246). Normal cells typically resist TRAIL-mediated apoptosis because of their low receptor expression (247). In colon adenocarcinoma models, CerS6 overexpression enhanced CD95 activation and apoptosis, whereas knockdown of CerS6 abolished these effects (248).

In breast cancer, CerS2 and CerS6 levels are elevated in nearly half of tumour samples relative to normal tissues, suggesting that their products – C16-ceramide and C24-ceramide – may promote survival rather than apoptosis (249). In contrast, within GBM, CerS2 and CerS6 overexpression enhances caspase activation, while silencing their expression suppresses it (156, 250). Notably, low ceramide levels are associated with higher-grade gliomas and increased GBM cell viability (156).

#### *1.2.2.4 Ceramides' role in regulating autophagy*

Building on their established role in apoptosis, ceramides also regulate autophagic pathways that determine cellular fate by influencing both survival and death. Autophagy is a highly conserved recycling mechanism that targets misfolded proteins or damaged organelles for lysosome degradation (251). While the primary function of autophagy is cell survival, dysregulated or prolonged autophagy activation can result in cell death (252, 253). Ceramides have been implicated in autophagy regulation (254). Most studies describe ceramide involvement primarily during the initiation and degradation phases of autophagy, with limited research on their role in elongation. Class I PI3K and Akt are inhibitors of autophagy. C2 or C6-ceramide can activate protein phosphatase 2A, blocking Akt signalling, thereby inducing autophagy in HT-29 (human colon) and MCF-7 (breast cancer) cell lines (255, 256). Edinger et al. showed that ceramides rapidly and significantly downregulate amino acid transporter proteins, inhibiting mTOR activity and inducing autophagy in a protein phosphatase 1 and protein phosphatase 2A-dependent manner (257). Similarly, C2-ceramide inhibited the expression of a nutrient transporter, resulting in starvation and AMPK-dependent autophagy in murine prolymphocytic cells (258). Another study demonstrated that exogenous C2-ceramide led to higher Beclin1 expression and subsequent induction of autophagy (255).

At the molecular level, autophagy is regulated at multiple stages, and ceramides have been implicated in several initiation mechanisms, such as autophagy induction and pre-autophagosomal formation. For instance, it has been shown that ceramide induces JNK activation, leading to BCL-2 phosphorylation (259). Phosphorylated BCL-2 results in its dissociation from Beclin1, removing its inhibitory role on autophagy. Treatments that elevate the levels of long-chain ceramides potentiate this effect. Another study demonstrated that treating nasopharyngeal and hepatocellular

carcinoma cells with ceramide potentiates Beclin1 expression, thus inducing autophagy (260). Concerning pre-autophagosomal formation, sphingosine-1-phosphate (**S1P**) may influence the formation of autophagosomes via LC3β lipidation and thus anchoring to the autophagosomal membrane. Additionally, Sphk (an enzyme that catalyzes the phosphorylation of sphingosine to S1P) increases S1P levels and has been shown to enhance preautophagosomal formation in primary neurons significantly, enhancing overall autophagosome formation (261). Sentelle et al. provided evidence that C18-pyridinium ceramide treatment, or endogenous C18-ceramide by CerS1 expression, mediated autophagic cell death independent of apoptosis. Instead, C18-ceramide induced lethal autophagy via LC3βII lipidation and selective targeting of mitochondria through direct interaction between ceramide and LC3βII upon Drp1-dependent mitochondrial fission (262). The association between mitochondria and ER membranes can serve as a membrane source for phagophore formation, whereby lipid rafts play a key role. Ganglioside GD3 is a downstream product of ceramides and a component of lipid rafts that binds to the Beclin1 complex (263, 264). In this way, GD3 helps to recruit components necessary for autophagosomal formation. Like other lipid rafts, GD3 also plays a role in membrane fluidity and curvature (193).

Ceramides have also been implicated in regulating autophagy during fusion, degradation, and overall autophagic flux, but to a very limited extent. C1P synthesis was recently reported to induce $Ca^{2+}$-dependent lysosomal fusion, leading to an increase in vesicle fusion. Levels of C1P rose significantly during phagocytosis, suggesting that C1P might be involved in autophagosome-lysosome fusion (265). Some reports show C18-ceramide's involvement in regulation at the degradation step of autophagy, where it can induce the selective targeting of mitochondria (266, 267). In addition to their role in regulating degradation in autophagy, ceramides also serve as autophagic substrates (268). It has been shown that the fusion step of autophagy depends on lipid

composition in the cell, such as ceramide levels (269). Another study demonstrated myristate's ability to enhance autophagic flux in a C14-ceramide and CerS5-dependent manner, indicating a role for ceramide in modulating autophagy flux (270).

Collectively, these findings highlight ceramides as multifaceted regulators of autophagy, acting at both the initiation and degradation stages to influence cancer cell fate through their effects on organelle dynamics, signalling, and membrane composition.

#### *1.2.2.5 Ceramides role in regulating autophagy in cancer*

As in the case of apoptosis, different studies implicate CerS and their products in the modulation of cancer due to their regulatory role in autophagy. However, these studies are mainly context-dependent, influenced by factors such as fatty acid chain length, subcellular location, the presence or absence of downstream targets, and the type of cancer being investigated.

In HT-29 colon carcinoma cells under starvation, BCL-2 overexpression inhibits autophagy, while C2 and C6-ceramide trigger autophagy. Specifically, C2-ceramide increased BNIP3 accumulation (271). The dissociation of the Beclin1:Bcl-2 complex is independent of BCL-2 phosphorylation, giving rise to two likely mechanisms through which ceramide dissociates this complex (272). The first is via JNK1 activation and subsequent BCL-2 phosphorylation, and the second is through an accumulation of BNIP3, which interferes with the Beclin1:BCL-2 complex.

Dbaibo et al. described that arsenic trioxide ($As_2O_3$) induces cytotoxic accumulation of overall ceramide in leukemia cells (HuT-102, C91-PI, and MT-2 cells) through inhibition of glucosylceramide synthase (273). It was demonstrated that $As_2O_3$ induced autophagic cell death in these cells, which was associated with increased Beclin1 expression. This lethal autophagy was inhibited when cells were treated with 3-MA (274). C2-ceramide has also been shown to trigger

autophagic cell death in malignant glioma cell lines (U373-MG and T98G) through disruption of mitochondrial membrane potential and BNIP3 activation (271). In leukemia cells (HL-60) as well as Chinese hamster ovary cells (**CHO**), ceramide-activated protein phosphatases inhibit mTOR, thereby inducing lethal autophagy (275). In another study that looked at ceramide's role in regulating autophagy in U251 and A172 brain cancer cells, CerS1 overexpression led to lethal autophagy (LC3B lipidation and P62 degradation) via inhibition of the PI3K/AKT pathway. Both CerS1 overexpression and exogenous C18-ceramide increased the occurrence of autophagosome formation (LC3 punctate) in both cell types (276).

Together, these findings highlight the isoform- and context-specific functions of CerS enzymes in modulating autophagy across different cancer types, demonstrating that shifts in ceramide metabolism can determine whether autophagy serves as a pro-survival or pro-death role.

### *1.2.3 Lipidomics and its application in cancer*

Lipids play a role in many key cellular processes. Their hydrophobic and heavily reduced characteristics designate them as major constituents of biological membranes and energy storage molecules. Lipids are also involved in both extracellular and intracellular signaling, where they transduce signals and potentiate or attenuate signaling cascades by acting as ligands, receptors, and second messengers. Altered lipid metabolism is among the most prominent metabolic alterations observed in cancer, where an increase in the biosynthesis or uptake of lipids can lead to changes in energy homeostasis and contribute to uncontrolled cell growth and tumour formation (195, 277). Thus, there must be well-established standardized methods for identifying and quantifying lipids to better understand their impact on cancer progression and therapeutic outcomes.

Lipidomics is the systems-level study of networks and pathways of lipids and is a subdiscipline of metabolomics. Like a genome or proteome that describes complete gene and protein profiles, a lipidome describes an exhaustive lipid profile (Lipid Metabolism and Lipidomics Application in Cancer Research Meixia Pan, Chao Qin, 2021). Over the past few decades, numerous contributions have led to advances in analytical method development for lipid characterization. Briefly, lipids are extracted from a biological source (e.g. cells, tissue, organ) and are then analyzed by variations of tandem chromatography (for separation), ionization, and mass spectrometry for identification (278). Well-developed lipidomic methods can lead to the discovery of lipid biomarkers for disease diagnosis and monitoring, as well as identifying potential therapeutic targets (279, 280).

Lipids have long been appreciated for playing critical roles in cancer pathogenesis. Studies investigating brain tissues of patients with GBM demonstrated that lipid droplets – structures not observed in normal brain tissue – are abundant in GBM. Still, the exact lipids, their functions, and the extent of their involvement in GBM and chemoresistance are not well understood (281). One study investigated lipid metabolism in glioblastoma stem cells and non-stem cells to better understand how lipid species vary among cellular microenvironments within a heterogenous tumour such as GBM. There is a striking difference in total lipid content between diverse cell populations from the same patient. Specifically, CSCs exhibit lower lipid droplet accumulation compared to non-CSCs in both organoid and xenograft tumours. Targeted lipidomic analysis of multiple patient-derived models also demonstrated a shift in lipid metabolism between GBM CSCs and non-CSCs – suggesting that lipids may play a role in maintaining specific microenvironments and highlighting their potential in depicting cellular state. These findings highlight the importance

of understanding how lipid content and metabolism differences influence cancer cell development and progression and how they might serve as therapeutic targets in treating GBM (282).

Another study by Soylemez et al. investigated differences in lipid profiles between patients with GBM and controls to identify potential biomarkers for GBM diagnosis using an untargeted lipidomic approach. Using quadruple time-of-flight liquid chromatography-mass spectrometry (**Q-TOF LC/MS**), they found differentially regulated lipid species between the two sample sets, predominantly ceramides, diacylglycerol (**DAGs**), triacylglycerols (**TAGs**), and sphingomyelins (283). Interestingly, in lipid-restricted growth conditions, GBM cells have been reported to alter their lipid composition utilizing *de novo* fatty acid synthesis. Taib et al. reported changes in the lipidomic profiles of U138 human GBM cells, primarily including phospholipids (**PLs**), DAGs, and TAGs, in response to the absence of serum lipids. These lipids have emerged as important mediators of signal transduction in numerous cell processes. Their findings suggested that monounsaturated FAs increased GBM proliferation, pointing to a novel lipid droplet-mediated pathway that may serve as a therapeutic target for patients with GBM (281).

Despite the recent and rapid evolution of lipidomics in basic science and cancer research, limitations still exist. Namely, the lack of methodological standardization poses challenges in reproducing results and may result in discrepancies in workflows, data processing, and interpretation – factors that complicate determining the precise involvement of lipid species in different cell mechanisms. Further, overreporting and misannotation remains an issue considering humans' vast diversity of human lipid species, highlighting the importance of carefully formulated and validated approaches when addressing specific research questions (284, 285).

In summary, robust and standardized lipidomic methodologies, coupled with in-depth data mining, can help researchers and clinicians better understand how lipids regulate specific

mechanisms in cancer. They also enable the discovery of novel biomarkers for diagnosis, monitoring, and therapeutic development, emphasizing the importance of integrating clinical phenotypes with lipidomic profiles to improve disease management and patient outcomes.

## *1.3 Hypothesis & Rationale*

### *1.3.1 Hypothesis*

Glioblastoma is an aggressive primary brain malignancy characterized by extensive molecular heterogeneity and resistance to therapy. Temozolomide (TMZ), administered alongside radiotherapy and surgery as part of standard of care treatment, exerts its cytotoxic effects primarily through DNA alkylation, which can promote cell-cycle arrest and apoptosis. However, the development of TMZ resistance remains a major barrier to effected treatment and disease control.

TMZ resistance is multifactorial and extends beyond alterations in DNA damage and repair. Cellular stress-response pathways, including autophagy, mitochondrial adaptation, and lipid metabolism, may contribute to the ability of GBM cells to survive therapeutic stress. Autophagy is a conserved intracellular degradation and recycling pathway that maintains cellular homeostasis and can have context-dependent tumour-suppressive or tumour-promoting functions. Alterations in autophagic flux may therefore contribute to the cellular phenotype associated with acquired TMZ resistance.

BCL2L13 is a mitochondrial BCL-2 family protein implicated in apoptosis, mitochondrial homeostasis, and mitophagy, making it a potential link between mitochondrial function and cellular stress responses in GBM. Ceramides and other sphingolipids similarly participate in apoptosis, autophagy, and cellular stress signalling. Ceramide synthases, including CerS2 and CerS6, generate ceramides with distinct acyl-chain compositions and may contribute to changes in sphingolipid profiles associated with therapeutic resistance.

Based on these relationships, we hypothesized that BCL2L13 contributes to the TMZ-resistant GBM phenotype through effects on autophagy and mitochondrial function and is associated with remodeling of ceramide and complex sphingolipid profiles, including lipid species associated with CerS2 and CerS6, with these effects differing between TMZ-resistant and TMZ-non-resistant GBM cells.

### *1.3.2 Objectives*

Objective 1:

To investigate the role of BCL2L13 in regulating autophagy, apoptosis, and mitochondrial bioenergetics in TMZ-resistant (**TMZ-R**) compared with TMZ-non-resistant (**TMZ-NR**) GBM cells.

Evaluation:

To investigate the role of BCL2L13 in TMZ chemoresistance, a TMZ-R U251 GBM model was generated using an 18-week pulsed TMZ exposure protocol. Chemoresistance was evaluated using cell viability, phase-contrast imaging, and flow cytometric analysis of apoptosis and cell-cycle distribution. Autophagy was assessed by examining LC3B-II and p62 dynamics over time and following treatment with bafilomycin A1, together with imaging of autophagic structures by transmission electron microscopy (**TEM**) and immunocytochemistry (**ICC**).

Objective 2:

To investigate the relationship between BCL2L13, CerS2 and CerS6, and ceramide and complex sphingolipid remodeling in TMZ-R and TMZ-NR GBM cells.

Evaluation:

To investigate the relationship between BCL2L13 and sphingolipid metabolism, targeted lipidomic profiling was performed in TMZ-R and TMZ-NR U251 cells with and without BCL2L13 knockdown. Ceramide and complex sphingolipid species were evaluated using lipid abundance profiles and multivariate analyses to identify lipidomic differences associated with TMZ resistance and BCL2L13 expression. Particular attention was given to ceramide species associated with CerS2 and CerS6 activity to examine their potential relationship with BCL2L13.

# CHAPTER 2: Materials and Methods

### *2.1 Reagents and antibodies*

Cell culture plastic ware, media, penicillin, streptomycin, and fetal bovine serum (**FBS**) were obtained from VWR (Toronto, ON, Canada). Autophagy inhibitor Bafilomycin A1 (Catalogue # B1793), propidium iodide (PI), 3-(4,5-dimethyl-2-thiazolyl)-2,5-diphenyl-2H-tetrazolium bromide (MTT), protease and phosphatase inhibitors were purchased from Sigma-Aldrich (Sigma-Aldrich, Oakville, CA). BCL2L13 short hairpin RNA (**shRNA**) and control shRNA were purchased from Santa Cruz Biotechnology, Inc. (Dallas, TX, USA). Puromycin dihydrochloride and Polybrene were purchased from Santa Cruz Biotechnology (Santa Cruz Biotechnology, US). BCL2L13 polyclonal antibody (Rabbit anti-human/mouse) was obtained from Proteintech (Rosemont, IL, USA). LC3β polyclonal antibody (Rabbit anti-human/mouse) was purchased from Sigma-Aldrich (Sigma-Aldrich, Oakville, CA). Glycerinaldehyde-3-phosphate-dehydrogenase (GAPDH) monoclonal antibody (Mouse anti-human/mouse) was purchased from Santa Cruz Biotechnology, Inc. (Dallas, TX, USA). All other primary antibodies were purchased from Cell Signaling Technology (Canada). Anti-rabbit IgG (whole molecule) and anti-mouse IgG (Fab

specific) peroxidase-conjugated secondary antibodies were purchased from Sigma-Aldrich (Sigma-Aldrich, Oakville, CA). Secondary conjugated-antibodies (donkey anti-rabbit IgG-AlexaFluor-594, IgG-AlexaFluor-488) were purchased from Jackson lab (CA, USA). Ponceau S solution was purchased from Sigma-Aldrich (Oakville, CA). Temozolomide (Cat. No. T2577) was purchased from Sigma-Aldrich (Oakville, CA).

**Table 2.1.** Primary antibodies are used in western blotting.

| Primary Antibody | Dilution | Source | Size (kDa) |
|---|---|---|---|
| LC3βI | 1:2500 | Sigma-Aldrich; | 16 |
| LC3βII | 1:2500 | Sigma-Aldrich; | 18 |
| p62/SQSTM1 | 1:1000 | Cell Signalling; | 62 |
| BCL2L13 | 1:3000 | Proteintech; | 75 |
| GAPDH | 1:1000 | Santa Cruz; | 37 |

**Table 3.2.** Secondary antibodies are used in western blotting.

| Secondary Antibody | Dilution | Source |
|---|---|---|
| Anti-Rabbit IgG | 1:5000 | Sigma-Aldrich |
| Anti-Mouse IgG | 1:3000 | Sigma-Aldrich |

### *2.2 Cell culture*

For all experiments, we used the U251-mKate human glioblastoma cell line. This cell line was developed by Dr. Marcel Bally at Experimental Therapeutics, British Columbia Cancer Agency, Vancouver, BC, Canada. Cancer cells were cultured in Dulbecco's Modified Eagle's Medium-high glucose (4 mg/ml) (DMEM) (CORNING; Cat #: 50-003-PB) supplemented with

10% FBS (Gibco, Cat #: 16000-044) and 1% penicillin and streptomycin. Cells were maintained in a humidified incubator in standard cell culture conditions (95% air and 5% $CO_2$ at 37°C). Stable BCL2L13 knockdown (KD) and negative control (scramble) were grown in the same medium plus puromycin (4 μg/ml) to ensure the selection of stably transfected cells.

### *2.3 Preparation of TMZ-resistant cells*

U251-mKate cells (developed by Dr. Marcel Bally, Experimental Therapeutics, British Columbia Cancer Agency, Vancouver, BC, Canada) were cultured in T75 tissue culture flasks in a complete media containing high glucose DMEM, 10% FBS (Gibco, Cat #: 16000-044), and 1% Penicillin-Streptomycin (Gibco, Cat #:15140-122) and incubated at 37°C, 5% $CO_2$, in a humidified incubator (Thermo Fischer Scientific, US). A pulsed-selection strategy was chosen to make a clinically relevant chemoresistant model (286). Once cells reached 70% confluence, they were treated with 100 μM TMZ (Sigma Aldrich, CAS #: 85622-93-1) over a three-week time period, followed by four weeks of TMZ-free media for recovery. Cells were cultured in complete media with 250 μM TMZ for three weeks, followed by another four weeks with TMZ-free media. The final population of U251-mKate cells resistant to 250 μM TMZ was selected and cultured in a complete media without TMZ for four weeks.

### *2.4 Immunoblotting*

Immunoblotting (western blotting) was used to detect protein expression. GAPDH and Ponceau S staining were used as loading controls. Briefly, cells were washed with phosphate buffered saline (**PBS**), and protein extracts were prepared in lysis buffer containing 20 mM Tris-HCl (pH 7.5), 0.5 mM phenylmehtylsulfonyl fluoride, 0.5% Nonidet P-40, 100 μM β-glycerol 3-

phosphate and 0.5% protease and phosphatase inhibitor cocktail. Cell lysate was subject to centrifugation at 10,000 g for 10 min at 4°C, and protein concentration was measured by Lowry protein assay. Next, proteins were separated by size using SDS-PAGE under reducing conditions and transferred to polyvinylidene difluoride membranes. Membranes were blocked with 5% skim milk in TBST (1X tris-buffered saline, 0.025% Tween 20RT) for 1 h at room temperature (**RT**). Blots were incubated overnight at 4°C with primary antibody in 1% skim milk in TBST, followed by incubation with HRP (horseradish peroxidase)-conjugated secondary antibody for 2 h at RT. Blots were washed with TBST for a total of 30 min prior to protein detection. Blots were developed by enhanced chemiluminescence detection (Amersham-Pharmacia Biotech) to visualize bands using Bio-Rad imager (Mississauga, ON, Canada). Image Lab Software offered by Bio-Rad imager was used to ensure linear exposure, and signals were visualized and quantified using the densitometry software Alpha Ease FC.

### *2.5 Transmission electron microscopy*

Autophagy was confirmed using transmission electron microscopy (**TEM**). Briefly, U251 GBM cells were cultured in 100 mm dishes in DMEM (10% FBS 1% P/S) in standard cell culture incubator conditions. Cells were fixed in Karnovsky fixative for 1 h at 4°C, and the pellet was resuspended in 5% sucrose in 0.1 M Sorenson's phosphate buffer overnight at 4°C. Cells were pelleted and post-fixed with 1% osmium tetroxide in 0.1 M Sorenson's buffer for 2 h. Next, cells were dehydrated and embedded in Embed 812 resin for sectioning. Thin sections (200 nm) were cut and placed on copper grids for staining and counter-staining with uranyl acetate and lead nitrate, respectively. Imaging was done using a Philips CM10 electron microscope.

### *2.6 Immunocytochemistry*

Immunocytochemistry (**ICC**) was used to detect changes in autophagy in U251 GBM cells and corresponding BCL2L13 KD transfectants. Cells were fixed with 3.7% formaldehyde and incubated at RT for 30 min. Samples were washed three times using Dulbecco's phosphate-buffered saline (**DPBS**) and kept in DPBS for 5 min each time. Fixed samples were permeabilized and blocked overnight at 4°C with a blocking buffer containing 5% IgG-free bovine serum albumin (**BSA**) (Jackson ImmunoResearch Laboratories) and 0.3% Triton X-100 (Bio Basic) in DPBS. The blocking buffer was replaced with an antibody solution containing 1% BSA, 0.3% Triton X-100, and conjugated antibodies in DPBS and incubated at 4°C overnight in the dark. The dilution ratio for the anti-LC3 rabbit polyclonal primary antibody was 1:2000 (Sigma, L7543). After removing the primary antibody, a secondary donkey anti-rabbit IgG antibody at 1:2000 dilution (Jackson ImmunoResearch Laboratories) was introduced and incubated at RT for 60 min in the dark. The nuclei staining solution was removed, and the samples were washed with DPBS three times and incubated for 5 min. The wells were partially filled with DPBS, and the samples were kept at 4°C in the dark until imaging was performed. Zeiss Axiovert 200 inverted microscope fitted with a Calibri 7 LED Light Source and Axiocam 702 mono camera. Quantification, scale bars, background subtract, and processing were done using Fiji (ImageJ) and Zen 2.3 Pro software. All experiments were repeated 3 times independently. A minimum of 10 pictures were taken per condition.

### *2.7 MTT viability assay*

Cell viability of U251 GBM cells (TMZ-NR, TMZ-R, BCL2L13 KD, and BCL2L13-wildtype (WT) was measured using MTT assay. Cells were grown to 50% confluence in high glucose DMEM with 10% FBS and 1% P/S. Cells were seeded (TMZ-NR: 50,000 cells/mL and

TMZ-R: 75,000 cells/mL) in 96-well U-bottom plates and treated with varying concentrations of BafA1 (1, 5, or 10 nM). Cell viability was assessed after 72 h. First, 20 µL of 5 mg/mL MTT (3-(4,5-dimethylthiazol-2-yl)-2,5-diphenyl-2H-tetrazolium bromide) was added to each well and incubated at 37°C and 5% $CO_2$ for 3 h. This assay is based on the reduction of MTT to its insoluble formazan, which is purple and absorbs electromagnetic radiation at 570nm. The reduction is facilitated by NAD(P)H-dependent cellular oxidoreductase enzymes active only in living cells with metabolic activity. Next, media was gently aspirated and 200 uL of dimethyl sulfoxide (**DMSO**) was mixed to each well. The plate was then incubated in the dark at RT for 25 min, and the absorbance was read at 570 nm using a Synergy H1 Microplate Reader. Relative cell viability (percent of control) was calculated using the equation: (mean OD (570 nm) of treated cells/mean OD (570 nm) of control cells) x 100. The treated cells were compared with control cells treated with DMSO vehicle only.

### *2.8 PrestoBlue viability assay*

According to the manufacturer's protocol, a viability assay was performed using PrestoBlue (Invitrogen, A13262). Briefly, 100 µl of 5 x $10^5$ cell/ml of U251-mKate cell TMZ-R and NR U251-mKate cells (U251) were cultured in 96-well plates (5 repeats for each group) and treated with TMZ-free or TMZ 250 µM-containing complete high glucose DMEM media for one day. Then, the media was removed, and cells were treated with 0-5000 µM of TMZ for 72 h. A working solution of PrestoBlue was prepared with a 1:10 dilution of stock solution. After three days of treatment, the media was replaced with 200 µL of working solution, and the plates were incubated in the $CO_2$ incubator for 30 min. Once incubated, 150 µL of each sample was transferred to a 96-

well plate. The fluorescent intensity was read using an Infinite M Nano plate reader (Tecan) via the i-control software (Tecan, Version 3.9.1.0) at two wavelengths: 560 nm and 590 nm.

### *2.9 Production of stable BCL2L13 knock down (KD) cell line*

Lentiviral transfection was used to silence BCL2L13 protein expression. U251 TMZ-R and NR GBM cells were seeded in a 12-well plate and cultured in DMEM (10% FBS and 1% P/S). At 40% confluency, cells were treated with 10 μg/mL polybrene (Santa Cruz Biotechnology, US) in pure DMEM medium (without FBS) and incubated for 1 h. Next, cells were introduced to viruses packed with shRNA – short hairpin RNA sequences complementary to the RNA encoding BCL2L13 protein in the host cell – which suppresses the translation of BCL2L13 RNA to protein. A lentivirus is a subclass of retroviruses that can integrate its genome into the host cell. Lentiviruses use enzymes reverse transcriptase (converts viral RNA into double-stranded DNA) and integrase (inserts viral DNA into host cell DNA). Further, these vectors encode antibiotic resistance genes to enable the selection of successfully transfected host cells, in this case through puromycin resistance. After the release of viral genetic material into the nucleus, the RNA of interest is transcribed using the cell's machineries. However, introducing exogenous RNA results in a cell response. To ensure that the effect of shRNA transfection is due to its specificity in knocking down protein expression, a negative control is needed where cells are exposed to transfection reagents and protocol but with lentiviral particles packed with scramble RNA (**scRNA**). scRNA has the same nucleotide composition but a different sequence than shRNA, so it does not target any mRNA. Cells were transfected at 30 multiplicity of infections overnight (12 h), then replenishing the medium for recovery for 48 h. The process from adding polybrene to transfecting and recovering cells was repeated once to ensure successful transfection. After

recovery, cells that incorporated shRNA and scRNA plasmids were selected using 4μg/ml puromycin dihydrochloride (Santa Cruz Biotechnology, US). BCL2L13 status was checked by western blot in isolated stable clones in both shRNA and transfected scramble cells.

### *2.10 Flow cytometry/Cell cycle analysis*

The Nicoletti method measured cellular apoptosis (287)**.** Briefly, U251 GBM cells (TMZ-NR, TMZ-R, BCL2L13-WT, BCL2L13-KD were seeded in a 12-well plate (50,000 cells/well for TMZ-NR cells and 75,000 cells/well for TMZ-R cells). Cells were grown to 60% confluence and treated with 250 μM TMZ for 48 h or 96 h. After the time point was reached, cells were detached with EDTA buffer and harvested by centrifugation at 800 g for 8 min at 4°C). Cells were washed once in PBS buffer before resuspending in a hypotonic PI lysis buffer (0.01% Triton x-100 and 1% sodium citrate, 40 μg/ml propidium iodide) and incubated at RT for 30 min in a dark environment and analyzed by flow cytometry. The stained cell samples were run on Beckman Coulter Cytoflex LX (Indianapolis, IN, USA). 50 mW 488 nm blue laser and 610/20 BandPass filter were used for proper excitation and emission of the propidium iodide. Single cell population was gated, and cell cycle analysis was performed to measure the percentage of cells at Sub-G0, G0-G1, S, and G2-M phases.

### *2.11 Measurement of mitochondrial respiration: Sea horse assay*

Mitochondrial respiration was measured using the Agilent Seahorse XFe24 analyzer by recording the oxygen consumption rate (**OCR**). Cells were seeded in their growth medium in XF cell culture 24-well microplates at approximately 0.3 x $10^6$ cells/well (U2521 TMZ-NR, TMZ-R, BCL2L13-KD, and scramble). On the day of the experiment, cells were washed twice with and

changed to XF base minimal DMEM containing glucose, L-glutamine, and sodium pyruvate (Agilent Technologies, Mississauga, ON). Cells were incubated at 37°C for 1 h prior to starting the assay. The seahorse analyzer measured the baseline OCR first, followed by protein leak using 1 μM of oligomycin. Maximal respiration was determined by injection of FCCP (2 μM) and non-mitochondrial respiration by adding 1 μM rotenone and 1 μM antimycin A. OCR was normalized by live cell count signal obtained by staining individual wells with Hoechst33342 (Invitrogen; Cat #:R37605) using Cytation 5 (Biotek). Maximal respiration was calculated by subtracting non-mitochondrial OCR from FCCP OCR. Spare capacity was determined by subtracting baseline OCR from FCCP OCR. Further, ATP production was calculated by subtracting Oligomycin OCR from baseline OCR. Finally, proton leak was measured by subtracting non-mitochondrial OCR from Oligomycin OCR. Data are presented as pmol of oxygen/minute/cell count.

### *2.12 Phase contrast*

Bright-field images were taken using an Axio Observer ZEISS microscope (ZEISS, Oberkochen, Germany) using 20x and 50x magnification objectives. Quantification, scale bars, background subtraction, and processing were done on Fiji (ImageJ) and Zen 2.3 Pro software.

### *2.13 Liquid chromatography-mass spectrometry (LC-MS/MS) for lipidomics analysis of ceramide species*

Lipid extraction used chloroform: methanol (C:M), 2:1 (v/v). Briefly, U251 GBM (NR, R, BCL2L13-KD, BCL2L13-WT) were grown to 100% confluency and collected using PBS 1X. After sonication and centrifugation (1000 g for 10 min), the supernatant was collected for each cell line. Then, a mixture of 100 μl of cell homogenate and 30 μl of the internal standard mixture was made. Samples were vortexed and centrifuged (3500 rpm at RT for 5 min). The lower phase was transferred to a different tube and dried under a stream of $N_2$ gas at RT. Lipids were then

reconstituted in 50 µl water-saturated butanol and sonicated for 10 min. In the last step, 50 µl of methanol with 10 mM ammonium formate was added, and samples were centrifuged (10000 g at RT for 10 min). Lipid internal standards were either odd-chain or deuterated and were not present endogenously. Samples were transferred into the micro insert in sample vials for lipid analysis. Lipids were separated on a LC-MS/MS platform using a chromatographic system. Instrument control and data processing were done with Analyst v1.6 and MultiQuant v2.1 software (AB Sciex, MA, USA). The separation was achieved on a Zorbax C18, 1.8 µm, 50 x 2.1 mm column (Agilent Technologies, Mississauga, ON). The flow rate was set to 300 µl/min using a linear gradient of mobile phase A and mobile phase B. Mobile phase A and B consisted of tetrahydrofuran, methanol, and water in a ratio of 20:20:60 (v/v/v) and 75:20:5 (v/v/v), respectively. Both A and B contained 10 mM ammonium formate. The elution program was as follows: start with 0% solvent B; increase to 100% B at 8.00 min; maintained at 100% B for 2.5 min; and back to 0% B for 0.5 min. The column was finally re-equilibrated to the starting conditions (0% mobile phase B) for 3 min before the next sample injection. Diacylglycerol (DG) and triacylglycerol (TG) species were separated in an isocratic fashion (100 µl/min) by employing 85% mobile phase B over 8 min. The analytical column and autosampler were maintained during the analysis at 50°C and 25°C, respectively. The injection volume was 5 µl.

*Mass Spectral Analysis:* Lipids eluted from the HPLC system were introduced into the AbSciex 4000 QTRAP triple quadrupole linear hybrid mass spectrometer. The mass spectrometer was operated in scheduled Multiple Reaction Monitoring (MRM) mode. 322 unique lipids spanning 25 lipid classes/subclasses were screened for targeted semi-quantitation. All lipid species other than fatty acids were scanned in positive electrospray ionization mode [**ESI+**]. The individual lipids in each lipid class were identified by lipid class-specific precursor ions or neutral

losses. Lipids were then quantified by comparing the deisotoped lipid peak areas against those of the class-specific internal standards added before lipid extraction. The total carbon number of the fatty acids represented lipids. In ESI+ mode, the instrument settings were optimized as follows: curtain gas (psi), 26; collision gas (nitrogen), medium; ion spray voltage (V), 5500; temperature (°C), 500.0; ion source gas 1 (psi), 40.0; ion and source gas 2 (psi), 30.0. The MRM detection window was fixed between 45 s and 90 s depending upon the chromatographic peak width of the lipid class. Isobaric species within the same class, such as PC(O) and PC(P), exhibited clear separation in this method. Also, molecular species within the same lipid class, which differ only in the number of double bonds, were well separated chromatographically. All analyses were performed with R software (version 4.1.1). Limma, pheatmap, and ggplot2 packages were used.

### *2.14 Statistics*

Data was repeated in at least three replicates and in three separate experiments independently for all experiments. Error bars depict ± standard deviation from the average values. Experiments with 4 or more conditions were analyzed using a one-way or two-way ANOVA with Tukey's test for multiple comparisons. Significance analysis was performed using a two-tailed t-test or one-way or two-way ANOVA using GraphPad Prism, where p-value = 0.05 and less was considered statistically significant.

*Lipidomics:* Lipid classification and annotation was done using LIPIDMAPS database based on molecular mass, isotope distribution, and collision-induced dissociation LC/MS data. Result and lipidomic data were analyzed using MetaboAnalyst 5.0, web version. Hierarchical clustering was visualized through heatmaps to display lipid abundance in different samples. Unsupervised principal component analysis was performed to visualize general lipid profile and grouping trends of all samples. Supervised partial least squares discriminant analysis was used to identify

differential lipids between primary and lymph node metastasis group, based on the values of variable importance in projection (VIP > 1.2) and false discovery rate (FDR < 0.05). These significant lipids were selected to predict protein interacting partners with each lipid, using Swiss Target Prediction. Gene Ontology (GO), Molecular function (MF), Kyoto Encyclopedia of Genes and Genomes analysis (**KEGG**), and protein-protein interactions were used for functional annotation of key prediction proteins using String and GProfiler web tools. Significance analysis was performed using a two-tailed t-test or one-way or two-way ANOVA using GraphPad Prism where p- value=0.05 and less was considered statistically significant.

# CHAPTER 3: Results

### *3.1 Temozolomide induces more cell death in U251 temozolomide non-resistant GBM cells.*

A 2D in vitro model of U251 TMZ-R GBM cells was developed over an 18-week period using a pulsed-selection strategy to establish a clinically relevant chemoresistant model. A pulsed-selection method is a strategy often used in vitro in which cells are given drug-free recovery periods, which are intended to mimic the cycles of chemotherapy that patients encounter during treatment (286). Clinically relevant cell lines are imperative to ensure that research findings are practically informative. The Presto Blue cell viability assay was used to demonstrate that TMZ-R GBM cells maintained greater viability than TMZ-NR cells following TMZ treatment, with approximately 50% viability maintained at 500 uM TMZ ($P < 0.0001$) (**Figure 3.1A**). For subsequent experiments, we kept the resistant cells in 250 uM TMZ and removed the TMZ 24 h before treatment conditions were applied. TMZ-NR GBM cells showed significant cell death at this concentration, whereas the population of U251 TMZ-R GBM cells is sustained ($P < 0.0001$).

Phase contrast microscopy showed differences in confluence, where the U251 TMZ-NR GBM cell population is dramatically reduced following 48 h of treatment with 100 uM TMZ compared to U251 TMZ-R GBM cells (**Figure 3.1B**). Further, phase contrast imaging revealed differences in morphology. U251 GBM cells are dendritic-like in nature with cytoplasmic prolongations known as filopodia. We observed that TMZ-NR cells were smaller, rounder in shape, had shorter filopodia, and grew closer to other cells. In contrast, TMZ-R cells had elongated, more distinct filopodia and were thinner and longer than TMZ-NR GBM cells.

Next, flow cytometry was used to investigate TMZ-induced apoptosis and the percentage of cells in different cell cycle phases after 48 h of treatment with 100 uM TMZ. The percentage of TMZ-NR cells in the sub-G0 phase (apoptotic cells) was significantly increased following TMZ treatment ($P < 0.0001$), whereas TMZ treatment had no significant effect in TMZ-R cells (**Figure 3.1C**). The percentage of cells in the G0-G1 phase significantly decreased in TMZ-NR cells following TMZ treatment ($P < 0.0001$), while TMZ-R cells showed no significant change (**Figure 3.1D**). Similarly, the percentage of TMZ-NR cells in the G2/M phase markedly increased ($P < 0.0001$) after treatment, while no significant change was observed in TMZ-R cells (**Figure 3.1E**). Lastly, both TMZ-NR and TMZ-R GBM cells showed no significant change ($P > 0.05$) in the proportion of cells in the S phase following 48 h of TMZ treatment (**Figure 3.1F**).

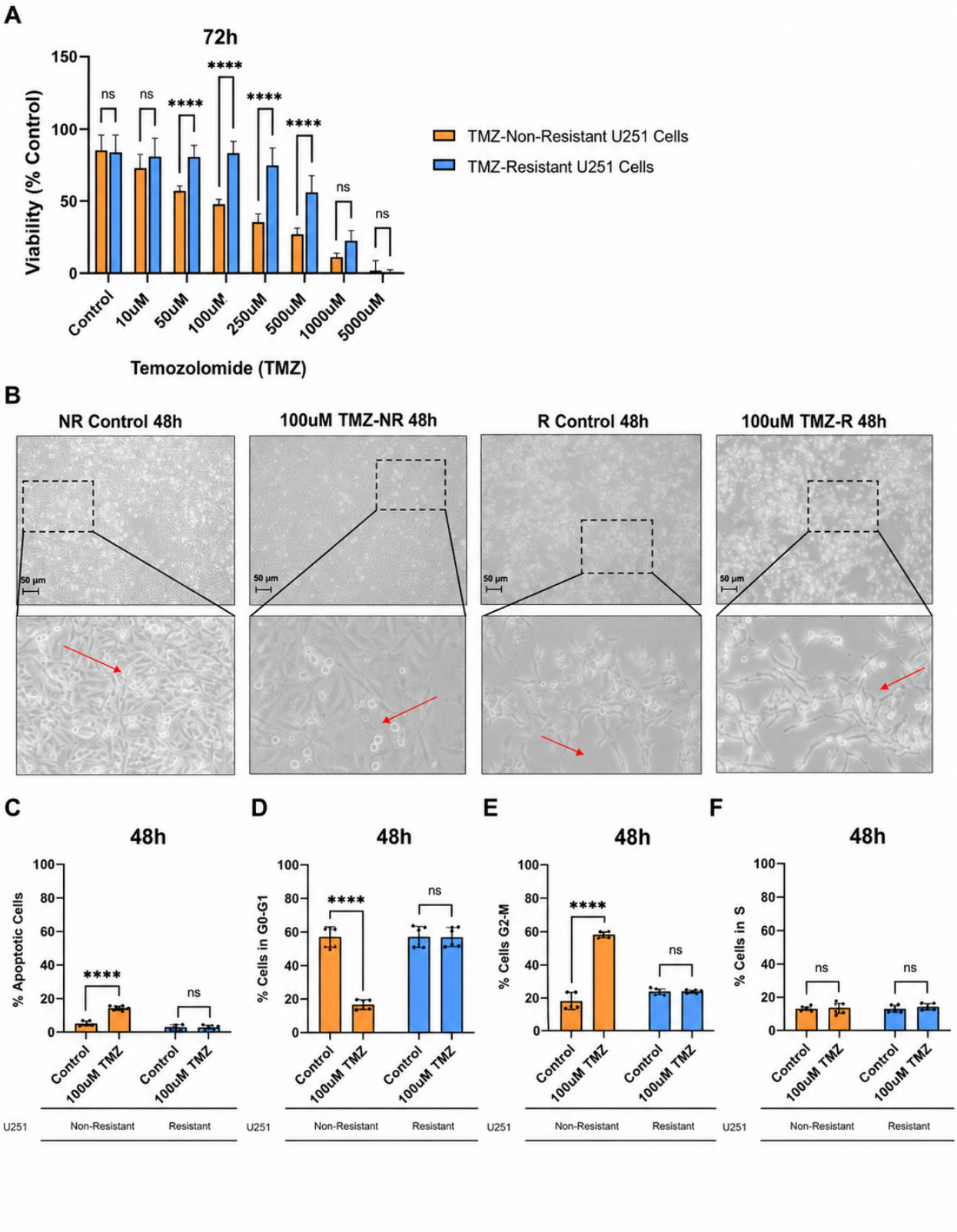
A
72h
Viability (% Control)
150
100
50
0
ns
ns
****
****
****
****
ns
ns
Control
10uM
50uM
100uM
250uM
500uM
1000uM
5000uM
Temozolomide (TMZ)
TMZ-Non-Resistant U251 Cells
TMZ-Resistant U251 Cells
B
NR Control 48h
100uM TMZ-NR 48h
R Control 48h
100uM TMZ-R 48h
50 µm
C
48h
% Apoptotic Cells
D
48h
% Cells in G0-G1
E
48h
% Cells G2-M
F
48h
% Cells in S
Control
100uM TMZ
U251
Non-Resistant
Resistant

**Figure 3.1. Temozolomide induces more cell death in TMZ-NR GBM cells.** (A) U251 TMZ-R and NR GBM cells were treated with 10-5000 μM TMZ or control medium for 72h, and cell viability was assessed using the PrestoBlue assay. (B) Phase-contrast microscopic images of U251 TMZ-R and NR GBM cells treated with TMZ (100 uM) or the corresponding control media for 48h. Scale bars = 50um. (C-F) U251 TMZ-NR and R GBM cells were treated with TMZ (100 uM) or corresponding control media for 48 h. Samples were collected and processed for propidium iodide flow cytometry to assess apoptosis and cell cycle distribution (G0/G1, G2/M, and S phases). Data represent three independent biological experiments and are presented as mean ± SD. Statistical significance is indicated in the figure (ns = $P > 0.05$, * = $P < 0.05$, ** = $P < 0.01$, *** = $P < 0.001$, **** = $P < 0.0001$).

### *3.2. Autophagy flux is impaired in TMZ-R GBM cells.*

Immunoblotting was used to investigate the level of LC3B-II and p62 expression, thereby providing an overview of autophagic activity in U251 TMZ-R and NR GBM cells. As previously mentioned, LC3B-II and p62 are common protein markers of autophagy activity due to their critical roles in autophagosomal processing. LC3B-II and p62 decreased over 72 hrs in TMZ-NR GBM cells; while their levels remained elevated in TMZ-R cells, consistent with impaired autophagic processing (**Figure 3.2A, B**) ($P < 0.01$).

In the next set of experiments, we used BafA1, which inhibits vacuolar H(+)-ATPase and blocks autophagic flux. An MTT cell viability assay was used to evaluate the cytotoxic effects of different concentrations of BafA1 (1, 5, and 10 nM) on U251 TMZ-R and NR GBM cells. The results showed that 10 nM BafA1 significantly decreased TMZ-NR GBM cells viability ($P < 0.001$), while no concentration of BafA1 induced significant cytotoxicity in TMZ-R GBM cells

(**Figure 3.2C**). Based on these toxicity studies, using immunoblotting, 5 nM BafA1 was selected as the dose used to compare autophagy flux between U251 TMZ-R and NR GBM cells. Treatment with 5 nM BafA1 for 72 h resulted in increased levels of both LC3B-II and p62 ($P < 0.01$) in TMZ-NR GBM cells (**Figure 3.2D, E**). In contrast, in TMZ-R cells, the same treatment had no significant effect on LC3B-II or p62 levels, consistent with impaired late-stage autophagic processing (**Figure 3.2D, E**).

Next, ICC imaging was used to visualize LC3B-positive puncta in TMZ-R cells compared with TMZ-NR cells. Both types of cells were grown for 72 h and processed for imaging. Samples were prepared stained cells using an LC3B antibody, allowing visualization of LC3B-positive puncta. More LC3B-positive puncta were observed in TMZ-R GBM cells, consistent with increased accumulation of autophagic structures (**Figure 3.2F**).

We also investigated the ultrastructure of TMZ-NR and R GBM cells using TEM to further evaluate autophagy. U251 TMZ-NR and R GBM cells were grown for 72 h, and samples were prepared for imaging. Autophagy was evaluated by quantifying cytosolic double-membrane autophagic vacuoles. The number of double-membrane autophagic vacuoles was significantly higher in TMZ-R GBM cells compared with TMZ-NR cells. (**Figure 3.2G, H**). This finding further supports the accumulation of autophagic structures and impaired late-stage autophagic processing in TMZ-R GBM cells.

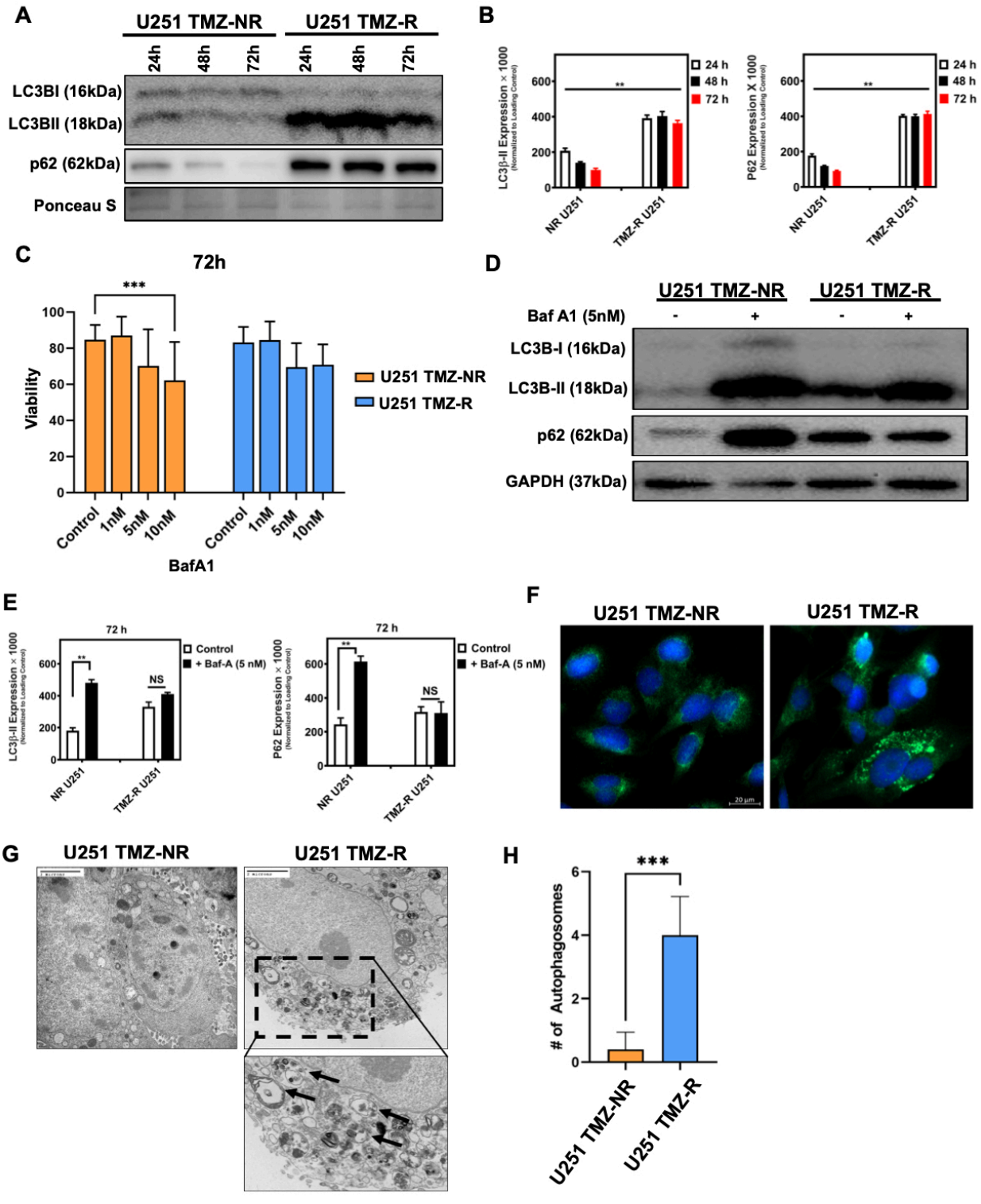
A
U251 TMZ-NR
U251 TMZ-R
24h
48h
72h
LC3BI (16kDa)
LC3BII (18kDa)
p62 (62kDa)
Ponceau S
B
LC3β-II Expression × 1000
(Normalized to Loading Control)
24 h
48 h
72 h
**
NR U251
TMZ-R U251
P62 Expression X 1000
C
72h
***
Viability
U251 TMZ-NR
U251 TMZ-R
Control
1nM
5nM
10nM
BafA1
D
Baf A1 (5nM)
LC3B-I (16kDa)
LC3B-II (18kDa)
p62 (62kDa)
GAPDH (37kDa)
E
72 h
Control
+ Baf-A (5 nM)
NS
F
20 μm
G
H
# of Autophagosomes

**Figure 3.2. Autophagy flux is impaired in TMZ-R GBM cells.** (A, B) U251 TMZ-NR and R GBM cells were grown for 72 h, with cell lysates prepared every 24 h. LC3B-II and p62 levels were evaluated by immunoblotting at 24, 48, and 72 h. Ponceau S was utilized as a loading control. (C) The cytotoxic effects of BafA1 (1, 5 and 10 nM) on U251 TMZ-NR and R GBM cells were determined via MTT assay over a 72 h period. (D, E) U251 TMZ-NR and R GBM cells were grown for 72 h in the presence or absence of BafA1 (5 nM). LC3B-II and p62 levels were evaluated by immunoblotting. GAPDH was utilized as a loading control. (F) U251 TMZ-NR and R GBM cells were grown for 72 h and processed for immunocytochemistry. LC3B-positive puncta were visualized using LC3B immunostaining. Scale bar = 20 um. (G, H) U251 TMZ-NR and R GBM cells were grown for 72 h and prepared for TEM. Autophagy was evaluated by quantifying cytosolic double-membrane autophagic vacuoles in 10 cells per condition. Data represent three independent biological experiments and are presented as mean ± SD. Statistical significance is indicated in the figure (ns = $P > 0.05$, * = $P < 0.05$, ** = $P < 0.01$, *** = $P < 0.001$, **** = $P < 0.0001$).

### *3.3 BCL2L13 has higher expression in U251 TMZ-R compared to TMZ-NR GBM cells.*

Immunoblotting was used to evaluate BCL2L13 expression in U251 TMZ-R and NR GBM cells. Cells were grown and collected every 24 h over 72 h to evaluate changes in BCL2L13 expression changes over time. These results showed that BCL2L13 expression was significantly higher in U251 TMZ-R GBM cells compared with TMZ-NR GBM cells at the 48 and 72 h time points ($P < 0.01$) (**Figure 3.3A, B**). Given the previously described roles of BCL2L13 in apoptosis, mitochondrial quality control, and autophagy-related processes, these findings prompted further

investigation of whether BCL2L13 may be associated with autophagy and cell-death responses in TMZ-R GBM cells (156).

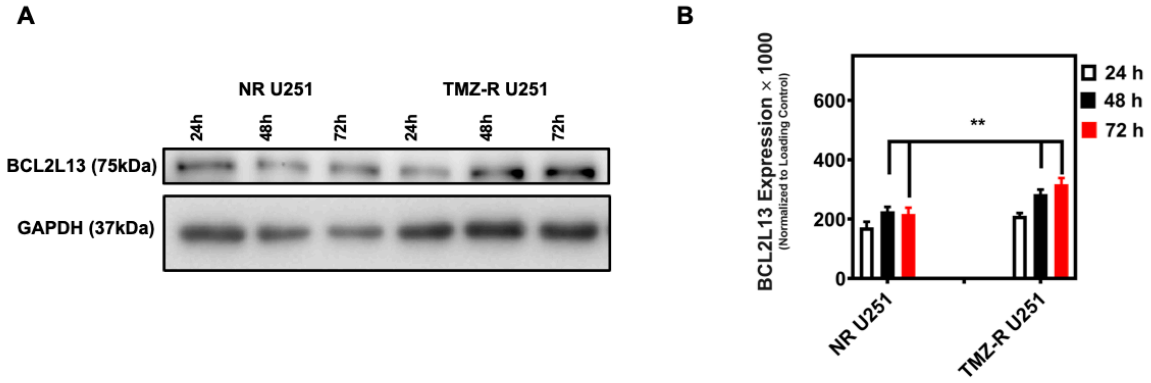


**Figure 3.3 BCL2L13 has higher expression in TMZ-R compared to TMZ-NR GBM cells.** (A, B) U251 TMZ-NR and R GBM cells were grown for 72 h. Cell lysates were prepared at 24, 48, and 72 h, and BCL2L13 expression was evaluated by immunoblotting. GAPDH was utilized as a loading control. Data represent three independent biological experiments and are presented as mean ± SD. Statistical significance is indicated in the figure (ns = $P > 0.05$, * = $P < 0.05$, ** = $P < 0.01$, *** = $P < 0.001$, **** = $P < 0.0001$).

### *3.4 BCL2L13 does not change TMZ-induced apoptosis in U251 TMZ-R GBM cells.*

To investigate the impact of BCL2L13 expression in U251 TMZ-R and NR GBM cells on autophagy, apoptosis, and their response to TMZ, we first sought to knock down its expression by transfecting cells with a lentivirus encoding BCL2L13-targeted shRNA. In this setting, lentiviral transduction enables stable, long-term RNA silencing in host cells. The immunoblot results showed successful knockdown of the BCL2L13 protein (**Figure 3.4A)**. Next, we used TEM to investigate if there were changes in the number of autophagic vacuoles in U251 TMZ-R and NR GBM cells (BCL2L13 KD and scramble). The results showed that BCL2L13 KD did not

significantly change the number of cytosolic double membrane vacuoles in U251 TMZ-NR and R GBM cells ($P > 0.05$) (**Figure 3.4B, C**).

Next, we evaluated the impact of BCL2L13 expression on autophagy-marker dynamics and U251 TMZ-NR and R GBM cells using BafA1 (5 nM, 72 hrs). The results showed that knocking down BCL2L13 significantly increased LC3B-II in U251 TMZ-NR GBM cells while significantly decreasing levels in U251 TMZ-R GBM cells without BafA1 treatment. In contrast, BCL2L13 KD did not induce a significant change in p62 levels in TMZ-NR cells while significantly decreasing p62 levels in TMZ-R cells in the absence of Baf-A1 treatment. Treatment with BafA1 significantly increased LC3B-II and decreased p62 degradation in TMZ-NR GBM cells, and BCL2L13 expression did not change this effect. On the other hand, BafA1 treatment did not have a significant effect on LC3B-II and p62 levels in TMZ-R cells, while BCL2L13 expression did not change this effect (**Figure 3.4D, E**). We then used flow cytometry to investigate the role of BCL2L13 expression in the response of U251-TMZ-R and NR GBM cells to TMZ-induced apoptosis and the percentage of cells in different phases of the cell cycle after treating cells with 100 μM TMZ for 48 and 96 hrs. The results showed that BCL2L13 expression did not significantly change TMZ-induced apoptosis in both NR and R GBM cells after 48 and 96 hrs ($P > 0.05$). The results indicated that knocking down BCL2L13 in U251 TMZ-NR cells for 48 hrs significantly reduced the percentage of cells in the G2-M phase of the cell cycle. Additionally, in U251 TMZ-R (both scramble and BCL2L13 KD) GBM cells, the number of cells in the G0-G1 phase decreased after 96 hrs (**Figures 3.4F, G**).

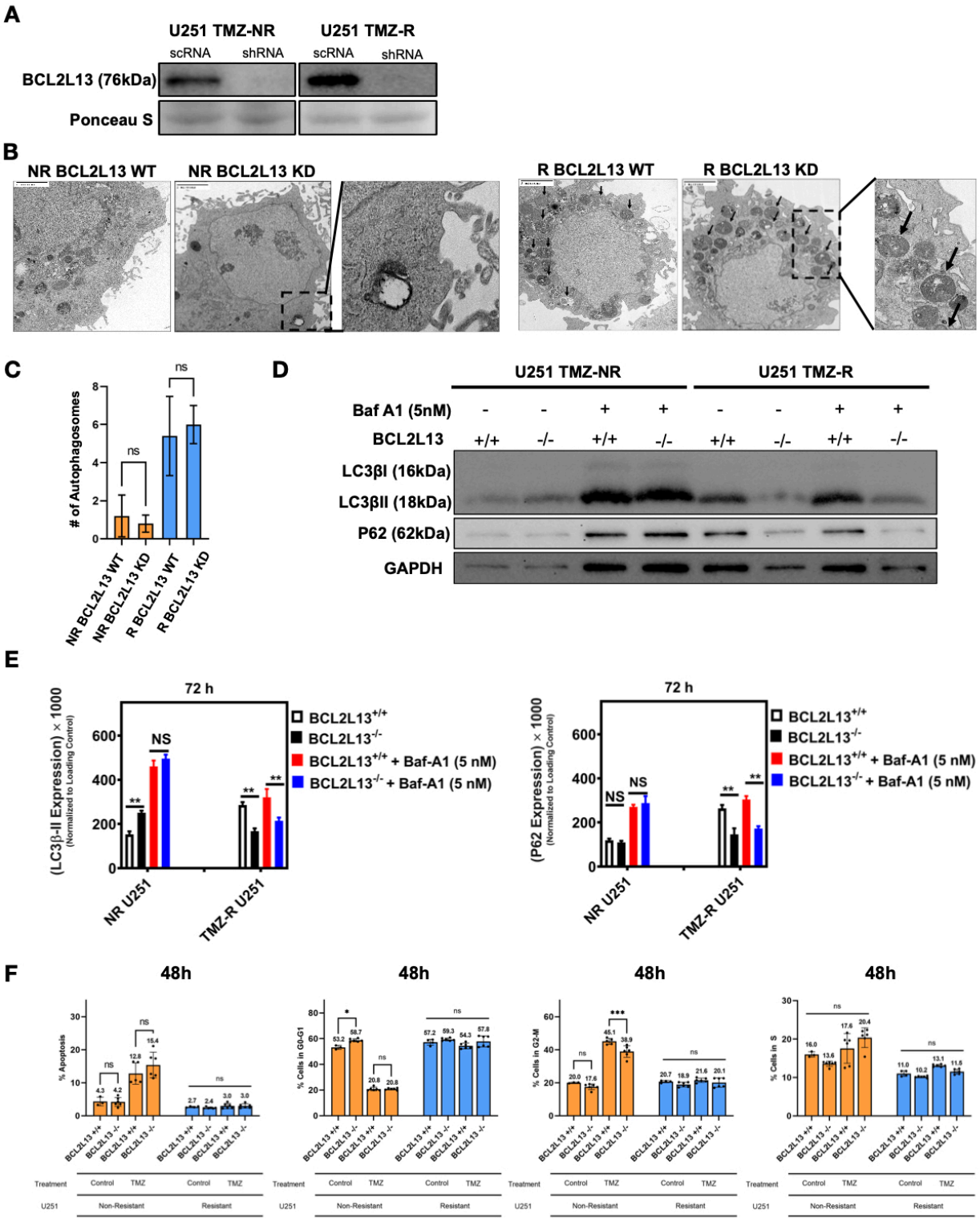
A
U251 TMZ-NR
U251 TMZ-R
scRNA
shRNA
scRNA
shRNA
BCL2L13 (76kDa)
Ponceau S
B
NR BCL2L13 WT
NR BCL2L13 KD
R BCL2L13 WT
R BCL2L13 KD
C
# of Autophagosomes
ns
ns
NR BCL2L13 WT
NR BCL2L13 KD
R BCL2L13 WT
R BCL2L13 KD
D
U251 TMZ-NR
U251 TMZ-R
Baf A1 (5nM)
BCL2L13
LC3βI (16kDa)
LC3βII (18kDa)
P62 (62kDa)
GAPDH
E
72 h
(LC3β-II Expression) × 1000
(Normalized to Loading Control)
NS
BCL2L13+/+
BCL2L13-/-
BCL2L13+/+ + Baf-A1 (5 nM)
BCL2L13-/- + Baf-A1 (5 nM)
NR U251
TMZ-R U251
72 h
(P62 Expression) × 1000
(Normalized to Loading Control)
NS
NS
BCL2L13+/+
BCL2L13-/-
BCL2L13+/+ + Baf-A1 (5 nM)
BCL2L13-/- + Baf-A1 (5 nM)
NR U251
TMZ-R U251
F
48h
48h
48h
48h
% Apoptosis
% Cells in G0-G1
% Cells in G2-M
% Cells in S
Treatment
Control
TMZ
U251
Non-Resistant
Resistant

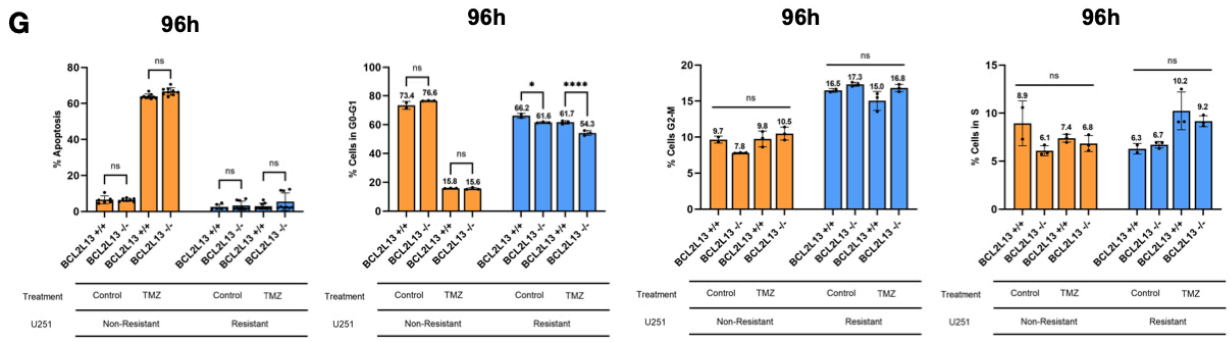


**Figure 4. BCL2L13 does not change TMZ-induced apoptosis in TMZ-R GBM cells.** (A) U251 TMZ-NR and TMZ-R were infected with scramble and BCL2L13 lentivirus (10 multiplicity of infections ). Cells were grown, and lysates were collected for further processing. Immunoblot of U251 TMZ-NR and TMZ-R (scramble and BCL2L13 KD) GBM cells demonstrates successful knockdown of BCL2L13. (B, C) Representative TEM images of U251 TMZ-NR and TMZ-R scramble and BCL2L13 KD cells after 72 h , with quantification of double-membrane autophagic vacuoles from 10 cells per condition. (D, E) Representative immunoblots and densitometric analysis of LC3B-II and p62 in TMZ-NR and TMZ-R scramble and BCL2L13-KD cells cultured for 72 h in the presence or absence of BafA1 (5 nM). GAPDH was used as a loading control. (F, G) U251 TMZ-NR and TMZ-R scramble and BCL2L13 KD cells were treated with TMZ (100 uM) or corresponding control medium for 48 h (F) or 96 h (G). Apoptosis and cell-cycle distribution (G0/G1, G2/M, and S phases) were assessed by propidium iodide flow cytometry. Data represent three independent biological experiments and are presented as mean ± SD. Statistical significance is indicated in the figure (ns = $P > 0.05$, * = $P < 0.05$, ** = $P < 0.01$, *** = $P < 0.001$, **** = $P < 0.0001$).

### *3.5 BCL2L13 knockdown differentially alters mitochondrial bioenergetics in TMZ-NR and TMZ-R GBM cells.*

Previous studies have shown that BCL2 family proteins are involved in various aspects of mitochondrial function (153, 288, 289). Figure 3.5 illustrates the impact of BCL2L13 KD on mitochondrial respiration in TMZ-NR and TMZ-R GBM cells, providing insight into how this protein is associated with energy metabolism in these cellular contexts. In Panel A, oxygen consumption rate (**OCR**) profiles over time show that NR control cells maintain the highest mitochondrial activity throughout, while TMZ-R cells show lower respiratory responses following FCCP addition, with minimal additional effect of BCL2L13 KD (**Figure 3.5A**).

Panel B highlights a clear baseline metabolic difference between NR and R cells: R control cells have significantly lower basal respiration compared to NR controls ($p < 0.05$), consistent with altered mitochondrial respiration associated with TMZ resistance. Importantly, BCL2L13 KD does not further impact basal respiration in TMZ-R cells (**Figure 3.5B**). In Panel C, maximal respiratory capacity after FCCP addition is high in TMZ-NR control cells but is significantly reduced in both TMZ-R control and TMZ-R BCL2L13 KD cells ($p < 0.0001$). BCL2L13 KD in TMZ-NR cells causes a non-significant reduction in maximal respiration, whereas resistant cells, with or without BCL2L13 knockdown, show similarly reduced capacity. Therefore, resistance is associated with a marked loss of maximal mitochondrial capacity. Although BCL2L13 KD produces a modest reduction in TMZ-NR cells, this difference was not statistically significant. No statistically significant difference is observed between TMZ-R control and TMZ-R KD cells, suggesting that in resistant cells, respiratory capacity is already compromised, and BCL2L13 KD has minimal additional effect (**Figure 3.5C**).

Panel D reflects similar trends in spare respiratory capacity: TMZ-NR control cells exhibit significantly greater capacity than all other groups ($p < 0.0001$), including TMZ-NR KD, TMZ-R

control, and TMZ-R KD. Thus, BCL2L13 KD significantly reduces spare respiratory capacity in TMZ-NR cells, while producing minimal additional impairment in TMZ-R cells (**Figure 3.5D**).

Panel E shows that ATP-linked respiration is highest in TMZ-NR control cells, with a significant reduction in TMZ-R control and TMZ-R KD cells ($P < 0.001$). Moreover, TMZ-NR KD also shows a non-significant decline compared to TMZ-NR control, though it remains significantly higher than TMZ-R KD ($p < 0.05$). These findings indicate that BCL2L13 KD produces a modest, non-significant reduction in ATP-linked respiration in TMZ-NR cells, while having minimal additional effect in the TMZ-R background (**Figure 3.5E**). In Panel F, proton leak is significantly elevated in TMZ-R cells compared with TMZ-NR controls and is further increased following BCL2L13 KD in TMZ-NR cells ($P < 0.0001$), consistent with altered mitochondrial coupling (**Figure 3.5F**). Lastly, Panel G reveals that non-mitochondrial oxygen consumption is significantly higher in TMZ-NR KD compared with TMZ-R KD ($P < 0.05$), while no significant difference is observed between TMZ-NR control and TMZ-NR KD cells (**Figure 3.5G**).

Overall, TMZ resistance is associated with reduced basal and maximal respiration, diminished spare respiratory capacity, reduced ATP-linked respiration, and increased proton leak. BCL2L13 KD has a greater effect on mitochondrial bioenergetics in TMZ-NR cells, significantly reducing spare respiratory capacity and increasing proton leak, while maximal and ATP-linked respiration show more modest, non-significant reductions. In TMZ-R, where mitochondrial respiratory capacity is already compromised, BCL2L13 KD produces minimal additional impairment. Together, these findings support a context-dependent association between BCL2L13 and mitochondrial bioenergetics rather than establishing BCL2L13 as a direct determinant of mitochondrial function.

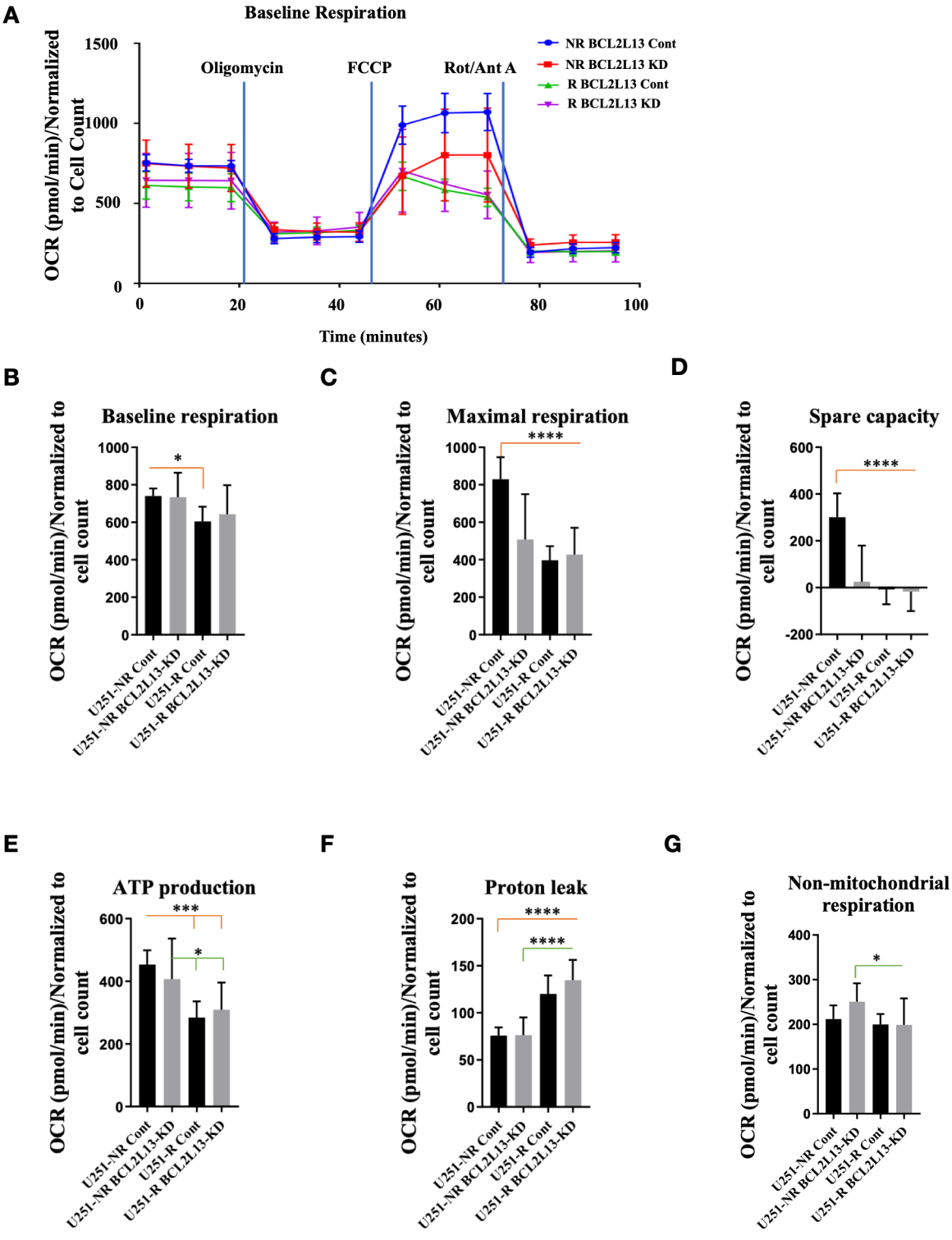
A
Baseline Respiration
OCR (pmol/min)/Normalized to Cell Count
Time (minutes)
Oligomycin
FCCP
Rot/Ant A
NR BCL2L13 Cont
NR BCL2L13 KD
R BCL2L13 Cont
R BCL2L13 KD
B
Baseline respiration
C
Maximal respiration
D
Spare capacity
E
ATP production
F
Proton leak
G
Non-mitochondrial respiration
OCR (pmol/min)/Normalized to cell count
U251-NR Cont
U251-NR BCL2L13-KD
U251-R Cont
U251-R BCL2L13-KD

**Figure 3.5. Effect of BCL2L13 knockdown on mitochondrial respiration in TMZ-NR and TMZ-R GBM cells.** (A) OCR traces from the Seahorse mitochondrial stress test. Following sequential addition of oligomycin, FCCP, and rotenone/antimycin A. (B-G) Quantification of (B) basal respiration, (C) maximal respiration, (D) spare respiratory capacity, (E) ATP-linked respiration, (F) proton leak, and (G) non-mitochondrial respiration in TMZ-NR and TMZ-R control and BCL2L13-KD cells. Data are presented as mean ± SD from at least three replicates in three independent experiments. Experiments with four or more conditions were analyzed using one-way or two-way ANOVA with Tukey's post hoc test for multiple comparisons. Statistical significance is indicated in the figure (ns = $P > 0.05$, * = $P < 0.05$, ** = $P < 0.01$, *** = $P < 0.001$, **** = $P < 0.0001$).

### *3.6 TMZ resistance is associated with distinct lipidomic remodeling further modified by BCL2L13 knockdown*

Targeted lipidomic analysis revealed distinct ceramide and complex sphingolipid profiles across TMZ-NR and TMZ-R cells with and without BCL2L13 knockdown. The heatmap (**Figure 3.6A**) demonstrated differences in ceramide and glycosylated ceramide subclasses across the four experimental groups. Both TMZ-NR and TMZ-R WT cells generally displayed higher dihydroceramides (dhCer) and monohexosylceramides (MHC) than their respective KD counterparts. In TMZ-R KD cells, several dihexosylceramide (DHC) and trihexosylceramide (THC) species, including 18:0, 20:0, and 22:0 species, were enriched, demonstrating subclass- and chain-length-specific remodeling associated with BCL2L13 KD. Principal component analysis (**PCA; Figure 3.6B**) demonstrated clear separation between TMZ-NR and TMZ-R samples. PC1 accounted for 65.7% of the total variance and represented the dominant separation between TMZ-Nr and TMZ-R cells, while PC2 accounted for an additional 17.9% of the variance. Together, PC1

and PC2 explained 83.6% of the total variance in the lipidomic dataset. TMZ-NR WT and KD samples showed substantial overlap, whereas TMZ-R WT and KD samples showed comparatively greater separation along PC2. These findings indicate that TMZ resistance represented the dominant source of global lipidomic variation, while BCL2L13 KD was associated with comparatively subtler, context-dependent differences.

The ceramide profile (**Figure 3.6C**) demonstrated chain-length-specific differences across experimental groups. Cer 16:0, a ceramide species associated with CerS6 activity, was highest in TMZ-R KD cells and was significantly elevated relative to TMZ-NR WT cells ($p \leq 0.0001$). Cer 22:0, associated with CerS2 activity, was significantly elevated in TMW-R WT relative to TMZ-NR WT cells ($p \leq 0.01$) and decreased following BCL2L13 KD in TMZ-R cells. Cer 18:0 was also significantly elevated in TMZ-R WT relative to TMz-NR WT cells ($p \leq 0.001$) and decreased following BCL2L13 KD. Cer 20:0 showed a similar abundance pattern. Cer 24:0 was highest in TMZ-R WT and decreased following KD, while Cer 24:1 was also highest in TMZ-R WT and lowest in TMZ-R KD cells. Together, these profiles demonstrate chain-length-specific ceramide remodeling associated with TMZ resistance and BCL2L13 KD.

In the dhCer panel (**Figure 3.6D**), dhCer 16:0 was significantly elevated in TMZ-R WT and TMZ-R KD relative to TMZ-NR WT cells (both $p \leq 0.0001$) and significantly decreased following BCL2L13 knockdown in TMZ-R cells ($p \leq 0.0001$). dhCer 18:0, 20:0, and 22:0 were generally enriched in TMZ-R cells, particularly TMZ-R WT, with dhCer 22:0 significantly elevated in TMZ-R KD relative to TMZ-NR WT cells ($p \leq 0.05$). dhCer 24:0 and 24:1 were consistently higher in TMZ-R than TMZ-NR cells, demonstrating a resistance-associated enrichment of very-long-chain dhCer species.

MHC species (**Figure 3.6E**) largely mirrored these patterns. MHC 16:0 was highest in TMZ-R WT cells, while MHC 24:0 was significantly elevated in TMZ-R WT relative to TMZ-NR WT cells ($p \leq 0.01$) and decreased following BCL2L13 knockdown. MHC 24:1 was significantly elevated in TMZ-R WT relative to TMZ-NR WT cells ($p \leq 0.0001$) and decreased significantly following BCL2L13 knockdown in TMZ-R cells ($p \leq 0.05$). MHC 24:1 also differed significantly between TMZ-NR WT and TMZ-R KD cells ($p \leq 0.05$).

DHC profiles (**Figure 3.6F**) demonstrated substantial resistance-associated enrichment. DHC 16:0 was significantly elevated in both TMZ-R WT and TMZ-R KD relative to TMZ-NR WT cells (both $p \leq 0.0001$). DHC 22:0 was significantly elevated in TMZ-R WT ($p \leq 0.05$) and TMZ-R KD ($p \leq 0.01$) relative to TMZ-NR WT cells. Very-long-chain DHC 24:0 and DHC 24:1 were also significantly elevated in both TMZ-R WT and TMZ-R KD relative to TMZ-NR WT cells (all $p \leq 0.0001$). Together, these findings demonstrate prominent enrichment of multiple DHC species in the TMZ-resistant background regardless of BCL2L13 expression.

THC profiles (**Figure 3.6G**) demonstrated additional context-dependent remodeling. THC 16:0 was significantly lower in TMZ-R WT relative to TMZ-NR WT cells ($p \leq 0.0001$), while BCL2L13 knockdown significantly increased THC 16:0 in TMZ-R cells ($p \leq 0.001$). TMZ-R KD remained significantly lower than TMZ-NR WT ($p \leq 0.05$). THC 18:0, 20:0, and 22:0 were highest in TMZ-R KD cells, while THC 24:0 and 24:1 displayed more variable patterns across experimental groups. THC 24:1 was significantly lower in TMZ-R WT relative to TMZ-NR WT cells ($p \leq 0.01$). Overall, Figures 3.6C–G demonstrate chain-length-, subclass-, and resistance-dependent differences in ceramide and complex sphingolipid profiles associated with BCL2L13 knockdown.

Partial Least Squares Discriminant Analysis (**PLS-DA**) was performed to identify sphingolipid species contributing to discrimination between WT and BCL2L13 KD samples. Variable Importance in Projection (VIP) scores > 1.2 were considered important contributors to group discrimination. In TMZ-NR cells (**Figure 3.6H**), prominent discriminating species included Cer 20:0, DHC 20:0, DHC 24:1, DHC 24:0, dhCer 22:0, and DHC 16:0. In TMZ-R cells (**Figure 3.6I**), Cer 22:0 and THC 18:0 were identified as prominent discriminating species. These findings identify lipid species contributing to WT/KD discrimination within each resistance condition without independently establishing the direction or statistical significance of abundance changes.

Under BCL2L13 knockdown conditions in TMZ-NR cells, KEGG pathway enrichment analysis identified several significantly enriched pathways (**Figure 3.6J**). The top five pathways based on false discovery rate (**FDR**) were steroid hormone biosynthesis, arachidonic acid metabolism, linoleic acid metabolism, alpha-linolenic acid metabolism, and neuroactive ligand–receptor interaction, all with an FDR of 2.55e-07. These results demonstrate pathway-level differences associated with BCL2L13 KD in TMZ-NR cells. In TMZ-R cells with BCL2L13 KD, KEGG pathway enrichment analysis (**Figure 3.6K**) identified two significantly enriched pathways. Neuroactive ligand–receptor interaction was the most strongly enriched pathway (enrichment strength = 1.34, FDR = 3.92e-13), followed by the calcium signaling pathway (enrichment strength = 1.21, FDR = 3.3e-04). Together, these findings demonstrate distinct pathway-level changes associated with BCL2L13 KD in TMZ-R cells.

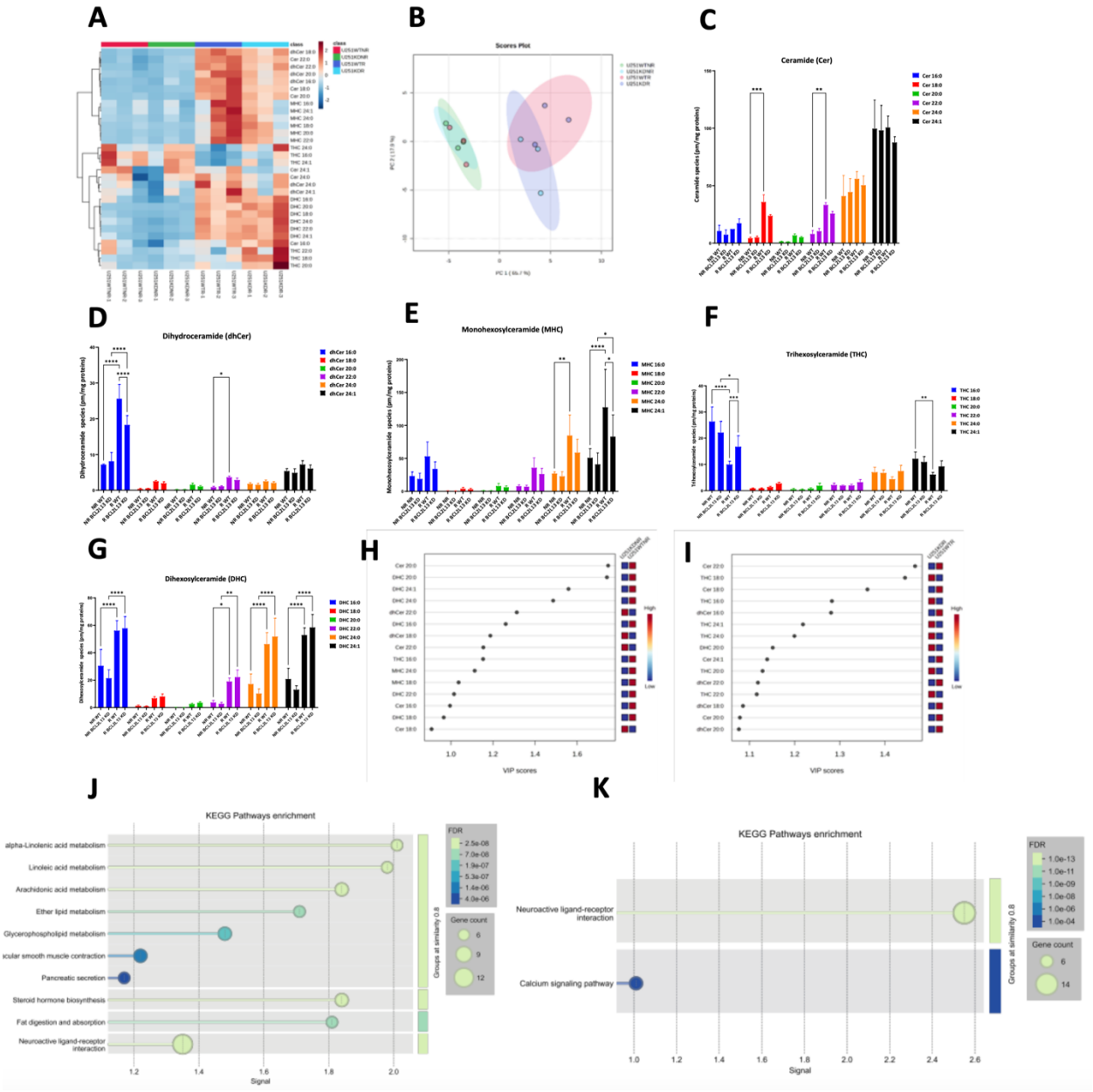


**Figure 6. Targeted lipidomic profiling of ceramide and complex sphingolipid remodeling in TMZ-NR and TMZ-R GBM cells following BCL2L13 knockdown.** (A) Heatmap of ceramide and complex sphingolipid subclasses across TMZ-NR WT, TMZ-NR KD, TMZ-R WT, and TMZ-R KD cells. TMZ-NR and TMZ-R WT cells generally exhibited higher dihydroceramides (dhCer) and monohexosylceramides (MHC) than their respective KD counterparts, while several dihexosylceramide (DHC) and trihexosylceramide (THC) species were enriched in TMZ-R KD

cells. (B) Principal component analysis (PCA) demonstrated predominant separation between TMZ-NR and TMZ-R conditions along PC1 (65.7% variance), while PC2 accounted for 17.9% of the variance; together, PC1 and PC2 accounted for 83.6% of the total variance. TMZ-NR WT and KD samples showed substantial overlap, while comparatively greater separation between TMZ-R WT and KD samples was observed along PC2. (C) Ceramide profiles demonstrated chain-length-specific differences. Cer 16:0 was highest in TMZ-R KD cells and significantly elevated relative to TMZ-NR WT cells ($p \leq 0.001$). Cer 22:0 was significantly elevated in TMZ-R WT relative to TMZ-NR WT cells ($p \leq 0.01$) and decreased following BCL2L13 knockdown in TMZ-R cells. Cer 18:0 was also significantly elevated in TMZ-R WT relative to TMZ-NR WT ($p \leq 0.001$). (D) dhCer 16:0 was significantly elevated in TMZ-R WT and TMZ-R KD relative to TMZ-NR WT (both $p \leq 0.0001$) and significantly decreased following BCL2L13 knockdown in TMZ-R cells ($p \leq 0.0001$). dhCer 22:0 was significantly elevated in TMZ-R KD relative to TMZ-NR WT ($p \leq 0.05$), while very-long-chain dhCer species were generally enriched in TMZ-R cells. (E) MHC 24:0 was significantly elevated in TMZ-R WT relative to TMZ-NR WT ($p \leq 0.01$). MHC 24:1 was significantly elevated in TMZ-R WT relative to TMZ-NR WT ($p \leq 0.0001$), decreased following BCL2L13 knockdown in TMZ-R cells ($p \leq 0.05$), and differed significantly between TMZ-NR WT and TMZ-R KD ($p \leq 0.05$). (F) DHC 16:0 was significantly elevated in both TMZ-R WT and TMZ-R KD relative to TMZ-NR WT (both $p \leq 0.0001$). DHC 22:0 was significantly elevated in TMZ-R WT ($p \leq 0.05$) and TMZ-R KD ($p \leq 0.01$) relative to TMZ-NR WT, while DHC 24:0 and 24:1 were significantly elevated in both resistant groups relative to TMZ-NR WT (all $p \leq 0.0001$). (G) THC profiles demonstrated context-dependent differences. THC 16:0 was significantly lower in TMZ-R WT relative to TMZ-NR WT ($p \leq 0.0001$) and significantly increased following BCL2L13 knockdown in TMZ-R cells ($p \leq 0.001$). THC 24:1 was significantly lower in TMZ-R

WT relative to TMZ-NR WT ($p \leq 0.01$). (H) PLS-DA/VIP analysis comparing TMZ-NR WT and BCL2L13 KD cells identified Cer 20:0, DHC 20:0, DHC 24:1, DHC 24:0, dhCer 22:0, and DHC 16:0 as prominent discriminating species. VIP scores > 1.2 were considered important contributors to group discrimination. (I) PLS-DA/VIP analysis comparing TMZ-R WT and BCL2L13 KD cells identified Cer 22:0 and THC 18:0 as prominent discriminating species. (J) KEGG pathway enrichment analysis following BCL2L13 knockdown in TMZ-NR cells identified steroid hormone biosynthesis, arachidonic acid metabolism, linoleic acid metabolism, alpha-linolenic acid metabolism, and neuroactive ligand–receptor interaction as the top five enriched pathways (FDR = $2.55 \times 10^{-7}$). (K) KEGG pathway enrichment analysis following BCL2L13 knockdown in TMZ-R cells identified neuroactive ligand–receptor interaction (enrichment strength = 1.34, FDR = $3.92 \times 10^{-13}$) and calcium signaling (enrichment strength = 1.21, FDR = 0.00033) as significantly enriched pathways. Statistical significance is indicated in the figure (ns = P > 0.05, * = P < 0.05, ** = P < 0.01, *** = P <0.001, **** = P < 0.0001).

# CHAPTER 4: Discussion

In the realm of GBM, TMZ resistance often finds its roots in disrupted cell death and autophagy mechanisms. Adept at evading apoptosis, GBM cells further fortify their resistance through alterations in apoptotic pathways. These alterations, including mutations in genes like TP53 and changes in pro- and anti-apoptotic proteins, contribute to treatment resistance (290, 291). Concurrently, autophagy can paradoxically bolster cell survival under stress conditions. In GBM, upregulated autophagy aids cancer cells withstanding chemotherapy by eliminating damaged organelles and proteins, thereby sustaining cellular metabolism and growth (292, 293). Due to the multifaceted nature of these resistance mechanisms, pinpointing precise targets for intervention remains a significant scientific and clinical challenge.

BCL2L13 is a pivotal protein with multifaceted roles in cancer, particularly GBM, and is involved in both apoptosis and mitophagy in GBM (294). Elevated levels of BCL2L13 have been observed in GBM, and it has also been identified as a ceramide synthase inhibitor (156). Additionally, it enhances mitophagy by promoting mitochondrial fission through dynamin-1-like protein (**DNM1L**) (295). Furthermore, BCL2L13 influences apoptosis. Previous research demonstrated that overexpression of BCL2L13 in GBM cells significantly inhibits caspase activation, whereas silencing BCL2L13 leads to increased caspase maturation (156). Together, these findings position BCL2L13 at an intersection between apoptosis, mitochondrial homeostasis, autophagy, and ceramide metabolism. To elucidate the role of BCL2L13 in TMZ-R and TMZ-NR GBM cells, this study examined BCL2L13 expression, autophagic flux, mitochondrial bioenergetics, and lipidomic remodeling in both cellular contexts.

Acquired TMZ resistance significantly limits treatment effectiveness, with over 90% of recurrent gliomas not responding to a second cycle of chemotherapy (296). Numerous studies

have investigated TMZ resistance using established GBM cell lines that are either naturally TMZ-NR or TMZ-R due to genomic alterations in MGMT or p53, revealing mechanisms of inherited TMZ resistance (297, 298). However, there are only a few studies on acquired TMZ resistance, primarily because developing models of acquired resistance through chronic TMZ treatment is time-consuming (100, 297, 299). Using our acquired TMZ-R U251 GBM model, our findings reveal that TMZ-R cells demonstrate lower susceptibility to TMZ, sustained regrowth, reduced apoptotic-like morphology, reduced G2/M cell-cycle arrest, and reduced apoptosis compared with TMZ-NR cells. These characteristics closely resemble acquired TMZ resistance and support the use of this 18-week pulsed TMZ selection protocol to generate an acquired TMZ-resistant U251 GBM model. Consistent with these findings, Zhu et al. (299) reported increased proliferative capacity, reduced G2/M arrest, increased DNA replication, and diminished apoptosis following TMZ exposure in resistant GBM cells. TMZ preferentially induced G2/M arrest in our TMZ-NR cells, consistent with previous reports (300, 301), whereas TMZ-R cells exhibited substantially lessG2/M arrest and apoptosis following treatment. Together, these findings validate the resistant phenotype of the model and provide the experimental context in which the subsequent autophagic, mitochondrial, and lipidomic differences were examines.

After establishing TMZ resistance, we investigated autophagy as a potential component of the resistant phenotype. Autophagy has a complex relationship with TMZ resistance and can support cancer cell survival by removing damaged cellular components and maintaining metabolic homeostasis during therapeutic stress (302, 303). Chemoradiotherapy can induce autophagy in glioma, and modulation of autophagy has consequently been investigated as a strategy for altering treatment sensitivity (302, 304). Induced autophagy has been reported to delay radiation-induced cell death and contribute to TMZ resistance (305, 306), while inhibition of autophagy-related

processes can increase sensitivity to TMZ or radiotherapy in experimental models (307). A mechanistic study demonstrated that sertindole inhibited autophagic flux by suppressing the lysosomal enzymes CTSD and CTSB, thereby reducing glioblastoma cell growth (308). Although autophagy commonly promotes tumour cell survival, it can also contribute to programmed.cell death, highlighting is context-dependent role in glioma therapy (309).

The current study identified impaired autophagic flux in TMZ-R GBM cells. Previous research examining LC3, Beclin 1, and autophagic flux in low- and high-grade gliomas reported higher expression of autophagy proteins and greater autophagic turnover in high-grade gliomas (310). However, inhibition of late-stage autophagy can impair cellular energy recycling and cause accumulation of nondegradable autophagic vesicles, ultimately promoting tumour cell death (304). Furthermore, combining autophagy flux inhibitors with autophagy-inducing therapies, such as radiotherapy or TMZ, may enhance autophagosome accumulation and increase tumour cell sensitivity to cytotoxic treatment. Accordingly, autophagy inhibitors such as CQ or HCQ have been investigated as strategies to enhance therapeutic sensitivity (311, 312).

The cell cycle is tightly regulated by checkpoints that coordinate cell growth, DNA replication, and division process of cell division, and it is controlled by various checkpoints that ensure proper division and DNA integrity (313). Autophagy flux can influence cell cycle progression by maintaining cellular energy availability and removing damaged cellular components that can hinder cell division. During cellular stress, autophagy provides metabolites that support survival and can delay cell-cycle progression until conditions improve (314, 315). Autophagy can also regulate cell-cycle proteins, including the cyclin-dependent kinase inhibitors p21 and p27, thereby influencing cell-cycle progression (316, 317).

Inhibition of autophagic flux can further disrupt cell-cycle progression through the accumulation of damaged proteins and organelles, contributing to oxidative stress, DNA damage, and activation of cell-cycle checkpoints (317, 318). Impaired degradation of cell-cycle regulators, including cyclin D1, may also contribute to cell-cycle arrest (317). Furthermore, disruption of autophagic recycling can compromise cellular energy and nutrient availability required for progression through energy-demanding phases of the cell cycle, including S and G2/M (319).

Cj et al. (310) attributed elevated autophagy protein levels in high-grade glioma to increased autophagic turnover. However, elevated autophagy proteins may reflect either increased autophagic activity or impaired degradation at a late stage of the pathway. Therefore, autophagic flux must be assessed to distinguish between these possibilities. An autophagic flux assay using BafA1 was performed to distinguish between increased autophagic activity and impaired degradation. In TMZ-NR cells, LC3B-II and p62 decreased over 72 h, while BafA1 treatment caused their accumulation, consistent with intact autophagic flux. In contrast, LC3B-II and p62 accumulated over time in TMZ-R cells, with no further accumulation following BafA1 treatment, indicating impaired late-stage autophagic turnover. Consistent with these findings, ICC and TEM demonstrated increased LC3B puncta and accumulation of double-membrane autophagic vacuoles in TMZ-R cells. Together, these findings support impaired autophagic flux in TMZ-R GBM cells, with accumulation of autophagic material resulting from defective late-stage turnover rather than increased autophagic activity.

Given the observed differences in autophagic flux between TMZ-NR and TMZ-R cells, we next investigated BCL2L13, a protein implicated in mitochondrial homeostasis, mitophagy, and apoptosis. BCL2L13 has been associated with mitochondrial membrane potential regulation and cell survival and death (294), while higher expression levels in GBM has been associated with

tumour progression and resistance to apoptosis (294, 320). BCL2L13 has also been shown to promote DNM1L-mediated mitochondrial fission and mitophagy in GBM (295). Furthermore, Jensen et al. demonstrated that BCL2L13 overexpression inhibited caspase activation, whereas BCL2L13 silencing increased caspase maturation, supporting an anti-apoptotic role in GBM cells (156). In the present study, BCL2L13 expression was significantly higher in TMZ-R than TMZ-NR cells. This finding prompted further investigation of whether BCL2L13 was associated with the altered autophagic and cell-death responses observed in the resistant phenotype.

To investigate the relationship between BCL2L13 and autophagy, BCL2L13 was knocked down in TMZ-NR and TMZ-R GBM cells. BCL2L13 knockdown produced distinct autophagic responses depending on resistance status. In TMZ-NR cells, knockdown increased LC3B-II without significantly altering p62, whereas in TMZ-R cells, knockdown decreased LC3B-II and increased p62 degradation. BafA1 further increased LC3B-II accumulation in TMZ-NR cells but produced little additional change in TMZ-R cells. Together, these findings suggest that BCL2L13 is associated with context-dependent alterations in autophagy-related markers, without producing a corresponding significant change in autophagic vacuole accumulation.

This context-dependent relationship is consistent with previous evidence linking BCL2L13 to autophagic processes. BCL2L13 can interact with LC3B and recruit the ULK1 complex during mitophagy, supporting its proposed function as a mammalian homologue of ATG32 (321). BCL2L13 has also been shown to promote DNM1L-mediated mitochondrial fission and mitophagy in GBM cells (295).

Despite its reported anti-apoptotic role, BCL2L13 knockdown did not significantly alter TMZ-induced apoptosis in TMZ-R cells in the present study. Previous work demonstrated that BCL2L13 can inhibit apoptosis in GBM through interactions involving CerS2 and CerS6, limiting

BAX activation, mitochondrial outer membrane permeabilization (MOMP), cytochrome c release, and subsequent caspase activation (156, 320, 322). However, BCL2L13 can exhibit context-dependent apoptotic functions; its overexpression in HEK293T and HeLa cells has been shown to induce cytochrome c release and apoptosis (153, 320).

In PC3 cells, BCL2L13 was also shown to interact with adenine nucleotide translocator (ANT), promoting cytochrome c release through alterations in mitochondrial permeability (154). BCL2L13 therefore has reported roles in both apoptosis and mitophagy, potentially linking mitochondrial quality control with cell-death regulation(323, 324).

Previous studies have shown that BCL-2 family proteins regulate mitochondrial function beyond their canonical roles in apoptosis (289). For example, BCL-xL interacts with F1FO ATP synthase to reduce proton leak and enhance ATP generation (325), while MCL-1contributes to the maintenance of oxidative phosphorylation (326, 327). Pro-apoptotic BCL-2 family members also contribute to metabolic regulation; for example, the BH3-only protein BAD associates with mitochondrial glucokinase, linking glycolysis with apoptosis signaling (328). Accordingly, alterations in BCL-2 family activity can affect cellular bioenergetics (329). BCL-2 can also modulate mitochondrial bioenergetics indirectly through $Ca^{2+}$ signaling by binding IP3 receptors at the endoplasmic reticulum and limiting $Ca^{2+}$ release to mitochondria (330).

Mechanistically, BCL2L13 has been shown to promote DNM1L-dependent mitochondrial fission and mitophagy, contributing to GBM cell proliferation and invasion (295). These findings suggest that elevated BCL2L13 in GBM may support mitochondrial homeostasis under cellular stress. Beyond cancer, BCL2L13 has also been implicated in regulating calcium homeostasis at ER–mitochondria contact sites in muscle cells (331), further supporting its broader involvement

in mitochondrial physiology. BCL2L13 has additionally been associated with mitochondrial bioenergetics and oxidative phosphorylation (320).

Metabolic reprogramming is a hallmark of GBM and contributes to therapy resistance. GBM cells can preferentially utilize glycolysis even in the presence of oxygen through the Warburg effect (332). In our Seahorse assays, TMZ-R GBM cells exhibited significantly lower basal oxygen consumption rates than TMZ-NR cells, demonstrating reduced basal mitochondrial respiration. This metabolic difference is consistent with reports that stem-like or drug-resistant glioma cells can exhibit attenuated maximal respiration and spare respiratory capacity (333). Although previous studies suggest that TMZ-R glioma cells may retain dependence on mitochondrial function, as inhibition of OXPHOS can preferentially affect TMZ-R cells (334), our findings demonstrate that TMZ resistance was associated with compromised mitochondrial respiratory capacity.

BCL2L13 knockdown in TMZ-NR GBM cells reduced mitochondrial respiratory flexibility. Under FCCP-induced stress, BCL2L13-deficient TMZ-NR cells showed reduced maximal respiration and spare respiratory capacity, resembling the compromised respiratory phenotype observed in TMZ-R cells. In contrast, BCL2L13 knockdown had comparatively little additional effect on mitochondrial respiration in TMZ-R cells, suggesting that the already compromised respiratory phenotype associated with TMZ resistance may limit the detectable effect of BCL2L13 loss. Together, these findings suggest that BCL2L13 is associated with the maintenance of mitochondrial respiratory capacity, with its effects being more evident in TMZ-NR than TMZ-R cells.

BCL2L13 knockdown also affected mitochondrial respiratory function, although these effects varied with TMZ resistance status. The reduced maximal respiration and spare respiratory capacity observed following BCL2L13 knockdown in TMZ-NR cells indicate a diminished ability

to respond to energetic stress. In contrast, TMZ-R cells already exhibited reduced mitochondrial respiratory function, with BCL2L13 knockdown producing comparatively little additional impairment. Together, these findings further support a context-dependent association between BCL2L13 and mitochondrial bioenergetics in GBM cells.

In GBM cells, BCL2L13 has been shown to promote DNM1L-mediated mitochondrial fission and mitophagy (295). supporting a role in mitochondrial quality control. However, the effects of BCL2L13 appear to be context-dependent. In differentiating stem cells, BCL2L13 knockdown was associated with increased mitophagy and a shift toward glycolytic metabolism, potentially as a compensatory response to mitochondrial stress (288). Together, these findings suggest that BCL2L13 may influence mitochondrial turnover and metabolic function in a cell context-dependent manner.

Beyond GBM, BCL2L13 has been implicated in mitochondrial metabolism and apoptosis across different cellular contexts. During adipocyte differentiation, BCL2L13 silencing impaired oxidative phosphorylation and was associated with a shift toward glycolytic metabolism (288). BCL2L13 has also been reported to interact with mitochondrial proteins including VDAC and ANT, linking it to regulation of mitochondrial membrane permeabilization and cytochrome c release (335). Conversely, BCL2L13 overexpression has demonstrated pro-apoptotic activity in other cellular contexts, further highlighting its context-dependent functions (153).

Together, these findings highlight the context-dependent role of BCL2L13 in mitochondrial function. In the present study, BCL2L13 knockdown reduced maximal respiration and spare respiratory capacity in TMZ-NR cells, resulting in a respiratory phenotype that more closely resembled TMZ-R cells. In contrast, BCL2L13 knockdown produced comparatively little additional impairment in TMZ-R cells, which already exhibited reduced mitochondrial respiratory

capacity. These findings suggest that BCL2L13 is associated with the maintenance of mitochondrial respiratory capacity in TMZ-NR cells, whereas TMZ resistance appears to be the dominant determinant of the compromised mitochondrial phenotype in TMZ-R cells.

Lipid metabolism has an important role in GBM progression and therapeutic resistance. Our findings demonstrate resistance-associated ceramide remodeling with additional context-dependent changes following BCL2L13 knockdown, supporting an association between BCL2L13 and sphingolipid metabolism. Lipids contribute to cell growth, proliferation, apoptosis, chemotherapeutic response, and drug resistance in cancer, and glioma cells exhibit substantial alterations in lipid metabolism (281, 336, 337). Taib et al. demonstrated accumulation of several lipid classes in GBM cells, including ceramides, phospholipids, diglycerides, triglycerides, and sphingomyelins. GBM cells can also rely on de novo lipid synthesis under nutrient-deprived conditions, highlighting lipid metabolism as a potential therapeutic vulnerability (281). Among these lipids, ceramides are particularly relevant because of their roles in apoptosis and autophagy and their previously reported association with BCL2L13 (156).

Previous studies suggest that targeting ceramide metabolism may influence therapeutic response in GBM. Manipulation of ceramide metabolic pathways, including inhibition of glucosylceramide synthase, has been investigated as a strategy to increase ceramide accumulation and promote apoptosis (338). Navone et al. demonstrated that luteolin shifted the sphingolipid rheostat toward ceramide production and increased TMZ sensitivity in primary GBM stem cells (339). Together, these findings support continued investigation of ceramide and sphingolipid metabolism as potential therapeutic targets in GBM.

Ceramides have important signaling roles in cellular stress responses, apoptosis, proliferation, and differentiation (156). Within sphingolipid metabolism, ceramide generally

promotes cell death, whereas sphingosine-1-phosphate (S1P) promotes cell survival and chemoresistance. Ceramide can also promote lethal mitophagy, in which extensive mitochondrial degradation contributes to apoptosis-independent cancer cell death (340). The balance between ceramide and S1P, often referred to as the sphingolipid rheostat, therefore influences cancer cell survival, and shifting this balance toward ceramide signaling may promote tumour cell death (341). Ceramide synthases also contribute to mitochondrial outer membrane MOMP and cytochrome c release during apoptosis, further linking ceramide metabolism to apoptotic regulation in GBM (156).

CerS2 and CerS6 generate distinct ceramide species and have been implicated in apoptotic regulation in GBM. Previous studies demonstrated that CerS2 and CerS6 overexpression enhanced caspase activation in GBM cells, whereas their inhibition reduced this response (156). BCL2L13 has been reported to interact with CerS2 and CerS6 and inhibit their activity (342). BCL2L13 knockdown has also been shown to increase CerS2 and CerS6 activity at the mitochondrial membrane (156). These findings provided the rationale for investigating whether BCL2L13 knockdown was associated with changes in ceramide profiles in the present study. Reduced ceramide levels have also been associated with higher-grade gliomas and enhanced GBM cell survival (156, 250), further supporting the relevance of ceramide metabolism to GBM biology.

Our results demonstrated distinct lipid profiles between TMZ-NR and TMZ-R GBM cells, with TMZ resistance representing the predominant source of lipidomic variation. The heatmap showed that dhCer and MHC species were generally higher in TMZ-NR and TMZ-R WT cells than in their respective BCL2L13 KD counterparts. In TMZ-R cells, BCL2L13 knockdown was associated with enrichment of several DHC and THC species, including THC 18:0, 20:0, and 22:0.

Together, these findings indicate that BCL2L13 knockdown is associated with subclass- and chain-length-specific lipid remodeling rather than a uniform increase or decrease in ceramide species.

dhCer species have been implicated in autophagy, oxidative and ER stress, as well as immunoregulatory and antiproliferative processes. Oxidative stress and hypoxia may also promote dhCer accumulation (343). dhCers have been shown to promote autophagosome formation in prostate cancer cells following treatment with fenretinide, a dihydroceramide desaturase inhibitor, or exogenous short-chain dhCer (344). Subsequent studies further supported a role for dhCer in autophagy (345, 346). In GBM, accumulation of dihydrosphingosine and dhCer, together with ER stress and autophagy, has been associated with cell death following combined sphingosine kinase inhibition and TMZ treatment (347).

Our findings demonstrated chain-length-specific differences in ceramide profiles across TMZ resistance and BCL2L13 knockdown conditions. Cer 18:0 was significantly elevated in TMZ-R WT compared with TMZ-NR WT cells and decreased following BCL2L13 knockdown in TMZ-R cells. Similar patterns were observed for Cer 20:0 and Cer 22:0, with Cer 22:0 significantly elevated in TMZ-R WT compared with TMZ-NR WT cells. Cer 24:0 and Cer 24:1 were also highest in TMZ-R WT cells and decreased following BCL2L13 knockdown. CerS2 preferentially synthesizes very-long-chain ceramides, including C20–C26 species, while BCL2L13 has been reported to inhibit CerS2 and CerS6 activity (156). These findings are therefore consistent with a context-dependent association between BCL2L13 and CerS-associated ceramide remodeling, although the present lipidomic analysis does not directly establish altered CerS activity. CerS2 is the only CerS containing motifs similar to S1P receptors, and S1P has been reported to inhibit ceramide synthesis in cells overexpressing CerS2 (348, 349). CerS2 has an important role in sphingolipid metabolism and has been implicated in cellular proliferation,

apoptosis, and tissue homeostasis. CerS2-deficient mice exhibit increased hepatocyte proliferation and apoptosis as well as pathological changes in the brain (207, 350, 351), suggesting that loss of CerS2 may contribute to carcinogenic processes. CerS2 has also been implicated in cellular responses to radiation, with overexpression associated with delayed apoptosis (349, 352). Furthermore, CerS2 suppression has been associated with ER stress, activation of the unfolded protein response (UPR), and increased autophagy (250, 353). CerS2 loss has also been associated with altered expression of cell-cycle regulators and genes involved in signaling and fatty acid metabolism (250, 353). Together, these studies demonstrate that CerS2 influences multiple cellular stress and metabolic pathways relevant to cancer.

Cer 16:0 also demonstrated a resistance-dependent response to BCL2L13 knockdown, with the highest levels observed in TMZ-R KD cells and the lowest levels in TMZ-NR KD cells. This contrasting response indicates that BCL2L13 knockdown is associated with context-dependent Cer 16:0 remodeling rather than a uniform increase in Cer 16:0. CerS6 preferentially synthesizes C14 and C16 ceramides and has been implicated in cancer development (249). CerS6 activity has been associated with apoptotic signaling through CD95 and tumour cell death(244, 354), while CerS6 knockdown has been reported to protect against apoptosis (248). In head and neck squamous cell carcinoma, CerS6 downregulation reduced Cer 16:0 and was associated with ER stress and activation of the unfolded protein response, whereas CerS6 overexpression promoted proliferation (355). CerS6 has also been implicated in TRAIL-mediated apoptosis, with CerS6 overexpression restoring TRAIL sensitivity in resistant colon carcinoma cells (248). CerS6-dependent ceramide signaling has additionally been associated with CD95-mediated chemotherapy responses (356). ROS can also contribute to oxidative mitochondrial damage and apoptotic signaling (357).

Together, these studies highlight the context-dependent role of CerS6 and Cer 16:0 in cancer cell stress and apoptotic responses.

Knockdown of BCL2L13 in TMZ-NR cells led to significant enrichment of lipid metabolic pathways, including steroid hormone biosynthesis, arachidonic acid, linoleic acid, and α-linolenic acid metabolism (all FDR ≈2.5×10^–7) (Figure 6J). These findings suggest that loss of BCL2L13 perturbs lipid homeostasis, consistent with its role in autophagy and mitochondrial function. Notably, autophagy (particularly lipophagy) is essential for mobilizing cholesterol and fatty acids for steroidogenesis; inhibiting autophagy can dysregulate steroid hormone production and lipid metabolism gene expression (358). BCL2L13 itself is a mitophagy receptor required for clearing damaged mitochondria (178). Its deficiency leads to accumulation of dysfunctional mitochondria and oxidative stress, forcing cells to rewire their metabolism (178). Accordingly, anti-apoptotic BCL-2 family proteins are known to support mitochondrial energetics beyond apoptosis – for example, BCL-2/BCL-XL overexpression enhances oxidative phosphorylation and ATP generation in cancer cells (increasing Complex I activity and oxygen consumption (359). Loss of BCL2L13 would thus be expected to compromise respiratory capacity and trigger compensatory upregulation of lipid biosynthetic pathways to meet energy demands. This aligns with our observation of increased LC3-II in BCL2L13-depleted sensitive cells (indicative of altered autophagic flux) (Figure 4) and the enrichment of lipid-signaling KEGG pathways, pointing to a metabolic stress response. Supporting this, Seahorse analysis (**Figure 5**) revealed that BCL2L13 knockdown in TMZ-NR cells led to marked reductions in maximal and spare respiratory capacity and modestly impaired ATP-linked respiration, mimicking the low-capacity phenotype seen in resistant cells. These bioenergetic deficits may promote compensatory activation of lipid biosynthesis and remodeling pathways identified in KEGG enrichment.

In TMZ-R cells, BCL2L13 knockdown primarily altered signaling pathways. KEGG analysis identified Neuroactive Ligand–Receptor Interaction as the top hit (14 genes, FDR ~3.9×10^–13) and the Calcium Signaling pathway as second (6 genes, FDR ~3.3×10^–4). These shifts highlight that disrupting BCL2L13 in the resistant context affects cell communication and $Ca^{2+}$-homeostasis more than core metabolism. Notably, BCL-2 family proteins are key modulators of intracellular $Ca^{2+}$ dynamics. For example, BCL-2 localized to the ER inhibits IP3 receptor–mediated $Ca^{2+}$ release, thereby dampening calcium signaling and apoptotic cascades (360). Thus, BCL2L13 loss may exacerbate $Ca^{2+}$ dysregulation in TMZ-resistant cells, consistent with the enrichment of calcium-signaling genes (e.g. NOS2, HTR2C, TACR3). Furthermore, enrichment of the neuroactive ligand–receptor pathway (including opioid, cannabinoid, and serotonin receptors) suggests a broader stress-adaptive response in resistant GBM cells lacking BCL2L13. Such receptors have been implicated in glioma survival and may be upregulated as a compensatory mechanism when mitochondrial and autophagic function is impaired, echoing the known crosstalk between mitochondrial stress and cell signaling pathways (361). Overall, our KEGG analysis suggests that BCL2L13 depletion induces profound metabolic remodeling in TMZ-NR cells, favouring lipid-related pathways, while provoking alterations in $Ca^{2+}$-linked signaling and receptor networks in TMZ-R cells. These findings are consistent with the established role of BCL2L13 in mitophagy and the broader influence of BCL-2 family proteins on cellular metabolism and calcium homeostasis. Furthermore, Seahorse metabolic profiling (**Figure 5**) demonstrated that BCL2L13 knockdown in TMZ-R cells, which already exhibit profoundly reduced respiratory function, does not further impair maximal or ATP-linked respiration but exacerbates proton leak, highlighting persistent mitochondrial dysfunction potentially linked to calcium signaling alterations identified by KEGG analysis.

# CHAPTER 5: Future Directions

## *5.1 Investigating the roles of CerS2 and CerS6*

To further elucidate the roles of ceramide synthase 2 (CerS2) and ceramide synthase 6 (CerS6) in TMZ resistance, future studies should directly manipulate CerS2 and CerS6 in TMZ-R and TMZ-NR GBM cells. These enzymes generate distinct ceramide species, with CerS2 preferentially synthesizing very-long-chain ceramides and CerS6 primarily generating C16 ceramide. These ceramide species have distinct roles in cellular signaling, apoptosis, and stress responses (294).

The present lipidomic findings demonstrated resistance- and chain-length-dependent ceramide remodeling associated with BCL2L13 KD. Direct genetic or pharmacological manipulation of CerS2 and CerS6, followed by lipidomic analysis and functional assessment of autophagy, apoptosis, and TMZ sensitivity, would help determine whether these enzymes contribute to the observed lipid remodeling and cellular phenotypes. Comparing these effects between TMZ-R and TMZ-NR cells would further establish whether CerS-associated functions depend on TMZ resistance status.

Importantly, these experiments would provide functional evidence beyond the associations identified by the present lipidomic analysis and clarify whether CerS2- or CerS6-associated pathways represent potential therapeutic vulnerabilities in TMZ-R GBM.

## *5.2 Investigating the relationship between autophagy flux Inhibition and the unfolded protein response (UPR)*

The unfolded protein response (UPR) is closely interconnected with autophagy during cellular stress and may contribute to the impaired autophagic flux observed in TMZ-R cells. UPR

activation can modulate autophagy through several signaling mechanisms (362). The UPR is activated in response to the accumulation of misfolded proteins in the endoplasmic reticulum (ER). It aims to restore ER homeostasis by enhancing protein folding capacity, degrading misfolded proteins, and attenuating protein synthesis. However, prolonged UPR activation can lead to cell death. The UPR is primarily mediated through the PERK, IRE1α, and ATF6 signaling branches, which coordinate cellular responses to endoplasmic reticulum (ER) stress and have been implicated in autophagy regulation (363). Future studies should determine whether impaired autophagic flux in TMZ-R cells is associated with altered UPR activation by comparing UPR-related proteins and signaling pathways between TMZ-R and TMZ-NR cells following TMZ treatment. In particular, assessment of PERK/eIF2α/ATF4, IRE1α/XBP1, and ATF6 signaling alongside autophagic flux would help define the relationship between ER stress and the autophagic phenotype identified in TMZ-R cells (363). Genetic or pharmacological modulation of these pathways could then determine whether altered UPR signaling contributes to impaired autophagic flux and whether its modulation influences TMZ-induced apoptosis.

### *5.3 Subcellular fractionation and lipidomics*

To further characterize the lipid remodeling identified in the present study, future studies should combine subcellular fractionation with targeted lipidomics in TMZ-R and TMZ-NR GBM cells. Isolation of mitochondrial, cytosolic, and nuclear fractions would allow determination of whether the observed lipid alterations, including changes in ceramide species, are localized to specific cellular compartments.

Mitochondrial lipid composition is particularly relevant because alterations in membrane lipids can influence mitochondrial membrane integrity, respiratory function, and the release of pro-apoptotic factors (364). Compartment-specific analysis could therefore help determine whether the

ceramide remodeling observed in TMZ-R cells and following BCL2L13 knockdown is associated with the mitochondrial and apoptotic phenotypes identified in the present study.

Cytosolic lipids can also function as signaling molecules that influence pathways involved in autophagy and apoptosis, while nuclear lipids can affect processes including chromatin organization, gene transcription, and DNA repair (365). Comparing lipid profiles across these compartments would provide greater insight into the cellular localization and potential functional significance of the lipid alterations associated with TMZ resistance and BCL2L13 knockdown.

Together, subcellular fractionation and lipidomics would extend the present whole-cell lipidomic analysis by determining where resistance- and BCL2L13-associated lipid remodeling occurs and provide a foundation for subsequent functional investigation of these lipid changes.

### *5.4 Therapeutic targeting of TMZ-R GBM cells*

If TMZ-R GBM cells could be selectively targeted, the distinct cellular vulnerabilities identified in the present study may provide opportunities for combination treatment strategies. TMZ-R cells exhibited impaired autophagic flux, reduced mitochondrial capacity, and distinct ceramide remodeling compared with TMZ-NR cells. These differences suggest that therapeutic strategies directed specifically towards the resistant population could exploit pathways important for TMZ-R cell survival while maintaining the activity of TMZ against responsive tumour cells.

One potential strategy would be to further disrupt autophagic or mitochondrial homeostasis in TMZ-R cells. Autophagy inhibitors have been investigated as a means of enhancing therapeutic sensitivity in GBM (311, 312). Mitochondrial metabolism may represent another therapeutic vulnerability, as inhibition of oxidative phosphorylation has been reported to preferentially affect TMZ-R GBM cells (334). Although BCL2L13 KD did not restore TMZ-induced apoptosis in the present study, it's context-dependent associations with autophagy,

mitochondrial function, and lipid remodeling suggest that BCL2L13-associated pathways may reveal additional therapeutic vulnerabilities in TMZ-R GBM.

Alternatively, the distinct sphingolipid profiles observed in TMZ-R cells support investigation of ceramide metabolism as a therapeutic target. Manipulation of sphingolipid metabolism has been shown to influence GBM cell survival and response to TMZ (338, 339). Future studies could determine whether targeting CerS2-, CerS6-, or other sphingolipid-associated pathways selectively compromises TMZ-R cell survival.

A potential therapeutic approach could therefore combine TMZ with an agent that specifically targets vulnerabilities in TMZ-R cells, such as altered autophagy, mitochondrial function, or lipid metabolism. This combination could target both TMZ-NR and TMZ-R tumour cell populations. Future studies in patient-derived and in vivo GBM models would be required to evaluate the efficacy and selectivity of this approach.

# CHAPTER 6: Conclusion

Glioblastoma remains one of the most aggressive and treatment-resistant malignancies, with the development of TMZ resistance representing a major obstacle to successful treatment. In this study, we investigated the role of BCL2L13 in autophagy, mitochondrial function, and ceramide metabolism in TMZ-resistant glioblastoma cells. Our findings demonstrate that TMZ-resistant cells exhibit impaired autophagy flux, reduced sensitivity to TMZ-induced apoptosis, compromised mitochondrial respiratory capacity, and distinct sphingolipid remodeling. Furthermore, BCL2L13 expression was significantly elevated in TMZ-resistant cells, supporting it's potential role for BCL2L13 in resistance-associated cellular adaptation.

BCL2L13 knockdown produced context-dependent effects in TMZ-resistant and TMZ-non-resistant cells. Although BCL2L13 knockdown did not significantly alter TMZ-induced apoptosis or autophagosome accumulation, changes in autophagy-related markers were observed and differed according to resistance status. BCL2L13 knockdown was also associated with altered mitochondrial respiration, with effects on maximal respiration and spare respiratory capacity being more evident in TMZ-non-resistant cells. Lipidomic analysis revealed resistance-, subclass-, and chain-length-specific remodeling of ceramide and related sphingolipid species associated with BCL2L13 knockdown. Importantly, TMZ resistance remained the predominant determinant of the mitochondrial and lipidomic phenotypes. Together, these findings support a context-dependent association between BCL2L13, autophagy, mitochondrial function, and ceramide metabolism in glioblastoma.

Collectively, this work demonstrates that BCL2L13 is associated with cellular pathways that differ according to TMZ resistance status. Rather than acting as a direct determinant of TMZ resistance, BCL2L13 may contribute to resistance-associated changes in autophagy, mitochondrial bioenergetics, and ceramide lipid remodeling. This study provides a foundation for future studies investigating BCL2L13-associated pathways, CerS2 and CerS6 function, UPR signaling, and compartment-specific lipid remodeling, as well as whether these pathways represent therapeutic vulnerabilities that can be selectively exploited in TMZ-resistant glioblastoma.

# CHAPTER 7: Bibliography


1. Khosla D. Concurrent therapy to enhance radiotherapeutic outcomes in glioblastoma. Ann Transl Med. 2016;4(3):54.
2. Treton Smith YY, Emily Walker, Faith Davis. Brain Tumour Registry of Canada (BTRC): Incidence Report 2010-2015 2019 [Available from: https://braintumourregistry.ca/incidence-report/.
3. Louis DN, Perry A, Reifenberger G, von Deimling A, Figarella-Branger D, Cavenee WK, et al. The 2016 World Health Organization Classification of Tumors of the Central Nervous System: a summary. Acta Neuropathol. 2016;131(6):803-20.
4. Freeman MR, Rowitch DH. Evolving concepts of gliogenesis: a look way back and ahead to the next 25 years. Neuron. 2013;80(3):613-23.
5. Liu Y, Lang F, Chou FJ, Zaghloul KA, Yang C. Isocitrate Dehydrogenase Mutations in Glioma: Genetics, Biochemistry, and Clinical Indications. Biomedicines. 2020;8(9).
6. Han S, Liu Y, Cai SJ, Qian M, Ding J, Larion M, et al. IDH mutation in glioma: molecular mechanisms and potential therapeutic targets. Br J Cancer. 2020;122(11):1580-9.
7. Louis DN, Perry, A, Wesseling P, et al. . The 2021 WHO Classification of Tumors of the Central Nervous System: a summary. Neuro Oncol. 2021;23(8):1231-51.
8. Institute NC. NCI Dictionaries 2022 [cited 2022. Available from: https://www.cancer.gov/publications/dictionaries/cancer-terms/def/five-year-survival-rate.
9. Ostrom QT, Gittleman H, Xu J, Kromer C, Wolinsky Y, Kruchko C, et al. CBTRUS Statistical Report: Primary Brain and Other Central Nervous System Tumors Diagnosed in the United States in 2009-2013. Neuro Oncol. 2016;18(suppl_5):v1-v75.
10. Stupp R, Hegi ME, Mason WP, van den Bent MJ, Taphoorn MJ, Janzer RC, et al. Effects of radiotherapy with concomitant and adjuvant temozolomide versus radiotherapy alone on survival in glioblastoma in a randomised phase III study: 5-year analysis of the EORTC-NCIC trial. Lancet Oncol. 2009;10(5):459-66.
11. Fan TY, Wang H, Xiang P, Liu YW, Li HZ, Lei BX, et al. Inhibition of EZH2 reverses chemotherapeutic drug TMZ chemosensitivity in glioblastoma. Int J Clin Exp Pathol. 2014;7(10):6662-70.
12. Marusyk A, Polyak K. Tumor heterogeneity: causes and consequences. Biochim Biophys Acta. 2010;1805(1):105-17.
13. Junttila MR, de Sauvage FJ. Influence of tumour micro-environment heterogeneity on therapeutic response. Nature. 2013;501(7467):346-54.
14. Daneman R, Prat A. The blood-brain barrier. Cold Spring Harb Perspect Biol. 2015;7(1):a020412.
15. Wu SK, Tsai CL, Huang Y, Hynynen K. Focused Ultrasound and Microbubbles-Mediated Drug Delivery to Brain Tumor. Pharmaceutics. 2020;13(1).
16. Weller M, van den Bent M., Presser M, et al. . EANO guidelines on the diagnosis and treatment of diffuse gliomas of adulthood. Nature Reviews Clinical Oncology. 2021;18:170-86.
17. Rice T. LD, Molinaro AM, et al. Understanding inherited genetic risk of adult glioma - a review. Neuro-Oncology Practice. 2016;3(1):10-6.

18. Kinnersley B HR, Bondy ML. Genome-wide association studies in glioma. Cancer Epidemiology, Biomarkers & Prevention. 2018;27(4):418-28.
19. Shete S HF, Robertson LB, et al. . Genome-wide association study indentifies five susceptibility loci for glioma. Nature Genetics. 2009;41(8):899-904.
20. Alonso MM, Gomez-Manzano C, Bekele BN, Yung WK, Fueyo J. Adenovirus-based strategies overcome temozolomide resistance by silencing the O6-methylguanine-DNA methyltransferase promoter. Cancer Res. 2007;67(24):11499-504.
21. Stevens MF, Gescher A, Hickman JA, Vaughan K, Simmonds RJ. alpha-Hydroxylated triazenes: potential active metabolites of anti-tumour dimethyltriazenes [proceedings]. J Pharm Pharmacol. 1978;30 Suppl:48P.
22. Agarwala SS, Kirkwood JM. Temozolomide, a novel alkylating agent with activity in the central nervous system, may improve the treatment of advanced metastatic melanoma. Oncologist. 2000;5(2):144-51.
23. Tisdale M. Antitumour imidazotetrazines--XI: effect of 8-carbamoyl-3-methylimidazo[5,1-d]-1,2,3,5-tetrazin-4(3H)-one [CCRG 81045; M and B 39831 NSC 362856] on poly(ADP-ribose) metabolism. Br J Cancer. 1985(52):789-92.
24. Friedman HS, Kerby T, Calvert H. Temozolomide and treatment of malignant glioma. Clin Cancer Res. 2000;6(7):2585-97.
25. Lee SY. Temozolomide resistance in glioblastoma multiforme. Genes Dis. 2016;3(3):198-210.
26. Strobel H, Baisch T, Fitzel R, Schilberg K, Siegelin MD, Karpel-Massler G, et al. Temozolomide and Other Alkylating Agents in Glioblastoma Therapy. Biomedicines. 2019;7(3).
27. Lips J, Kaina B. Repair of O(6)-methylguanine is not affected by thymine base pairing and the presence of MMR proteins. Mutat Res. 2001;487(1-2):59-66.
28. Denny BJ, Wheelhouse RT, Stevens MF, Tsang LL, Slack JA. NMR and molecular modeling investigation of the mechanism of activation of the antitumor drug temozolomide and its interaction with DNA. Biochemistry. 1994;33(31):9045-51.
29. U.S. Food & Drug Administration USA: FDA; 1999 [Available from: https://www.accessdata.fda.gov/drugsatfda_docs/nda/99/21029_Temodar.cfm.
30. Shao L, Wang Y, Chang J, Luo Y, Meng A, Zhou D. Hematopoietic stem cell senescence and cancer therapy-induced long-term bone marrow injury. Transl Cancer Res. 2013;2(5):397-411.
31. Giudice V, Selleri C. Aplastic anemia: Pathophysiology. Semin Hematol. 2022;59(1):13-20.
32. Aster JC SR. Clinical manifestations, diagnosis, and classification of myelodysplastic syndromes 2024 [updated June 2024. Available from: https://www-uptodate-com.uml.idm.oclc.org/contents/clinical-manifestations-diagnosis-and-classification-of-myelodysplastic-syndromes-mds?search=Clinical%20manifestations%2C%20diagnosis%2C%20and%20classification%20of%20myelodysplastic%20syndromes&source=search_result&selectedTitle=1~150&usage_type=default&display_rank=1.
33. Stupp R, Mason WP, van den Bent MJ, Weller M, Fisher B, Taphoorn MJ, et al. Radiotherapy plus concomitant and adjuvant temozolomide for glioblastoma. N Engl J Med. 2005;352(10):987-96.

34. Weller M, Cloughesy T, Perry JR, Wick W. Standards of care for treatment of recurrent glioblastoma--are we there yet? Neuro Oncol. 2013;15(1):4-27.
35. Yoshimoto K, Mizoguchi M, Hata N, Murata H, Hatae R, Amano T, et al. Complex DNA repair pathways as possible therapeutic targets to overcome temozolomide resistance in glioblastoma. Front Oncol. 2012;2:186.
36. Bell EH, Zhang P, Fisher BJ, Macdonald DR, McElroy JP, Lesser GJ, et al. Association of MGMT Promoter Methylation Status With Survival Outcomes in Patients With High-Risk Glioma Treated With Radiotherapy and Temozolomide: An Analysis From the NRG Oncology/RTOG 0424 Trial. JAMA Oncol. 2018;4(10):1405-9.
37. Weller M, Tabatabai G, Kastner B, Felsberg J, Steinbach JP, Wick A, et al. MGMT Promoter Methylation Is a Strong Prognostic Biomarker for Benefit from Dose-Intensified Temozolomide Rechallenge in Progressive Glioblastoma: The DIRECTOR Trial. Clin Cancer Res. 2015;21(9):2057-64.
38. Pieper RO, Costello JF, Kroes RA, Futscher BW, Marathi U, Erickson LC. Direct correlation between methylation status and expression of the human O-6-methylguanine DNA methyltransferase gene. Cancer Commun. 1991;3(8):241-53.
39. Hanihara M, Miyake K, Watanabe A, Yamada Y, Oishi N, Kawataki T, et al. Assessment of MGMT methylation status using high-performance liquid chromatography in newly diagnosed glioblastoma. Clin Epigenetics. 2020;12(1):174.
40. Watts GS, Pieper RO, Costello JF, Peng YM, Dalton WS, Futscher BW. Methylation of discrete regions of the O6-methylguanine DNA methyltransferase (MGMT) CpG island is associated with heterochromatinization of the MGMT transcription start site and silencing of the gene. Mol Cell Biol. 1997;17(9):5612-9.
41. Kitange GJ, Carlson BL, Mladek AC, Decker PA, Schroeder MA, Wu W, et al. Evaluation of MGMT promoter methylation status and correlation with temozolomide response in orthotopic glioblastoma xenograft model. J Neurooncol. 2009;92(1):23-31.
42. Minniti G SM, Arcella A, Buttarelli F, D'Elia A, Lanzetta G, Esposito V, Scarpino S, Maurizi Enrici R, Giangaspero F. Correlation between O6-methylguanine-DNA methyltransferase and survival in elderly patients with glioblastoma treated with radiotherapy plus concomitant and adjuvant temozolomide. J Neurooncol. 2011(102):311-6.
43. Li Q GJ, Wang W, Wang D. Relationship between MGMT gene expression and treatment effectiveness and prognosis in glioma. Oncol Lett. 2017;14:229-33.
44. Butler M, Pongor L, Su YT, Xi L, Raffeld M, Quezado M, et al. MGMT Status as a Clinical Biomarker in Glioblastoma. Trends Cancer. 2020;6(5):380-91.
45. Wang L, Li Z, Liu C, Chen L, Liu L, Hu Z, et al. Comparative assessment of three methods to analyze MGMT methylation status in a series of 350 gliomas and gangliogliomas. Pathol Res Pract. 2017;213(12):1489-93.
46. Preusser M, Charles Janzer R, Felsberg J, Reifenberger G, Hamou MF, Diserens AC, et al. Anti-O6-methylguanine-methyltransferase (MGMT) immunohistochemistry in glioblastoma multiforme: observer variability and lack of association with patient survival impede its use as clinical biomarker. Brain Pathol. 2008;18(4):520-32.
47. Wu S, Li X, Gao F, de Groot JF, Koul D, Yung WKA. PARP-mediated PARylation of MGMT is critical to promote repair of temozolomide-induced O6-methylguanine DNA damage in glioblastoma. Neuro Oncol. 2021;23(6):920-31.

48. McDonald KL, Tabone T, Nowak AK, Erber WN. Somatic mutations in glioblastoma are associated with methylguanine-DNA methyltransferase methylation. Oncol Lett. 2015;9(5):2063-7.
49. Egana L, Auzmendi-Iriarte J, Andermatten J, Villanua J, Ruiz I, Elua-Pinin A, et al. Methylation of MGMT promoter does not predict response to temozolomide in patients with glioblastoma in Donostia Hospital. Sci Rep. 2020;10(1):18445.
50. Li GM. Mechanisms and functions of DNA mismatch repair. Cell Res. 2008;18(1):85-98.
51. Iyer RR, Pluciennik A, Burdett V, Modrich PL. DNA mismatch repair: functions and mechanisms. Chem Rev. 2006;106(2):302-23.
52. Kat A, Thilly WG, Fang WH, Longley MJ, Li GM, Modrich P. An alkylation-tolerant, mutator human cell line is deficient in strand-specific mismatch repair. Proc Natl Acad Sci U S A. 1993;90(14):6424-8.
53. Shinsato Y, Furukawa T, Yunoue S, Yonezawa H, Minami K, Nishizawa Y, et al. Reduction of MLH1 and PMS2 confers temozolomide resistance and is associated with recurrence of glioblastoma. Oncotarget. 2013;4(12):2261-70.
54. McFaline-Figueroa JL, Braun CJ, Stanciu M, Nagel ZD, Mazzucato P, Sangaraju D, et al. Minor Changes in Expression of the Mismatch Repair Protein MSH2 Exert a Major Impact on Glioblastoma Response to Temozolomide. Cancer Res. 2015;75(15):3127-38.
55. Cahill DP, Levine KK, Betensky RA, Codd PJ, Romany CA, Reavie LB, et al. Loss of the mismatch repair protein MSH6 in human glioblastomas is associated with tumor progression during temozolomide treatment. Clin Cancer Res. 2007;13(7):2038-45.
56. Krokan HE, Bjoras M. Base excision repair. Cold Spring Harb Perspect Biol. 2013;5(4):a012583.
57. Almeida KH, Sobol RW. A unified view of base excision repair: lesion-dependent protein complexes regulated by post-translational modification. DNA Repair (Amst). 2007;6(6):695-711.
58. Serrano-Heras G, Castro-Robles B, Romero-Sanchez CM, Carrion B, Barbella-Aponte R, Sandoval H, et al. Involvement of N-methylpurine DNA glycosylase in resistance to temozolomide in patient-derived glioma cells. Sci Rep. 2020;10(1):22185.
59. Agnihotri S, Gajadhar AS, Ternamian C, Gorlia T, Diefes KL, Mischel PS, et al. Alkylpurine-DNA-N-glycosylase confers resistance to temozolomide in xenograft models of glioblastoma multiforme and is associated with poor survival in patients. J Clin Invest. 2012;122(1):253-66.
60. Chen J, Li Y, Yu TS, McKay RM, Burns DK, Kernie SG, et al. A restricted cell population propagates glioblastoma growth after chemotherapy. Nature. 2012;488(7412):522-6.
61. Qianquan MWLCXea. Canacer Stem Cells and Immunosuppressive Microenvironment in Gloma. Frontiers in Immunology. 2018;9.
62. Galli R, Binda E, Orfanelli U, Cipelletti B, Gritti A, De Vitis S, et al. Isolation and characterization of tumorigenic, stem-like neural precursors from human glioblastoma. Cancer Res. 2004;64(19):7011-21.
63. Huang Z, Cheng L, Guryanova OA, Wu Q, Bao S. Cancer stem cells in glioblastoma--molecular signaling and therapeutic targeting. Protein Cell. 2010;1(7):638-55.
64. Lee J, Kotliarova S, Kotliarov Y, Li A, Su Q, Donin NM, et al. Tumor stem cells derived from glioblastomas cultured in bFGF and EGF more closely mirror the phenotype and genotype of primary tumors than do serum-cultured cell lines. Cancer Cell. 2006;9(5):391-403.

65. Pollard SM, Yoshikawa, K., Clarke, I. D, et al. Glioma stem cell lines expanded in adherent culture have tumor-specific phenotypes and are suitablefor chemical and genetic screens. Cell Stem Cell. 2009;4:568-80.
66. Singh SK, Hawkins C, Clarke ID, Squire JA, Bayani J, Hide T, et al. Identification of human brain tumour initiating cells. Nature. 2004;432(7015):396-401.
67. Gilbert CA, Ross AH. Cancer stem cells: cell culture, markers, and targets for new therapies. J Cell Biochem. 2009;108(5):1031-8.
68. Joo KM, Kim SY, Jin X, Song SY, Kong DS, Lee JI, et al. Clinical and biological implications of CD133-positive and CD133-negative cells in glioblastomas. Lab Invest. 2008;88(8):808-15.
69. Rasper M, Schafer A, Piontek G, Teufel J, Brockhoff G, Ringel F, et al. Aldehyde dehydrogenase 1 positive glioblastoma cells show brain tumor stem cell capacity. Neuro Oncol. 2010;12(10):1024-33.
70. Tomita H, Tanaka K, Tanaka T, Hara A. Aldehyde dehydrogenase 1A1 in stem cells and cancer. Oncotarget. 2016;7(10):11018-32.
71. Munthe S, Sorensen MD, Thomassen M, Burton M, Kruse TA, Lathia JD, et al. Migrating glioma cells express stem cell markers and give rise to new tumors upon xenografting. J Neurooncol. 2016;130(1):53-62.
72. Meacham CE, Morrison SJ. Tumour heterogeneity and cancer cell plasticity. Nature. 2013;501(7467):328-37.
73. Auffinger B, Tobias AL, Han Y, Lee G, Guo D, Dey M, et al. Conversion of differentiated cancer cells into cancer stem-like cells in a glioblastoma model after primary chemotherapy. Cell Death Differ. 2014;21(7):1119-31.
74. Fessler E, Borovski T, Medema JP. Endothelial cells induce cancer stem cell features in differentiated glioblastoma cells via bFGF. Mol Cancer. 2015;14:157.
75. Olmez I, Shen W, McDonald H, Ozpolat B. Dedifferentiation of patient-derived glioblastoma multiforme cell lines results in a cancer stem cell-like state with mitogen-independent growth. J Cell Mol Med. 2015;19(6):1262-72.
76. Rath BH, Wahba A, Camphausen K, Tofilon PJ. Coculture with astrocytes reduces the radiosensitivity of glioblastoma stem-like cells and identifies additional targets for radiosensitization. Cancer Med. 2015;4(11):1705-16.
77. Bao S, Wu Q, McLendon RE, Hao Y, Shi Q, Hjelmeland AB, et al. Glioma stem cells promote radioresistance by preferential activation of the DNA damage response. Nature. 2006;444(7120):756-60.
78. Mani SA, Guo W, Liao MJ, Eaton EN, Ayyanan A, Zhou AY, et al. The epithelial-mesenchymal transition generates cells with properties of stem cells. Cell. 2008;133(4):704-15.
79. Hombach-Klonisch S, Mehrpour M, Shojaei S, Harlos C, Pitz M, Hamai A, et al. Glioblastoma and chemoresistance to alkylating agents: Involvement of apoptosis, autophagy, and unfolded protein response. Pharmacol Ther. 2018;184:13-41.
80. Meyer M, Reimand J, Lan X, Head R, Zhu X, Kushida M, et al. Single cell-derived clonal analysis of human glioblastoma links functional and genomic heterogeneity. Proc Natl Acad Sci U S A. 2015;112(3):851-6.
81. Hutvagner G, Zamore PD. A microRNA in a multiple-turnover RNAi enzyme complex. Science. 2002;297(5589):2056-60.

82. O'Brien J, Hayder H, Zayed Y, Peng C. Overview of MicroRNA Biogenesis, Mechanisms of Actions, and Circulation. Front Endocrinol (Lausanne). 2018;9:402.
83. Vickers KC, Palmisano BT, Shoucri BM, Shamburek RD, Remaley AT. MicroRNAs are transported in plasma and delivered to recipient cells by high-density lipoproteins. Nat Cell Biol. 2011;13(4):423-33.
84. Tabet F, Vickers KC, Cuesta Torres LF, Wiese CB, Shoucri BM, Lambert G, et al. HDL-transferred microRNA-223 regulates ICAM-1 expression in endothelial cells. Nat Commun. 2014;5:3292.
85. Goldie BJ, Dun MD, Lin M, Smith ND, Verrills NM, Dayas CV, et al. Activity-associated miRNA are packaged in Map1b-enriched exosomes released from depolarized neurons. Nucleic Acids Res. 2014;42(14):9195-208.
86. Tomar MS, Kumar A, Srivastava C, Shrivastava A. Elucidating the mechanisms of Temozolomide resistance in gliomas and the strategies to overcome the resistance. Biochim Biophys Acta Rev Cancer. 2021;1876(2):188616.
87. Comincini S, Allavena G, Palumbo S, Morini M, Durando F, Angeletti F, et al. microRNA-17 regulates the expression of ATG7 and modulates the autophagy process, improving the sensitivity to temozolomide and low-dose ionizing radiation treatments in human glioblastoma cells. Cancer Biol Ther. 2013;14(7):574-86.
88. Ujifuku K. MS, Takakura M., et al. . miR-195, miR-455-3p and miR-10a(*) are implicated in acquired temozolomide resistance in glioblastoma multiforme cells. Cancer Letters. 2010;296:241-8.
89. Tian T, Mingyi M, Qiu X, Qiu Y. MicroRNA-101 reverses temozolomide resistance by inhibition of GSK3beta in glioblastoma. Oncotarget. 2016;7(48):79584-95.
90. Shi L, Chen J, Yang J, Pan T, Zhang S, Wang Z. MiR-21 protected human glioblastoma U87MG cells from chemotherapeutic drug temozolomide induced apoptosis by decreasing Bax/Bcl-2 ratio and caspase-3 activity. Brain Res. 2010;1352:255-64.
91. Wong ST, Zhang XQ, Zhuang JT, Chan HL, Li CH, Leung GK. MicroRNA-21 inhibition enhances in vitro chemosensitivity of temozolomide-resistant glioblastoma cells. Anticancer Res. 2012;32(7):2835-41.
92. Cancer Genome Atlas Research N. Comprehensive genomic characterization defines human glioblastoma genes and core pathways. Nature. 2008;455(7216):1061-8.
93. Mizoguchi M, Guan Y, Yoshimoto K, Hata N, Amano T, Nakamizo A, et al. MicroRNAs in Human Malignant Gliomas. J Oncol. 2012;2012:732874.
94. Srinivasan S, Patric IR, Somasundaram K. A ten-microRNA expression signature predicts survival in glioblastoma. PLoS One. 2011;6(3):e17438.
95. Liu X. ABC Family Transporters. Singapore: Springer; 2019.
96. Dean M, Rzhetsky A, Allikmets R. The human ATP-binding cassette (ABC) transporter superfamily. Genome Res. 2001;11(7):1156-66.
97. Tarling EJ, de Aguiar Vallim TQ, Edwards PA. Role of ABC transporters in lipid transport and human disease. Trends Endocrinol Metab. 2013;24(7):342-50.
98. Bojanic DD, Tarr PT, Gale GD, Smith DJ, Bok D, Chen B, et al. Differential expression and function of ABCG1 and ABCG4 during development and aging. J Lipid Res. 2010;51(1):169-81.
99. Eckford PD, Sharom FJ. ABC efflux pump-based resistance to chemotherapy drugs. Chem Rev. 2009;109(7):2989-3011.

100. Perazzoli G, Prados J, Ortiz R, Caba O, Cabeza L, Berdasco M, et al. Temozolomide Resistance in Glioblastoma Cell Lines: Implication of MGMT, MMR, P-Glycoprotein and CD133 Expression. PLoS One. 2015;10(10):e0140131.
101. Schaich M, Kestel L, Pfirrmann M, Robel K, Illmer T, Kramer M, et al. A MDR1 (ABCB1) gene single nucleotide polymorphism predicts outcome of temozolomide treatment in glioblastoma patients. Ann Oncol. 2009;20(1):175-81.
102. Elshazly AM, Gewirtz DA. Is Autophagy Inhibition in Combination with Temozolomide a Therapeutically Viable Strategy? Cells. 2023;12(4).
103. Glick D, Barth S, Macleod KF. Autophagy: cellular and molecular mechanisms. J Pathol. 2010;221(1):3-12.
104. Li Y, Chen Y. AMPK and Autophagy. Adv Exp Med Biol. 2019;1206:85-108.
105. Kim J KM, Viollet B, Huan K.L. AMPK and mTOR regulate autophagy through direct phosphorylation of Ulk1. Nature. 2011(13):132-41.
106. Li X, He S, Ma B. Autophagy and autophagy-related proteins in cancer. Mol Cancer. 2020;19(1):12.
107. Russell RC, Tian Y, Yuan H, Park HW, Chang YY, Kim J, et al. ULK1 induces autophagy by phosphorylating Beclin-1 and activating VPS34 lipid kinase. Nat Cell Biol. 2013;15(7):741-50.
108. Chun Y, Kim J. AMPK-mTOR Signaling and Cellular Adaptations in Hypoxia. Int J Mol Sci. 2021;22(18).
109. Mizushima N, Yoshimori T, Ohsumi Y. The role of Atg proteins in autophagosome formation. Annu Rev Cell Dev Biol. 2011;27:107-32.
110. Lamb CA, Yoshimori T, Tooze SA. The autophagosome: origins unknown, biogenesis complex. Nat Rev Mol Cell Biol. 2013;14(12):759-74.
111. Mizushima N, Noda T, Yoshimori T, Tanaka Y, Ishii T, George MD, et al. A protein conjugation system essential for autophagy. Nature. 1998;395(6700):395-8.
112. Kabeya Y, Mizushima N, Ueno T, Yamamoto A, Kirisako T, Noda T, et al. LC3, a mammalian homologue of yeast Apg8p, is localized in autophagosome membranes after processing. EMBO J. 2000;19(21):5720-8.
113. Yang Z, Wilkie-Grantham RP, Yanagi T, Shu CW, Matsuzawa S, Reed JC. ATG4B (Autophagin-1) phosphorylation modulates autophagy. J Biol Chem. 2015;290(44):26549-61.
114. Kabeya Y, Mizushima N, Ueno T, Yamamoto A, Kirisako T, Noda T, et al. LC3, a mammalian homologue of yeast Apg8p, is localized in autophagosome membranes after processing. 2000;19(21):5720-8.
115. Kabeya Y, Mizushima N, Yamamoto A, Oshitani-Okamoto S, Ohsumi Y, Yoshimori TJJocs. LC3, GABARAP and GATE16 localize to autophagosomal membrane depending on form-II formation. 2004;117(13):2805-12.
116. Li J, Chen X, Kang R, Zeh H, Klionsky DJ, Tang DJA. Regulation and function of autophagy in pancreatic cancer. 2020:1-22.
117. Wang T, Hu J, Luo H, Li H, Zhou J, Zhou L, et al. Photosensitizer and Autophagy Promoter Coloaded ROS-Responsive Dendrimer-Assembled Carrier for Synergistic Enhancement of Tumor Growth Suppression. Small. 2018;14(38):e1802337.
118. Qu X, Yu J, Bhagat G, Furuya N, Hibshoosh H, Troxel A, et al. Promotion of tumorigenesis by heterozygous disruption of the beclin 1 autophagy gene. J Clin Invest. 2003;112(12):1809-20.

119. Zhang B, Liu, L. Autophagy is a double-edged sword in therapy of colorectal cancer. Oncology Letters. 2021;21(378).
120. Luo T, Fu J, Xu A, Su B, Ren Y, Li N, et al. PSMD10/gankyrin induces autophagy to promote tumor progression through cytoplasmic interaction with ATG7 and nuclear transactivation of ATG7 expression. Autophagy. 2016;12(8):1355-71.
121. Mizushima N, et al. Autophagy fights disease through cellular self-digestion. Nature. 2008;451(7182).
122. Ravikumar B, et al. Regulation of mammalian autophagy in physiology and pathophysiology. Physiol Rev. 2010;90(4).
123. Liang XH, Jackson S, Seaman M, Brown K, Kempkes B, Hibshoosh H, et al. Induction of autophagy and inhibition of tumorigenesis by beclin 1. Nature. 1999;402(6762):672-6.
124. Shen Y, Li DD, Wang LL, Deng R, Zhu XF. Decreased expression of autophagy-related proteins in malignant epithelial ovarian cancer. Autophagy. 2008;4(8):1067-8.
125. Takamura A, Komatsu M, Hara T, Sakamoto A, Kishi C, Waguri S, et al. Autophagy-deficient mice develop multiple liver tumors. Genes Dev. 2011;25(8):795-800.
126. Roy BC, Ahmed I, Ramalingam S, Jala V, Haribabu B, Ramamoorthy P, et al. Co-localization of autophagy-related protein p62 with cancer stem cell marker dclk1 may hamper dclk1's elimination during colon cancer development and progression. Oncotarget. 2019;10(24):2340-54.
127. Song J, Guo X, Xie X, Zhao X, Li D, Deng W, et al. Autophagy in hypoxia protects cancer cells against apoptosis induced by nutrient deprivation through a Beclin1-dependent way in hepatocellular carcinoma. J Cell Biochem. 2011;112(11):3406-20.
128. Tang T, Xia Q, Xi M. Dihydroartemisinin and its anticancer activity against endometrial carcinoma and cervical cancer: involvement of apoptosis, autophagy and transferrin receptor. Singapore medical journal. 2021;62(2):96-103.
129. Ozates NP, Sogutlu F, Lerminoglu F, Demir B, Gunduz C, Shademan B, et al. Effects of rapamycin and AZD3463 combination on apoptosis, autophagy, and cell cycle for resistance control in breast cancer. Life Sci. 2021;264:118643.
130. Han M, Qian X, Cao H, Wang F, Li X, Han N, et al. lncRNA ZNF649-AS1 Induces Trastuzumab Resistance by Promoting ATG5 Expression and Autophagy. Mol Ther. 2020;28(11):2488-502.
131. Harder BG, Peng S, Sereduk CP, Sodoma AM, Kitange GJ, Loftus JC, et al. Inhibition of phosphatidylinositol 3-kinase by PX-866 suppresses temozolomide-induced autophagy and promotes apoptosis in glioblastoma cells. Mol Med. 2019;25(1):49.
132. Liu J, Liu Y, Wang Y, Li C, Xie Y, Klionsky DJ, et al. TMEM164 is a new determinant of autophagy-dependent ferroptosis. Autophagy. 2022:1-12.
133. Han S, Zhu L, Zhu Y, Meng Y, Li J, Song P, et al. Targeting ATF4-dependent pro-survival autophagy to synergize glutaminolysis inhibition. Theranostics. 2021;11(17):8464-79.
134. Yang ZJ, Chee CE, Huang S, Sinicrope FA. The role of autophagy in cancer: therapeutic implications. Mol Cancer Ther. 2011;10(9):1533-41.
135. Kondo Y, Kanzawa T, Sawaya R, Kondo S. The role of autophagy in cancer development and response to therapy. Nat Rev Cancer. 2005;5(9):726-34.

136. Bak DH, Kang SH, Choi DR, Gil MN, Yu KS, Jeong JH, et al. Autophagy enhancement contributes to the synergistic effect of vitamin D in temozolomide-based glioblastoma chemotherapy. Exp Ther Med. 2016;11(6):2153-62.
137. Carmo A, Carvalheiro H, Crespo I, Nunes I, Lopes MC. Effect of temozolomide on the U-118 glioma cell line. Oncol Lett. 2011;2(6):1165-70.
138. Liu X, Sun K, Wang H, Dai Y. Knockdown of retinoblastoma protein may sensitize glioma cells to cisplatin through inhibition of autophagy. Neurosci Lett. 2016;620:137-42.
139. Hu YL, DeLay M, Jahangiri A, Molinaro AM, Rose SD, Carbonell WS, et al. Hypoxia-induced autophagy promotes tumor cell survival and adaptation to antiangiogenic treatment in glioblastoma. Cancer Res. 2012;72(7):1773-83.
140. Wojton J, Meisen WH, Kaur B. How to train glioma cells to die: molecular challenges in cell death. J Neurooncol. 2016;126(3):377-84.
141. Kanzawa T, Germano IM, Komata T, Ito H, Kondo Y, Kondo S. Role of autophagy in temozolomide-induced cytotoxicity for malignant glioma cells. Cell Death Differ. 2004;11(4):448-57.
142. Cory S, Adams JM. The Bcl2 family: regulators of the cellular life-or-death switch. Nat Rev Cancer. 2002;2(9):647-56.
143. Sato T, Irie S, Krajewski S, Reed JC. Cloning and sequencing of a cDNA encoding the rat Bcl-2 protein. Gene. 1994;140(2):291-2.
144. Andreu-Fernandez V, Sancho M, Genoves A, Lucendo E, Todt F, Lauterwasser J, et al. Bax transmembrane domain interacts with prosurvival Bcl-2 proteins in biological membranes. Proc Natl Acad Sci U S A. 2017;114(2):310-5.
145. Goping IS, Gross A, Lavoie JN, Nguyen M, Jemmerson R, Roth K, et al. Regulated targeting of BAX to mitochondria. J Cell Biol. 1998;143(1):207-15.
146. Singh R, Letai A, Sarosiek K. Regulation of apoptosis in health and disease: the balancing act of BCL-2 family proteins. Nat Rev Mol Cell Biol. 2019;20(3):175-93.
147. Shimizu S, Konishi A, Kodama T, Tsujimoto Y. BH4 domain of antiapoptotic Bcl-2 family members closes voltage-dependent anion channel and inhibits apoptotic mitochondrial changes and cell death. Proc Natl Acad Sci U S A. 2000;97(7):3100-5.
148. Lomonosova E, Chinnadurai G. BH3-only proteins in apoptosis and beyond: an overview. Oncogene. 2008;27 Suppl 1:S2-19.
149. Karch J, Molkentin JD. Regulated necrotic cell death: the passive aggressive side of Bax and Bak. Circ Res. 2015;116(11):1800-9.
150. Willis SN, Fletcher JI, Kaufmann T, van Delft MF, Chen L, Czabotar PE, et al. Apoptosis initiated when BH3 ligands engage multiple Bcl-2 homologs, not Bax or Bak. Science. 2007;315(5813):856-9.
151. Tait SW, Green DR. Mitochondrial regulation of cell death. Cold Spring Harb Perspect Biol. 2013;5(9).
152. Letai A, Bassik MC, Walensky LD, Sorcinelli MD, Weiler S, Korsmeyer SJ. Distinct BH3 domains either sensitize or activate mitochondrial apoptosis, serving as prototype cancer therapeutics. Cancer Cell. 2002;2(3):183-92.
153. Kataoka T, Holler N, Micheau O, Martinon F, Tinel A, Hofmann K, et al. Bcl-rambo, a novel Bcl-2 homologue that induces apoptosis via its unique C-terminal extension. J Biol Chem. 2001;276(22):19548-54.

154. Kim JY, So KJ, Lee S, Park JH. Bcl-rambo induces apoptosis via interaction with the adenine nucleotide translocator. FEBS Lett. 2012;586(19):3142-9.
155. Kaufmann T, Schlipf S, Sanz J, Neubert K, Stein R, Borner C. Characterization of the signal that directs Bcl-x(L), but not Bcl-2, to the mitochondrial outer membrane. J Cell Biol. 2003;160(1):53-64.
156. Jensen SA, Calvert AE, Volpert G, Kouri FM, Hurley LA, Luciano JP, et al. Bcl2L13 is a ceramide synthase inhibitor in glioblastoma. Proc Natl Acad Sci U S A. 2014;111(15):5682-7.
157. Thul PJ, Akesson L, Wiking M, Mahdessian D, Geladaki A, Ait Blal H, et al. A subcellular map of the human proteome. Science. 2017;356(6340).
158. Uhlen M, Fagerberg L, Hallstrom BM, Lindskog C, Oksvold P, Mardinoglu A, et al. Proteomics. Tissue-based map of the human proteome. Science. 2015;347(6220):1260419.
159. Boumela I, Assou S, Aouacheria A, Haouzi D, Dechaud H, De Vos J, et al. Involvement of BCL2 family members in the regulation of human oocyte and early embryo survival and death: gene expression and beyond. Reproduction. 2011;141(5):549-61.
160. Avila-Arcos MC, McManus KF, Sandoval K, Rodriguez-Rodriguez JE, Villa-Islas V, Martin AR, et al. Population History and Gene Divergence in Native Mexicans Inferred from 76 Human Exomes. Mol Biol Evol. 2020;37(4):994-1006.
161. Nakazawa M, Matsubara H, Matsushita Y, Watanabe M, Vo N, Yoshida H, et al. The Human Bcl-2 Family Member Bcl-rambo Localizes to Mitochondria and Induces Apoptosis and Morphological Aberrations in Drosophila. PLoS One. 2016;11(6):e0157823.
162. Okamoto K, Kondo-Okamoto N, Ohsumi Y. Mitochondria-anchored receptor Atg32 mediates degradation of mitochondria via selective autophagy. Dev Cell. 2009;17(1):87-97.
163. Murakawa T, Okamoto K, Omiya S, Taneike M, Yamaguchi O, Otsu K. A Mammalian Mitophagy Receptor, Bcl2-L-13, Recruits the ULK1 Complex to Induce Mitophagy. Cell Rep. 2019;26(2):338-45 e6.
164. Hashino T, Matsubara H, Xu J, Tanaka R, Kusagawa E, Ueda Y, et al. PGAM5 interacts with Bcl-rambo and regulates apoptosis and mitophagy. Exp Cell Res. 2022;420(1):113342.
165. Ke PY. Diverse Functions of Autophagy in Liver Physiology and Liver Diseases. Int J Mol Sci. 2019;20(2).
166. Parzych KR, Klionsky DJ. An overview of autophagy: morphology, mechanism, and regulation. Antioxid Redox Signal. 2014;20(3):460-73.
167. Ma C, Xia F, Kelley SO. Mitochondrial Targeting of Probes and Therapeutics to the Powerhouse of the Cell. Bioconjug Chem. 2020;31(12):2650-67.
168. Spinelli JB, Haigis MC. The multifaceted contributions of mitochondria to cellular metabolism. Nat Cell Biol. 2018;20(7):745-54.
169. Fakouri NB, Hansen TL, Desler C, Anugula S, Rasmussen LJ. From Powerhouse to Perpetrator-Mitochondria in Health and Disease. Biology (Basel). 2019;8(2).
170. Sun N, Youle RJ, Finkel T. The Mitochondrial Basis of Aging. Mol Cell. 2016;61(5):654-66.
171. Fang EF, Scheibye-Knudsen M, Chua KF, Mattson MP, Croteau DL, Bohr VA. Nuclear DNA damage signalling to mitochondria in ageing. Nat Rev Mol Cell Biol. 2016;17(5):308-21.
172. Rodriguez-Enriquez S, Kai Y, Maldonado E, Currin RT, Lemasters JJ. Roles of mitophagy and the mitochondrial permeability transition in remodeling of cultured rat hepatocytes. Autophagy. 2009;5(8):1099-106.

173. Byrnes K, Blessinger S, Bailey NT, Scaife R, Liu G, Khambu B. Therapeutic regulation of autophagy in hepatic metabolism. Acta Pharm Sin B. 2022;12(1):33-49.
174. Williams JA, Ding WX. Targeting Pink1-Parkin-mediated mitophagy for treating liver injury. Pharmacol Res. 2015;102:264-9.
175. Ueno T, Komatsu M. Autophagy in the liver: functions in health and disease. Nat Rev Gastroenterol Hepatol. 2017;14(3):170-84.
176. Novak I, Kirkin V, McEwan DG, Zhang J, Wild P, Rozenknop A, et al. Nix is a selective autophagy receptor for mitochondrial clearance. EMBO Rep. 2010;11(1):45-51.
177. Li M, Jia J, Zhang X, Dai H. Selective binding of mitophagy receptor protein Bcl-rambo to LC3/GABARAP family proteins. Biochem Biophys Res Commun. 2020;530(1):292-300.
178. Murakawa T, Yamaguchi O, Hashimoto A, Hikoso S, Takeda T, Oka T, et al. Bcl-2-like protein 13 is a mammalian Atg32 homologue that mediates mitophagy and mitochondrial fragmentation. Nat Commun. 2015;6:7527.
179. Ryan BJ, Hoek S, Fon EA, Wade-Martins R. Mitochondrial dysfunction and mitophagy in Parkinson's: from familial to sporadic disease. Trends Biochem Sci. 2015;40(4):200-10.
180. Ye X, Sun X, Starovoytov V, Cai Q. Parkin-mediated mitophagy in mutant hAPP neurons and Alzheimer's disease patient brains. Hum Mol Genet. 2015;24(10):2938-51.
181. Kitada T, Asakawa S, Hattori N, Matsumine H, Yamamura Y, Minoshima S, et al. Mutations in the parkin gene cause autosomal recessive juvenile parkinsonism. Nature. 1998;392(6676):605-8.
182. Valente EM, Abou-Sleiman PM, Caputo V, Muqit MM, Harvey K, Gispert S, et al. Hereditary early-onset Parkinson's disease caused by mutations in PINK1. Science. 2004;304(5674):1158-60.
183. Swerdlow RH, Burns JM, Khan SM. The Alzheimer's disease mitochondrial cascade hypothesis. J Alzheimers Dis. 2010;20 Suppl 2:S265-79.
184. Querfurth HW, LaFerla FM. Alzheimer's disease. N Engl J Med. 2010;362(4):329-44.
185. Kerr JS, Adriaanse BA, Greig NH, Mattson MP, Cader MZ, Bohr VA, et al. Mitophagy and Alzheimer's Disease: Cellular and Molecular Mechanisms. Trends Neurosci. 2017;40(3):151-66.
186. Liu X, Wang X, Zhang L, Zhou Y, Yang L, Yang M. By targeting apoptosis facilitator BCL2L13, microRNA miR-484 alleviates cerebral ischemia/reperfusion injury-induced neuronal apoptosis in mice. Bioengineered. 2021;12(1):948-59.
187. Wang B, Nie J, Wu L, Hu Y, Wen Z, Dong L, et al. AMPKalpha2 Protects Against the Development of Heart Failure by Enhancing Mitophagy via PINK1 Phosphorylation. Circ Res. 2018;122(5):712-29.
188. Banga S, Gao P, Shen X, Fiscus V, Zong WX, Chen L, et al. Legionella pneumophila inhibits macrophage apoptosis by targeting pro-death members of the Bcl2 protein family. Proc Natl Acad Sci U S A. 2007;104(12):5121-6.
189. Holleman A, den Boer ML, de Menezes RX, Cheok MH, Cheng C, Kazemier KM, et al. The expression of 70 apoptosis genes in relation to lineage, genetic subtype, cellular drug resistance, and outcome in childhood acute lymphoblastic leukemia. Blood. 2006;107(2):769-76.
190. Meng F, Zhang L, Zhang M, Ye K, Guo W, Liu Y, et al. Down-regulation of BCL2L13 renders poor prognosis in clear cell and papillary renal cell carcinoma. Cancer Cell Int. 2021;21(1):332.

191. van Meer G, Voelker DR, Feigenson GW. Membrane lipids: where they are and how they behave. Nat Rev Mol Cell Biol. 2008;9(2):112-24.
192. Soto-Avellaneda A, Morrison BE. Signaling and other functions of lipids in autophagy: a review. Lipids Health Dis. 2020;19(1):214.
193. Simons K, Sampaio JL. Membrane organization and lipid rafts. Cold Spring Harb Perspect Biol. 2011;3(10):a004697.
194. Di Paolo G, De Camilli P. Phosphoinositides in cell regulation and membrane dynamics. Nature. 2006;443(7112):651-7.
195. Snaebjornsson MT, Janaki-Raman S, Schulze A. Greasing the Wheels of the Cancer Machine: The Role of Lipid Metabolism in Cancer. Cell Metab. 2020;31(1):62-76.
196. Whitman M, Downes CP, Keeler M, Keller T, Cantley L. Type I phosphatidylinositol kinase makes a novel inositol phospholipid, phosphatidylinositol-3-phosphate. Nature. 1988;332(6165):644-6.
197. Berridge MJ, Irvine RF. Inositol trisphosphate, a novel second messenger in cellular signal transduction. Nature. 1984;312(5992):315-21.
198. Pettitt TR, Martin A, Horton T, Liossis C, Lord JM, Wakelam MJ. Diacylglycerol and phosphatidate generated by phospholipases C and D, respectively, have distinct fatty acid compositions and functions. Phospholipase D-derived diacylglycerol does not activate protein kinase C in porcine aortic endothelial cells. J Biol Chem. 1997;272(28):17354-9.
199. Hawkins PT, Anderson KE, Davidson K, Stephens LR. Signalling through Class I PI3Ks in mammalian cells. Biochem Soc Trans. 2006;34(Pt 5):647-62.
200. Fernandis AZ, Wenk MR. Membrane lipids as signaling molecules. Curr Opin Lipidol. 2007;18(2):121-8.
201. Henneberry AL, Wright MM, McMaster CR. The major sites of cellular phospholipid synthesis and molecular determinants of Fatty Acid and lipid head group specificity. Mol Biol Cell. 2002;13(9):3148-61.
202. Gault C, Obeid, L., Hannun, Y. Sphingolipids as Signalling and Regulatory Molecules: Landes Bioscience/Springer Science+Business Media, LLC; 2010.
203. Field BC, Gordillo R, Scherer PE. The Role of Ceramides in Diabetes and Cardiovascular Disease Regulation of Ceramides by Adipokines. Front Endocrinol (Lausanne). 2020;11:569250.
204. Hannun YA. Functions of ceramide in coordinating cellular responses to stress. Science. 1996;274(5294):1855-9.
205. Hannun YA, Obeid LM. Principles of bioactive lipid signalling: lessons from sphingolipids. Nat Rev Mol Cell Biol. 2008;9(2):139-50.
206. Pewzner-Jung Y, Ben-Dor S, Futerman AH. When do Lasses (longevity assurance genes) become CerS (ceramide synthases)?: Insights into the regulation of ceramide synthesis. J Biol Chem. 2006;281(35):25001-5.
207. Levy M, Futerman AH. Mammalian ceramide synthases. IUBMB Life. 2010;62(5):347-56.
208. Ogretmen B, Hannun YA. Biologically active sphingolipids in cancer pathogenesis and treatment. Nat Rev Cancer. 2004;4(8):604-16.
209. Ponnusamy S, Meyers-Needham M, Senkal CE, Saddoughi SA, Sentelle D, Selvam SP, et al. Sphingolipids and cancer: ceramide and sphingosine-1-phosphate in the regulation of cell death and drug resistance. Future Oncol. 2010;6(10):1603-24.

210. Dolgachev V, Farooqui MS, Kulaeva OI, Tainsky MA, Nagy B, Hanada K, et al. De novo ceramide accumulation due to inhibition of its conversion to complex sphingolipids in apoptotic photosensitized cells. J Biol Chem. 2004;279(22):23238-49.
211. Kitatani K, Idkowiak-Baldys J, Hannun YA. The sphingolipid salvage pathway in ceramide metabolism and signaling. Cell Signal. 2008;20(6):1010-8.
212. Laviad EL, Kelly S, Merrill AH, Jr., Futerman AH. Modulation of ceramide synthase activity via dimerization. J Biol Chem. 2012;287(25):21025-33.
213. Becker KP, Kitatani K, Idkowiak-Baldys J, Bielawski J, Hannun YA. Selective inhibition of juxtanuclear translocation of protein kinase C betaII by a negative feedback mechanism involving ceramide formed from the salvage pathway. J Biol Chem. 2005;280(4):2606-12.
214. Kitatani K, Idkowiak-Baldys J, Bielawski J, Taha TA, Jenkins RW, Senkal CE, et al. Protein kinase C-induced activation of a ceramide/protein phosphatase 1 pathway leading to dephosphorylation of p38 MAPK. J Biol Chem. 2006;281(48):36793-802.
215. Bose R, Verheij M, Haimovitz-Friedman A, Scotto K, Fuks Z, Kolesnick R. Ceramide synthase mediates daunorubicin-induced apoptosis: an alternative mechanism for generating death signals. Cell. 1995;82(3):405-14.
216. Blazquez C, Galve-Roperh I, Guzman M. De novo-synthesized ceramide signals apoptosis in astrocytes via extracellular signal-regulated kinase. FASEB J. 2000;14(14):2315-22.
217. Basnakian AG, Ueda N, Hong X, Galitovsky VE, Yin X, Shah SV. Ceramide synthase is essential for endonuclease-mediated death of renal tubular epithelial cells induced by hypoxia-reoxygenation. Am J Physiol Renal Physiol. 2005;288(2):F308-14.
218. Mesicek J, Lee H, Feldman T, Jiang X, Skobeleva A, Berdyshev EV, et al. Ceramide synthases 2, 5, and 6 confer distinct roles in radiation-induced apoptosis in HeLa cells. Cell Signal. 2010;22(9):1300-7.
219. Kerr JF, Wyllie AH, Currie AR. Apoptosis: a basic biological phenomenon with wide-ranging implications in tissue kinetics. Br J Cancer. 1972;26(4):239-57.
220. Kerr JF. History of the events leading to the formulation of the apoptosis concept. Toxicology. 2002;181-182:471-4.
221. Henry-Mowatt J, Dive C, Martinou JC, James D. Role of mitochondrial membrane permeabilization in apoptosis and cancer. Oncogene. 2004;23(16):2850-60.
222. Ganesan V, Walsh T, Chang KT, Colombini M. The dynamics of Bax channel formation: influence of ionic strength. Biophys J. 2012;103(3):483-91.
223. Bleicken S, Landeta O, Landajuela A, Basanez G, Garcia-Saez AJ. Proapoptotic Bax and Bak proteins form stable protein-permeable pores of tunable size. J Biol Chem. 2013;288(46):33241-52.
224. Colombini M. Membrane channels formed by ceramide. Handb Exp Pharmacol. 2013(215):109-26.
225. Siskind LJ, Davoody A, Lewin N, Marshall S, Colombini M. Enlargement and contracture of C2-ceramide channels. Biophys J. 2003;85(3):1560-75.
226. Kuwana T, Mackey MR, Perkins G, Ellisman MH, Latterich M, Schneiter R, et al. Bid, Bax, and lipids cooperate to form supramolecular openings in the outer mitochondrial membrane. Cell. 2002;111(3):331-42.

227. Ruvolo PP, Clark W, Mumby M, Gao F, May WS. A functional role for the B56 alpha-subunit of protein phosphatase 2A in ceramide-mediated regulation of Bcl2 phosphorylation status and function. J Biol Chem. 2002;277(25):22847-52.
228. Stiban J, Perera M. Very long chain ceramides interfere with C16-ceramide-induced channel formation: A plausible mechanism for regulating the initiation of intrinsic apoptosis. Biochim Biophys Acta. 2015;1848(2):561-7.
229. Laviad EL, Albee L, Pankova-Kholmyansky I, Epstein S, Park H, Merrill AH, Jr., et al. Characterization of ceramide synthase 2: tissue distribution, substrate specificity, and inhibition by sphingosine 1-phosphate. J Biol Chem. 2008;283(9):5677-84.
230. Chong SJF, Iskandar K, Lai JXH, Qu J, Raman D, Valentin R, et al. Serine-70 phosphorylated Bcl-2 prevents oxidative stress-induced DNA damage by modulating the mitochondrial redox metabolism. Nucleic Acids Res. 2020;48(22):12727-45.
231. Ruvolo PP, Deng X, Ito T, Carr BK, May WS. Ceramide induces Bcl2 dephosphorylation via a mechanism involving mitochondrial PP2A. J Biol Chem. 1999;274(29):20296-300.
232. Siskind LJ, Feinstein L, Yu T, Davis JS, Jones D, Choi J, et al. Anti-apoptotic Bcl-2 Family Proteins Disassemble Ceramide Channels. J Biol Chem. 2008;283(11):6622-30.
233. Chang KT, Anishkin A, Patwardhan GA, Beverly LJ, Siskind LJ, Colombini M. Ceramide channels: destabilization by Bcl-xL and role in apoptosis. Biochim Biophys Acta. 2015;1848(10 Pt A):2374-84.
234. De Giorgi F, Lartigue L, Bauer MK, Schubert A, Grimm S, Hanson GT, et al. The permeability transition pore signals apoptosis by directing Bax translocation and multimerization. FASEB J. 2002;16(6):607-9.
235. Smaili SS, Hsu YT, Sanders KM, Russell JT, Youle RJ. Bax translocation to mitochondria subsequent to a rapid loss of mitochondrial membrane potential. Cell Death Differ. 2001;8(9):909-20.
236. Hsu YT, Youle RJ. Bax in murine thymus is a soluble monomeric protein that displays differential detergent-induced conformations. J Biol Chem. 1998;273(17):10777-83.
237. Hsu YT, Wolter KG, Youle RJ. Cytosol-to-membrane redistribution of Bax and Bcl-X(L) during apoptosis. Proc Natl Acad Sci U S A. 1997;94(8):3668-72.
238. Oltvai ZN, Milliman CL, Korsmeyer SJ. Bcl-2 heterodimerizes in vivo with a conserved homolog, Bax, that accelerates programmed cell death. Cell. 1993;74(4):609-19.
239. Ganesan V, Perera MN, Colombini D, Datskovskiy D, Chadha K, Colombini M. Ceramide and activated Bax act synergistically to permeabilize the mitochondrial outer membrane. Apoptosis. 2010;15(5):553-62.
240. Belaud-Rotureau MA, Leducq N, Macouillard Poulletier de Gannes F, Diolez P, Lacoste L, Lacombe F, et al. Early transitory rise in intracellular pH leads to Bax conformation change during ceramide-induced apoptosis. Apoptosis. 2000;5(6):551-60.
241. Min J, Mesika A, Sivaguru M, Van Veldhoven PP, Alexander H, Futerman AH, et al. (Dihydro)ceramide synthase 1 regulated sensitivity to cisplatin is associated with the activation of p38 mitogen-activated protein kinase and is abrogated by sphingosine kinase 1. Mol Cancer Res. 2007;5(8):801-12.
242. Senkal CE, Ponnusamy S, Rossi MJ, Bialewski J, Sinha D, Jiang JC, et al. Role of human longevity assurance gene 1 and C18-ceramide in chemotherapy-induced cell death in human head and neck squamous cell carcinomas. Mol Cancer Ther. 2007;6(2):712-22.

243. Peter ME, Hadji A, Murmann AE, Brockway S, Putzbach W, Pattanayak A, et al. The role of CD95 and CD95 ligand in cancer. Cell Death Differ. 2015;22(5):885-6.
244. Walker T, Mitchell C, Park MA, Yacoub A, Graf M, Rahmani M, et al. Sorafenib and vorinostat kill colon cancer cells by CD95-dependent and -independent mechanisms. Mol Pharmacol. 2009;76(2):342-55.
245. LeBlanc HN, Ashkenazi A. Apo2L/TRAIL and its death and decoy receptors. Cell Death Differ. 2003;10(1):66-75.
246. Ivanov VN, Bhoumik A, Ronai Z. Death receptors and melanoma resistance to apoptosis. Oncogene. 2003;22(20):3152-61.
247. Hassanzadeh A, Farshdousti Hagh M, Alivand MR, Akbari AAM, Shams Asenjan K, Saraei R, et al. Down-regulation of intracellular anti-apoptotic proteins, particularly c-FLIP by therapeutic agents; the novel view to overcome resistance to TRAIL. J Cell Physiol. 2018;233(10):6470-85.
248. White-Gilbertson S, Mullen T, Senkal C, Lu P, Ogretmen B, Obeid L, et al. Ceramide synthase 6 modulates TRAIL sensitivity and nuclear translocation of active caspase-3 in colon cancer cells. Oncogene. 2009;28(8):1132-41.
249. Erez-Roman R, Pienik R, Futerman AH. Increased ceramide synthase 2 and 6 mRNA levels in breast cancer tissues and correlation with sphingosine kinase expression. Biochem Biophys Res Commun. 2010;391(1):219-23.
250. Alizadeh J, da Silva Rosa SC, Weng X, Jacobs J, Lorzadeh S, Ravandi A, et al. Ceramides and ceramide synthases in cancer: Focus on apoptosis and autophagy. Eur J Cell Biol. 2023;102(3):151337.
251. Levine B, Klionsky DJ. Development by self-digestion: molecular mechanisms and biological functions of autophagy. Dev Cell. 2004;6(4):463-77.
252. Qu X, Zou Z, Sun Q, Luby-Phelps K, Cheng P, Hogan RN, et al. Autophagy gene-dependent clearance of apoptotic cells during embryonic development. Cell. 2007;128(5):931-46.
253. Pattingre S, Tassa A, Qu X, Garuti R, Liang XH, Mizushima N, et al. Bcl-2 antiapoptotic proteins inhibit Beclin 1-dependent autophagy. Cell. 2005;122(6):927-39.
254. Young MM, Kester M, Wang HG. Sphingolipids: regulators of crosstalk between apoptosis and autophagy. J Lipid Res. 2013;54(1):5-19.
255. Scarlatti F, Bauvy C, Ventruti A, Sala G, Cluzeaud F, Vandewalle A, et al. Ceramide-mediated macroautophagy involves inhibition of protein kinase B and up-regulation of beclin 1. J Biol Chem. 2004;279(18):18384-91.
256. Schubert KM, Scheid MP, Duronio V. Ceramide inhibits protein kinase B/Akt by promoting dephosphorylation of serine 473. J Biol Chem. 2000;275(18):13330-5.
257. Billen LP, Kokoski CL, Lovell JF, Leber B, Andrews DW. Bcl-XL inhibits membrane permeabilization by competing with Bax. PLoS Biol. 2008;6(6):e147.
258. Guenther GG, Peralta ER, Rosales KR, Wong SY, Siskind LJ, Edinger AL. Ceramide starves cells to death by downregulating nutrient transporter proteins. Proc Natl Acad Sci U S A. 2008;105(45):17402-7.
259. Pattingre S, Bauvy C, Carpentier S, Levade T, Levine B, Codogno P. Role of JNK1-dependent Bcl-2 phosphorylation in ceramide-induced macroautophagy. J Biol Chem. 2009;284(5):2719-28.

260. Li DD, Wang LL, Deng R, Tang J, Shen Y, Guo JF, et al. The pivotal role of c-Jun NH2-terminal kinase-mediated Beclin 1 expression during anticancer agents-induced autophagy in cancer cells. Oncogene. 2009;28(6):886-98.
261. Moruno Manchon JF, Uzor NE, Dabaghian Y, Furr-Stimming EE, Finkbeiner S, Tsvetkov AS. Cytoplasmic sphingosine-1-phosphate pathway modulates neuronal autophagy. Sci Rep. 2015;5:15213.
262. Sentelle RD, Senkal CE, Jiang W, Ponnusamy S, Gencer S, Selvam SP, et al. Ceramide targets autophagosomes to mitochondria and induces lethal mitophagy. Nat Chem Biol. 2012;8(10):831-8.
263. Garofalo T, Matarrese P, Manganelli V, Marconi M, Tinari A, Gambardella L, et al. Evidence for the involvement of lipid rafts localized at the ER-mitochondria associated membranes in autophagosome formation. Autophagy. 2016;12(6):917-35.
264. Matarrese P, Garofalo T, Manganelli V, Gambardella L, Marconi M, Grasso M, et al. Evidence for the involvement of GD3 ganglioside in autophagosome formation and maturation. Autophagy. 2014;10(5):750-65.
265. Hinkovska-Galcheva VT, Boxer LA, Mansfield PJ, Harsh D, Blackwood A, Shayman JA. The formation of ceramide-1-phosphate during neutrophil phagocytosis and its role in liposome fusion. J Biol Chem. 1998;273(50):33203-9.
266. Mizumura K, Justice MJ, Schweitzer KS, Krishnan S, Bronova I, Berdyshev EV, et al. Sphingolipid regulation of lung epithelial cell mitophagy and necroptosis during cigarette smoke exposure. FASEB J. 2018;32(4):1880-90.
267. Dany M, Gencer S, Nganga R, Thomas RJ, Oleinik N, Baron KD, et al. Targeting FLT3-ITD signaling mediates ceramide-dependent mitophagy and attenuates drug resistance in AML. Blood. 2016;128(15):1944-58.
268. Hernandez-Diaz S, Soukup SF. The role of lipids in autophagy and its implication in neurodegeneration. Cell Stress. 2020;4(7):167-86.
269. Koga H, Kaushik S, Cuervo AM. Altered lipid content inhibits autophagic vesicular fusion. FASEB J. 2010;24(8):3052-65.
270. Russo SB, Baicu CF, Van Laer A, Geng T, Kasiganesan H, Zile MR, et al. Ceramide synthase 5 mediates lipid-induced autophagy and hypertrophy in cardiomyocytes. J Clin Invest. 2012;122(11):3919-30.
271. Daido S, Kanzawa T, Yamamoto A, Takeuchi H, Kondo Y, Kondo S. Pivotal role of the cell death factor BNIP3 in ceramide-induced autophagic cell death in malignant glioma cells. Cancer Res. 2004;64(12):4286-93.
272. Levine B, Sinha S, Kroemer G. Bcl-2 family members: dual regulators of apoptosis and autophagy. Autophagy. 2008;4(5):600-6.
273. Dbaibo GS, Kfoury Y, Darwiche N, Panjarian S, Kozhaya L, Nasr R, et al. Arsenic trioxide induces accumulation of cytotoxic levels of ceramide in acute promyelocytic leukemia and adult T-cell leukemia/lymphoma cells through de novo ceramide synthesis and inhibition of glucosylceramide synthase activity. Haematologica. 2007;92(6):753-62.
274. Qian W, Liu J, Jin J, Ni W, Xu W. Arsenic trioxide induces not only apoptosis but also autophagic cell death in leukemia cell lines via up-regulation of Beclin-1. Leuk Res. 2007;31(3):329-39.

275. Taniguchi M, Kitatani K, Kondo T, Hashimoto-Nishimura M, Asano S, Hayashi A, et al. Regulation of autophagy and its associated cell death by "sphingolipid rheostat": reciprocal role of ceramide and sphingosine 1-phosphate in the mammalian target of rapamycin pathway. J Biol Chem. 2012;287(47):39898-910.
276. Wang Z, Wen L, Zhu F, Wang Y, Xie Q, Chen Z, et al. Overexpression of ceramide synthase 1 increases C18-ceramide and leads to lethal autophagy in human glioma. Oncotarget. 2017;8(61):104022-36.
277. Rohrig F, Schulze A. The multifaceted roles of fatty acid synthesis in cancer. Nat Rev Cancer. 2016;16(11):732-49.
278. Rustam YH, Reid GE. Analytical Challenges and Recent Advances in Mass Spectrometry Based Lipidomics. Anal Chem. 2018;90(1):374-97.
279. Zhao YY, Cheng XL, Lin RC, Wei F. Lipidomics applications for disease biomarker discovery in mammal models. Biomark Med. 2015;9(2):153-68.
280. Sethi S, Brietzke E. Recent advances in lipidomics: Analytical and clinical perspectives. Prostaglandins Other Lipid Mediat. 2017;128-129:8-16.
281. Taïb B, Aboussalah AM, Moniruzzaman M, Chen S, Haughey NJ, Kim SF, et al. Lipid accumulation and oxidation in glioblastoma multiforme. Sci Rep. 2019;9(1):19593.
282. Shakya S, Gromovsky AD, Hale JS, Knudsen AM, Prager B, Wallace LC, et al. Altered lipid metabolism marks glioblastoma stem and non-stem cells in separate tumor niches. Acta Neuropathol Commun. 2021;9(1):101.
283. Soylemez B, Bulut Z, Sahin-Bolukbasi S. Investigating the Potential of Lipids for Use as Biomarkers for Glioblastoma via an Untargeted Lipidomics Approach. J Korean Neurosurg Soc. 2022.
284. Shevchenko A, Simons K. Lipidomics: coming to grips with lipid diversity. Nat Rev Mol Cell Biol. 2010;11(8):593-8.
285. Anderson A. Lipidomics in biomedical research: chance and challenges. Drug Discovery World2021.
286. McDermott M, Eustace AJ, Busschots S, Breen L, Crown J, Clynes M, et al. In vitro Development of Chemotherapy and Targeted Therapy Drug-Resistant Cancer Cell Lines: A Practical Guide with Case Studies. Front Oncol. 2014;4:40.
287. Nicoletti I MR, Di Virgilio F. . Common Methods for Measuring Apoptotic Cell Death by Flow Cytometry. Imaging Living Cells. 2003:215-28.
288. Fujiwara M, Tian L, Le PT, DeMambro VE, Becker KA, Rosen CJ, et al. The mitophagy receptor Bcl-2-like protein 13 stimulates adipogenesis by regulating mitochondrial oxidative phosphorylation and apoptosis in mice. J Biol Chem. 2019;294(34):12683-94.
289. Gimenez-Cassina A, Danial NN. Regulation of mitochondrial nutrient and energy metabolism by BCL-2 family proteins. Trends Endocrinol Metab. 2015;26(4):165-75.
290. Krakstad C, Chekenya M. Survival signalling and apoptosis resistance in glioblastomas: opportunities for targeted therapeutics. Mol Cancer. 2010;9:135.
291. Valdés-Rives SA, Casique-Aguirre D, Germán-Castelán L, Velasco-Velázquez MA, González-Arenas A. Apoptotic Signaling Pathways in Glioblastoma and Therapeutic Implications. Biomed Res Int. 2017;2017:7403747.

292. Sanati M, Binabaj MM, Ahmadi SS, Aminyavari S, Javid H, Mollazadeh H, et al. Recent advances in glioblastoma multiforme therapy: A focus on autophagy regulation. Biomed Pharmacother. 2022;155:113740.
293. Khan I, Baig MH, Mahfooz S, Rahim M, Karacam B, Elbasan EB, et al. Deciphering the Role of Autophagy in Treatment of Resistance Mechanisms in Glioblastoma. Int J Mol Sci. 2021;22(3).
294. Jacobs J, Iranpour R, Behrooz AB, da Silva Rosa SC, Ghavami S. The role of BCL2L13 in glioblastoma: turning a need into a target. Biochem Cell Biol. 2024;102(2):127-34.
295. Wang J, Chen A, Xue Z, Liu J, He Y, Liu G, et al. BCL2L13 promotes mitophagy through DNM1L-mediated mitochondrial fission in glioblastoma. Cell Death Dis. 2023;14(9):585.
296. Oliva CR, Nozell SE, Diers A, McClugage SG, 3rd, Sarkaria JN, Markert JM, et al. Acquisition of temozolomide chemoresistance in gliomas leads to remodeling of mitochondrial electron transport chain. J Biol Chem. 2010;285(51):39759-67.
297. Rabé M, Dumont S, Álvarez-Arenas A, Janati H, Belmonte-Beitia J, Calvo GF, et al. Identification of a transient state during the acquisition of temozolomide resistance in glioblastoma. Cell Death Dis. 2020;11(1):19.
298. Tiek DM, Rone JD, Graham GT, Pannkuk EL, Haddad BR, Riggins RB. Alterations in Cell Motility, Proliferation, and Metabolism in Novel Models of Acquired Temozolomide Resistant Glioblastoma. Sci Rep. 2018;8(1):7222.
299. Zhu Y, Chen Z, Kim SN, Gan C, Ryl T, Lesjak MS, et al. Characterization of Temozolomide Resistance Using a Novel Acquired Resistance Model in Glioblastoma Cell Lines. Cancers (Basel). 2022;14(9).
300. Barciszewska AM, Gurda D, Głodowicz P, Nowak S, Naskręt-Barciszewska MZ. A New Epigenetic Mechanism of Temozolomide Action in Glioma Cells. PLoS One. 2015;10(8):e0136669.
301. Hirose Y, Berger MS, Pieper RO. p53 effects both the duration of G2/M arrest and the fate of temozolomide-treated human glioblastoma cells. Cancer Res. 2001;61(5):1957-63.
302. Yan Y, Xu Z, Dai S, Qian L, Sun L, Gong Z. Targeting autophagy to sensitive glioma to temozolomide treatment. J Exp Clin Cancer Res. 2016;35:23.
303. Jiapaer S, Furuta T, Tanaka S, Kitabayashi T, Nakada M. Potential Strategies Overcoming the Temozolomide Resistance for Glioblastoma. Neurol Med Chir (Tokyo). 2018;58(10):405-21.
304. Koukourakis MI, Mitrakas AG, Giatromanolaki A. Therapeutic interactions of autophagy with radiation and temozolomide in glioblastoma: evidence and issues to resolve. Br J Cancer. 2016;114(5):485-96.
305. Ito H, Daido S, Kanzawa T, Kondo S, Kondo Y. Radiation-induced autophagy is associated with LC3 and its inhibition sensitizes malignant glioma cells. Int J Oncol. 2005;26(5):1401-10.
306. Lomonaco SL, Finniss S, Xiang C, Decarvalho A, Umansky F, Kalkanis SN, et al. The induction of autophagy by gamma-radiation contributes to the radioresistance of glioma stem cells. Int J Cancer. 2009;125(3):717-22.
307. Mitrakas AG, Kalamida D, Giatromanolaki A, Pouliliou S, Tsolou A, Kyranas R, et al. Autophagic flux response and glioblastoma sensitivity to radiation. Cancer Biol Med. 2018;15(3):260-74.
308. Liu B, Shi Y, Qin B, Cheng D, Nie Z, Zhai H, et al. Sertindole inhibits autophagic flux and glioma progression. MedComm – Oncology. 2023;2(2):e41.

309. Eskelinen EL. Doctor Jekyll and Mister Hyde: autophagy can promote both cell survival and cell death. Cell Death Differ. 2005;12 Suppl 2:1468-72.
310. Cj P, Hv E, Vijayakurup V, G RM, Nair S, Gopala S. High LC3/Beclin Expression Correlates with Poor Survival in Glioma: a Definitive Role for Autophagy as Evidenced by In Vitro Autophagic Flux. Pathol Oncol Res. 2019;25(1):137-48.
311. Bilger A, Bittner MI, Grosu AL, Wiedenmann N, Meyer PT, Firat E, et al. FET-PET-based reirradiation and chloroquine in patients with recurrent glioblastoma: first tolerability and feasibility results. Strahlenther Onkol. 2014;190(10):957-61.
312. Gewirtz DA. The Challenge of Developing Autophagy Inhibition as a Therapeutic Strategy. Cancer Res. 2016;76(19):5610-4.
313. Gousias K, Theocharous T, Simon M. Mechanisms of Cell Cycle Arrest and Apoptosis in Glioblastoma. Biomedicines. 2022;10(3).
314. Jin S, White E. Role of autophagy in cancer: management of metabolic stress. Autophagy. 2007;3(1):28-31.
315. Mizushima N, Komatsu M. Autophagy: renovation of cells and tissues. Cell. 2011;147(4):728-41.
316. Kang C, Elledge SJ. How autophagy both activates and inhibits cellular senescence. Autophagy. 2016;12(5):898-9.
317. Ziegler DV, Huber K, Fajas L. The Intricate Interplay between Cell Cycle Regulators and Autophagy in Cancer. Cancers (Basel). 2021;14(1).
318. Mathiassen SG, De Zio D, Cecconi F. Autophagy and the Cell Cycle: A Complex Landscape. Front Oncol. 2017;7:51.
319. Mizushima N, Klionsky DJ. Protein turnover via autophagy: implications for metabolism. Annu Rev Nutr. 2007;27:19-40.
320. Meng F, Sun N, Liu D, Jia J, Xiao J, Dai H. BCL2L13: physiological and pathological meanings. Cell Mol Life Sci. 2021;78(6):2419-28.
321. Murakawa T, Okamoto K, Omiya S, Taneike M, Yamaguchi O, Otsu K. A Mammalian Mitophagy Receptor, Bcl2-L-13, Recruits the ULK1 Complex to Induce Mitophagy. Cell Rep. 2019;26(2):338-45.e6.
322. Kalkavan H, Green DR. MOMP, cell suicide as a BCL-2 family business. Cell Death Differ. 2018;25(1):46-55.
323. Zimmermann M, Reichert AS. How to get rid of mitochondria: crosstalk and regulation of multiple mitophagy pathways. Biol Chem. 2017;399(1):29-45.
324. Onishi M, Yamano K, Sato M, Matsuda N, Okamoto K. Molecular mechanisms and physiological functions of mitophagy. Embo j. 2021;40(3):e104705.
325. Alavian KN, Li H, Collis L, Bonanni L, Zeng L, Sacchetti S, et al. Bcl-xL regulates metabolic efficiency of neurons through interaction with the mitochondrial F1FO ATP synthase. Nat Cell Biol. 2011;13(10):1224-33.
326. Perciavalle RM, Stewart DP, Koss B, Lynch J, Milasta S, Bathina M, et al. Anti-apoptotic MCL-1 localizes to the mitochondrial matrix and couples mitochondrial fusion to respiration. Nat Cell Biol. 2012;14(6):575-83.
327. Wang X, Bathina M, Lynch J, Koss B, Calabrese C, Frase S, et al. Deletion of MCL-1 causes lethal cardiac failure and mitochondrial dysfunction. Genes Dev. 2013;27(12):1351-64.

328. Danial NN, Gramm CF, Scorrano L, Zhang CY, Krauss S, Ranger AM, et al. BAD and glucokinase reside in a mitochondrial complex that integrates glycolysis and apoptosis. Nature. 2003;424(6951):952-6.
329. Lucantoni F, Salvucci M, Dussmann H, Lindner AU, Lambrechts D, Prehn JHM. BCL(X)L and BCL2 increase the metabolic fitness of breast cancer cells: a single-cell imaging study. Cell Death Differ. 2021;28(5):1512-31.
330. Rong YP, Aromolaran AS, Bultynck G, Zhong F, Li X, McColl K, et al. Targeting Bcl-2-IP3 receptor interaction to reverse Bcl-2's inhibition of apoptotic calcium signals. Mol Cell. 2008;31(2):255-65.
331. Grepper D, Tabasso C, Zanou N, Aguettaz AKF, Castro-Sepulveda M, Ziegler DV, et al. BCL2L13 at endoplasmic reticulum-mitochondria contact sites regulates calcium homeostasis to maintain skeletal muscle function. iScience. 2024;27(8):110510.
332. Singh N, Miner A, Hennis L, Mittal S. Mechanisms of temozolomide resistance in glioblastoma - a comprehensive review. Cancer Drug Resist. 2021;4(1):17-43.
333. Vlashi E, Lagadec C, Vergnes L, Matsutani T, Masui K, Poulou M, et al. Metabolic state of glioma stem cells and nontumorigenic cells. Proc Natl Acad Sci U S A. 2011;108(38):16062-7.
334. Zampieri LX, Sboarina M, Cacace A, Grasso D, Thabault L, Hamelin L, et al. Olaparib Is a Mitochondrial Complex I Inhibitor That Kills Temozolomide-Resistant Human Glioblastoma Cells. Int J Mol Sci. 2021;22(21).
335. Matsubara H, Tanaka R, Tateishi T, Yoshida H, Yamaguchi M, Kataoka T. The human Bcl-2 family member Bcl-rambo and voltage-dependent anion channels manifest a genetic interaction in Drosophila and cooperatively promote the activation of effector caspases in human cultured cells. Exp Cell Res. 2019;381(2):223-34.
336. Kwong SC, Jamil AHA, Rhodes A, Taib NA, Chung I. Metabolic role of fatty acid binding protein 7 in mediating triple-negative breast cancer cell death via PPAR-α signaling. J Lipid Res. 2019;60(11):1807-17.
337. Cheng H, Wang M, Su J, Li Y, Long J, Chu J, et al. Lipid Metabolism and Cancer. Life (Basel). 2022;12(6).
338. Giussani P, Bassi R, Anelli V, Brioschi L, De Zen F, Riccitelli E, et al. Glucosylceramide synthase protects glioblastoma cells against autophagic and apoptotic death induced by temozolomide and Paclitaxel. Cancer Invest. 2012;30(1):27-37.
339. Navone SE, Guarnaccia L, Rizzaro MD, Begani L, Barilla E, Alotta G, et al. Role of Luteolin as Potential New Therapeutic Option for Patients with Glioblastoma through Regulation of Sphingolipid Rheostat. Int J Mol Sci. 2023;25(1).
340. Sheridan M, Ogretmen B. The Role of Ceramide Metabolism and Signaling in the Regulation of Mitophagy and Cancer Therapy. Cancers (Basel). 2021;13(10).
341. Zaibaq F, Dowdy T, Larion M. Targeting the Sphingolipid Rheostat in Gliomas. Int J Mol Sci. 2022;23(16).
342. Ogretmen B. Sphingolipid metabolism in cancer signalling and therapy. Nat Rev Cancer. 2018;18(1):33-50.
343. Lachkar F, Ferré P, Foufelle F, Papaioannou A. Dihydroceramides: their emerging physiological roles and functions in cancer and metabolic diseases. Am J Physiol Endocrinol Metab. 2021;320(1):E122-e30.

344. Zheng W, Kollmeyer J, Symolon H, Momin A, Munter E, Wang E, et al. Ceramides and other bioactive sphingolipid backbones in health and disease: lipidomic analysis, metabolism and roles in membrane structure, dynamics, signaling and autophagy. Biochim Biophys Acta. 2006;1758(12):1864-84.
345. Gagliostro V, Casas J, Caretti A, Abad JL, Tagliavacca L, Ghidoni R, et al. Dihydroceramide delays cell cycle G1/S transition via activation of ER stress and induction of autophagy. Int J Biochem Cell Biol. 2012;44(12):2135-43.
346. Signorelli P, Munoz-Olaya JM, Gagliostro V, Casas J, Ghidoni R, Fabriàs G. Dihydroceramide intracellular increase in response to resveratrol treatment mediates autophagy in gastric cancer cells. Cancer Lett. 2009;282(2):238-43.
347. Noack J, Choi J, Richter K, Kopp-Schneider A, Régnier-Vigouroux A. A sphingosine kinase inhibitor combined with temozolomide induces glioblastoma cell death through accumulation of dihydrosphingosine and dihydroceramide, endoplasmic reticulum stress and autophagy. Cell Death Dis. 2014;5(9):e1425.
348. Shimeno H, Soeda S, Sakamoto M, Kouchi T, Kowakame T, Kihara T. Partial purification and characterization of sphingosine N-acyltransferase (ceramide synthase) from bovine liver mitochondrion-rich fraction. Lipids. 1998;33(6):601-5.
349. Mullen TD, Hannun YA, Obeid LM. Ceramide synthases at the centre of sphingolipid metabolism and biology. Biochem J. 2012;441(3):789-802.
350. Pewzner-Jung Y, Brenner O, Braun S, Laviad EL, Ben-Dor S, Feldmesser E, et al. A critical role for ceramide synthase 2 in liver homeostasis: II. insights into molecular changes leading to hepatopathy. J Biol Chem. 2010;285(14):10911-23.
351. Raichur S. Ceramide Synthases Are Attractive Drug Targets for Treating Metabolic Diseases. Front Endocrinol (Lausanne). 2020;11:483.
352. Panjarian S, Kozhaya L, Arayssi S, Yehia M, Bielawski J, Bielawska A, et al. De novo N-palmitoylsphingosine synthesis is the major biochemical mechanism of ceramide accumulation following p53 up-regulation. Prostaglandins Other Lipid Mediat. 2008;86(1-4):41-8.
353. Spassieva SD, Mullen TD, Townsend DM, Obeid LM. Disruption of ceramide synthesis by CerS2 down-regulation leads to autophagy and the unfolded protein response. Biochem J. 2009;424(2):273-83.
354. Mollinedo F, Gajate C. Fas/CD95 death receptor and lipid rafts: new targets for apoptosis-directed cancer therapy. Drug Resist Updat. 2006;9(1-2):51-73.
355. Senkal CE, Ponnusamy S, Bielawski J, Hannun YA, Ogretmen B. Antiapoptotic roles of ceramide-synthase-6-generated C16-ceramide via selective regulation of the ATF6/CHOP arm of ER-stress-response pathways. Faseb j. 2010;24(1):296-308.
356. Chae HD, Kim BM, Yun UJ, Shin DY. Deregulation of Cdk2 causes Bim-mediated apoptosis in p53-deficient tumors following actin damage. Oncogene. 2008;27(29):4115-21.
357. Slimen IB, Najar T, Ghram A, Dabbebi H, Ben Mrad M, Abdrabbah M. Reactive oxygen species, heat stress and oxidative-induced mitochondrial damage. A review. Int J Hyperthermia. 2014;30(7):513-23.
358. Esmaeilian Y, Hela F, Bildik G, Iltumur E, Yusufoglu S, Yildiz CS, et al. Autophagy regulates sex steroid hormone synthesis through lysosomal degradation of lipid droplets in human ovary and testis. Cell Death Dis. 2023;14(5):342.

359. Xu Y, Gao W, Zhang Y, Wu S, Liu Y, Deng X, et al. ABT737 reverses cisplatin resistance by targeting glucose metabolism of human ovarian cancer cells. Int J Oncol. 2018;53(3):1055-68.
360. Pinton P, Rizzuto R. Bcl-2 and Ca2+ homeostasis in the endoplasmic reticulum. Cell Death Differ. 2006;13(8):1409-18.
361. Chen YB, Aon MA, Hsu YT, Soane L, Teng X, McCaffery JM, et al. Bcl-xL regulates mitochondrial energetics by stabilizing the inner membrane potential. J Cell Biol. 2011;195(2):263-76.
362. Yan MM, Ni JD, Song D, Ding M, Huang J. Interplay between unfolded protein response and autophagy promotes tumor drug resistance. Oncol Lett. 2015;10(4):1959-69.
363. McQuiston A, Diehl JA. Recent insights into PERK-dependent signaling from the stressed endoplasmic reticulum. F1000Res. 2017;6:1897.
364. Mostafavi S, Eskandari N. Mitochondrion: Main organelle in orchestrating cancer escape from chemotherapy. Cancer Rep (Hoboken). 2024;7(2):e1942.
365. Lin Z, Long F, Kang R, Klionsky DJ, Yang M, Tang D. The lipid basis of cell death and autophagy. Autophagy. 2024;20(3):469-88.